NORTHWESTERN UNIVERSITY

An Investigation of the Cellular Mechanisms Underlying Hearing Sensitivity and Resistance to Noise Induced Traumas.

A DISSERTATION

SUBMITTED TO THE GRADUATE SCHOOL

IN PARTIAL FULFILLMENT OF THE REQUIREMENTS

for the degree

DOCTOR OF PHILOSOPHY

Field of Neuroscience

By

Miguel Angel Ramirez

EVANSTON, ILLINOIS

September 2022

Abstract

Perturbations to the physiology or impairments in the formation of synapses within the cochlea, specifically the ribbon synapses, result in decreased sensitivity to auditory stimuli. In example, prolonged exposure to moderately intense auditory stimuli, like power tools, can result in the swelling of nerve terminals, retraction of the postsynaptic membrane, and eventually the loss of ribbon synapses driving permanent hearing loss. Thus, understanding proteins which physically tether and organize these synaptic membranes, such as neuroligins and neurexins, will broaden our understanding of potentially protective mechanisms against the loss of hearing sensitivity. Moreover, we lack even a basic characterization of the molecular changes distinguishing permeant from temporary sensory hearing loss. Therefore, the goal of this thesis is two parts, the first is to characterize the impact of neuroligins with respect to ribbon synapse maturation and physiology. The second, is to broaden our understanding of the cochlear proteome with respect to noise exposure and recovery from noise induced trauma.

In chapters 3 and 4, I determined that *Nlgn3* expression dramatically increases throughout cochlear development, and that Nlgn1 and Nlgn3 are present at many of the same ribbon synapses. *Nlgn3* and *Nlgn1* single knock out (KO) cochleae have fewer ribbon synapses and mild hearing phenotypes based on auditory brain stem response recordings. Double KO cochlear phenotypes generally exceed the additive effects of the individual KO's, with the latency of sound-response being particularly severe. These observations indicate that Nlgn1 and Nlgn3 have largely overlapping yet essential functions in the maturation and function of cochlear ribbon synapses.

In chapter 5 I discuss the results of our quantitative proteomics analysis, which revealed that moderate and severe intensity noise cause proteotoxicity within the cochlea. Transcriptomic analysis determined that a subset of genes encoding proteins with elevated levels also have increased gene expression, including numerous proteasome subunits. Recovery period proteomics revealed that protein synthesis machinery is selectively up regulated. We report that over stimulation of the auditory system drives a robust cochlear proteotoxic stress response.

In chapter 6 I discussed preliminary data collected while investigating the protective effects of a drug known to induce the heat shock response with respect to noise exposure. In the latter portion of this chapter, I then discuss the presence of long-lived proteins within the cochlea and strategies for detecting low abundance proteins within the cochlea.

Together these chapters outline key efforts made during my doctoral training and reflect novel bodies of work which expand our understanding of cellular mechanisms underlying hearing and our sensitivity to noise induced hearing loss.

Acknowledgements

My journey as a budding scientist was not without its challenges and obstacles, it would be remised if I did not acknowledge the people in my life that have supported my endeavors. The amount of gratitude I feel for not only the training but the guidance I have received from Dr. Jeffrey Savas is impossible to overstate. When we embarked on this journey together, I don't think we would have predicted that we would go through multiple postdocs, a global pandemic, and a house renovation, in addition to the regular challenges of graduate school. To say I was wet behind the ears is an understatement, but somehow, we made it and the amount of growth I have gone through feels incredible. Jeff's support and approach to problems will forever shape how I view and analyze science. In my stay with the Savas lab, I have been gifted with a solid scientific foundation, an appreciation for how powerful an analytical tool mass spectrometry is, years of mice breeding headaches, and a deep appreciation for scientific rigor and reasoning.

Over the years the Savas lab has grown and shrunk but the incredible environment created in this space was one of the reasons coming into lab was always enjoyable. Tim, Natalia, and Nalini kept my spirits high over the years and I will cherish all of our time spent together, from sharing chicken nuggets to scouring conferences looking for free stuff, it was fun. To our tremendous lab manager, Seby Edessary, who was the glue that held the lab together, always supportive and willing to help, thank you. But most importantly, I must thank Nopporn Jongkamonwiwat for some of my most memorable experiences. Nop, with a perpetual smile on his face, is one of the warmest individuals I have ever had the pleasure of meeting. Although our time was short, I will always appreciate the long nights we spent listening to Madonna working on experiments and sharing stories. Thank you for having patience with me, for guiding me and

for teaching me not only ABRs but how to carry myself in an academic environment without losing my joy and empathy for those around me.

I'd also like to thank the members of my thesis committee – Anis Contractor, Jaime Garcia-Añoveros, and Kazuaki Homma – who have provided invaluable advice on the work that forms this thesis. Jaime for always contributing his vast knowledge to better aid in my understanding of the nuances related to hearing. Anis for encouraging me to take risks throughout my training but for also maintaining my expectations with the feasibility of experiments. Finally, Kazu for providing me an outlet to not only develop my skills as a presenter but also allowing me the opportunity to hear and discuss the work of others in our field on a weekly basis.

Lastly, I would like to thank my family for supporting me despite my mood swings and frustrations. My mother for always being by my side, offering advice, comfort, and providing a constant reminder of what my journey means in the grand scheme of things. To not overthink when things go wrong but to anticipate how to fix things before, they get that far. My father for always believing in me. My brothers, Despot included, for always cheering me up and making me laugh when I was at my lowest. My aunt and uncle who have been my rock these past few years, always supporting me and showering me with love. But finally, my wonderful partner, who has filled this pandemic with so much happiness, thank you for all that you do and all that you continue to do.

Contributions

Portions of this thesis are adapted from "Noise exposures causing hearing loss generate proteotoxic stress and activate the proteostasis network" by Jongkamonwiwat and Ramirez et al. (*Cell Reports* 2020) and "Cochlear Encoding of Sound requires Nlgn1 and Nlgn3" by Ramirez et al. (pending *iScience* 2022) The following important contributions were made by individuals other than Miguel Ramirez: Chapter 3: Yuzuru Ninoyu performed marmoset cochlear immunofluorescence. Chapter 4: Cayla Miller performed synaptic distance quantification. Seby Edassery aided in quantification of TMT data. Chapter 5: Nopporn Jongkamonwiwat and Anne C.Y. Wong. performed ABR and DPOAE experiments. Nopporn Jongkamonwiwat performed mass spectrometry analysis. Seby Edassery contributed to western blot analysis, and RNASeq analysis, finally Tirzah Abbott guided SEM data acquisition.

Dedicated to my late grandfather, Elias Sanchez.

“Ponte las pilas.”

Arrangement of the Dissertation

Title Page…… 1

Abstract……... 2

Acknowledgment…… 4

Contributions……... 6

Dedication……... 7

Table of Contents…… 8

List of Figures...…….11

Chapter 1: Introduction into Cellular Cochlear Biology…… 15

Overview of the Peripheral Auditory Circuit……..……..……..……16

How We Measure Hearing…..……...21

Organizers of the Cochlear Ribbon Synapse…….…….……22

Trans-synaptic Adhesion Molecules in the Context of Hearing……..……...23

What is Noise and How Does it Affect Us?...……..…….……25

What is a Proteome and How Does Proteomics Further Our Understanding of Hearing?...26

Chapter 2: Methods…..……..…….……30

Cochlear Functional Assays..……...……..31

Quantitative PCR……...……....33

RNAseq and Transcriptomic Quantification...…....……..33

RNAScope and CellProfiler Analysis…..……36

Metabolic Labeling of the Cochlea with ^{15}N Mouse Chow……...37

Preparation of Cochlear Extracts for ^{15}N Based Quantitation……37

Preparation of Cochlear Extracts for TMT Based Quantitation…….....38

Nanoflow LC with Multinotch MS2/MS3 Orbitrap Fusion MS analysis……39

Absolute Quantitation of Peptide / Protein Abundance ……40

Analysis of Tandem Mass Spectra…….…....41

Bioinformatic Analysis with PATHER AND STRING ……..…44

Heat Maps, Clustering and Volcano Pots for the Recovery Priod ……..…44

TUBE Pulldown Western Blot…..…….45

diGly Analysis of Protein Ubiquitination..…….46

Immunofluorescence with Confocal Analysis.……..……..…47

Quantification of Synapse Density, Volume, and Diversity…….…….….49

Synapse Distance Quantification……..…….….50

SEM Analysis...…….….51

Western Blot Analysis ……..……..…51

Quantification and Statistical Analysis..……..…52

Animal Experiments…….…..53

Chapter 3: Neuroligins and Neurexins Among the Cochlear Ribbon Synapses…….……..54

Introduction……55

Results……54

Neuroligins are Primarily Expressed by Cochlear Spiral Ganglion Neurons……54

Nlgn1 and *Nlgn3* Localize to Common and Distinct Ribbon Synapses…...…….65

Nlgn3 is Predominantly Expressed throughout Cochlear Ribbon Synapse Maturation but neither *Nlgn1* nor *Nlgn3* are Necessary for Synapse Formation. ……...…….75

Chapter 4: Maturation of Cochlear Ribbon Synapses is Dependent on Neuroligins 1 and 3……..…79

Introduction……80

Results……82

Ribbon Synapses are Significantly Fewer and Smaller in *Nlgn1/ 3* Double Knock Out Mice……82

Nlgn1 and *Nlgn3* are Required for Cochlear Ribbon Synapse Proteome Maintenance.....90

Absence of *Nlgn1* or *Nlgn3* Impairs Hearing……..93

Mice Lacking *Nlgn1* or *Nlgn3* are Highly Sensitive to Noise……...102

Chapter 5: Cochlear Proteome Remodeling After Noise……..…..…109

Introduction……..…110

Results……..112

Short-Term Noise Exposures Result in Temporary and Permanent Hearing Loss in Mice…… 112

Confirmation that Noise Exposure Unbalances the Cochlear Proteome……..…116

Exposure to Moderate Intensity Noise Leads to Reduced Ribbon Synapse Density, Modest Damage to Mechanotransduction Machinery, but not Cell Death……125

Hair Cells, Spiral Ganglion Neurons, and Additional Cochlear Cell Types Express Proteins with Altered Fold Change After Noise Exposure……...129

Noise Exposures Causing Hearing Loss Drive Cochlear Gene Expression.……135

Ubiquitin-proteasome System is Activated After Exposure to Moderate and Severe Intensity Noise…..……139

Protein Translation Machinery has Selectively Elevated Fold Change During the Recovery Period……...143

Chapter 6: Data in Progress: Mitigation of Cellular Stress Induced by Noise……..…..…149

Introduction and Preliminary Data……...150

Chapter 7: Data in Progress: The Investigation of Long-Lived Proteins within the Cochlea, and the Quantification of Low-Abundance Proteins in Complex Cochlear Samples……..161

Introduction and Preliminary Data……...161

Chapter 8: General Discussion…….174

Discussion I: Neuroligins and Hearing…….……..……..175

Discussion II: The Cellular Impact of Noise Exposure…….……..180

Chapter 9: References……...…….……184

List of figures

Figure 1. Overview of the cells within the Organ of Corti…….19

Figure 2. Positive and negative controls within the cochlea used for RNAScope expression analysis……...59

Figure 3. *Nlgn1 is* expressed by spiral ganglion neurons alongside *Nlgn3*…….61

Figure 4. *Nlgn1* and *Nlgn3* mRNAs are co-expressed among neurons in the cochlea……63

Figure 5. Western blot analysis of brain lysates validates Nlgn1 and Nlgn3 KO……..……67

Figure 6. Nlgn1 and Nlgn3 localize to cochlear ribbon synapses throughout the turns of the cochlea……...…69

Figure 7. The presence of Nlgn1 and Nlgn3 at cochlear ribbon synapses is conserved across species and position dependent along the modiolar-pillar axis in mice…….71

Figure 8. Cochlear ribbon synapses demonstrate a modiolar-pillar dependent pattern for Nlgn1 and Nlgn3……..73

Figure 9. Neuroligins are expressed throughout cochlear development but are not required for synapse formation……..77

Figure 10. Visualization of cochlear ribbon synapses across single and double neuroligin knock-outs compared to WT…….……85

Figure 11. Nlgn1 and 3 are required for cochlear ribbon synapse maturation……87

Figure 12. *Nlgn1/3* dKO cochlea have reduced levels of synaptic scaffolding proteins……..91

Figure 13. Comparison of *Nlgn1* KO and *Nlgn3* KO background strains observed comparable ABR responses……95

Figure 14. Nlgn1 and 3 are required for cochlear function……97

Figure 15. *Nlgn3* is overexpressed in *Nlgn1* KO cochlea……100

Figure 16. Nlgn1 KO and Nlgn3 KO background strains observe comparable susceptibility to noise and recovery…….104

Figure 17. *Nlgn3* KOs have increased sensitivity to noise……106

Figure 18. ABR and DPOAE cochlear functional assays to determine responses in FVB mice after 30 minutes of exposure to ambient, moderate, or severe noise (8-16 kHz)…….114

Figure 19. Assessment of significantly altered proteins from TMT analyses……119

Figure 20. Confirmation that noise exposures causing hearing loss unbalance the cochlea proteome……..121

Figure 21. Direct comparison of the cochlear proteome after 30-minute noise exposures causing temporary or permeant hearing loss…….123

Figure 22. Exposure to moderate and severe intensity noise alter stereocilia morphology and reduce synaptic density across the middle and base of the cochlea…….127

Figure 23. A proportion of hair cell enriched proteins are also significantly altered following damaging levels of noise exposure……...……131

Figure 24. Proteins regulated during noise exposure are expressed by HCs, SGNs, and supporting cells within the cochlea……133

Figure 25. RNA-Seq analysis demonstrated an overall increase in cochlear gene expression following exposure to moderate or severe intensity noise compared to ambient levels……137

Figure 26. The degree of ubiquitylation within the cochlea increases at progressively increasing levels of noise exposure compared to ambient controls……141

Figure 27. Proteomic assessment of the molecular mechanisms underlying the recovery of hearing sensitivity……145

Figure 28. Ribosomal proteins have elevated fold change during the hearing recovery period cochlear extracts after exposure to moderate or severe relative to ambient intensity noise……147

Figure 29. GFP signal intensity increases with noise exposure and is concentrated among the cells of the spiral bundle……...153

Figure 30. *GFP* is expressed among all cell types within the cochlea and expression is reduced following noise exposure……..……155

Figure 31. GFP levels increase 2 hours after exposure to 105 dB SPL noise…….……157

Figure 32. TRC051384 injections elevate GFP abundance prior to noise exposure which reduces cellular stress after noise exposure……...…159

Figure 33. GO analysis of long-lived proteins within the cochlear determined an enrichment in collogen and extracellular matrix proteins……167

Figure 34. Comparison of the theoretical top two most intense precursor and product ions with measured ions associated with Nlgn3……...169

Figure 35. Analysis of retention times associated with the 6 precursors used for PRM observed similar elution times across all trials……171

Figure 36. Comparison of DDA and S-PRM methods demonstrate increasing levels of selectivity for Nlgn3 product ions……..……173

Figure 37. Summary of the Impact of Neuroligin 1/3 on Ribbon Synapse Structure and Function……...182

Figure 38. Speculation on TRC051384's Effect on the Preservation of Hearing Following Noise……188

Chapter 1: **: Introduction into Cellular Cochlear Biology**

Peripheral auditory circuit

Hearing is critically dependent on the function of cochlear ribbon synapses, which are specialized cell junctions formed between mechanosensitive hair cells and a single auditory afferent nerve fiber (ANF) (Fettiplace, 2017). Upon auditory stimulation, energy carried by sound is transferred into the cochlea and transformed into a physical displacement of the endolymph inside the cochlear duct, resulting in the displacement of the basilar and tectorial membranes. The physical properties of the basilar membrane, which increases in width and decreases in stiffness from its base to its apex, allow for the encoding of different tones. As such, vibrations will travel along the basilar membrane until they reach a distance where a maximal amplitude of displacement is attained and then rapidly subsides. Generally, low-frequency sounds cause the apical end of the membrane to vibrate, and high-frequency sounds cause the basal end to vibrate. Thus, giving rise to the tonotopic map where any given tone will stimulate a localized region along the basilar membrane.

The region between the basilar and tectorial membranes is known as the organ of Corti, this region houses specialized mechanosensitive cells referred to as hair cells **(Figure 1)**. As the basilar membrane vibrates, a force is applied to the tops of the hair cells by the tectorial membrane leading to the deflection of the hair bundles atop inner hair cells. The force applied to the hair bundles pull open MET ion channels, located at the tips of the bundles, leading to a graded depolarization of the hair cell. Because the MET channels are largely indiscriminate with respect to ion permeability, the depolarization of the hair cell can vary and is largely dependent on the frequency with which the MET channels are opened.

The perception of loudness is typically related to sound pressure levels (SPL), which is measured in decibels (dB), is used to characterize the intensity of auditory stimuli. While sound intensity and SPL are distinct measures, they are intimately related. Therefore, as the sound intensity increases, the power carried by sound waves also increases, resulting in greater changes to local pressures because of the displacement of the cochlear fluid. Importantly, rather than transmitting a binary action potential, the inner hair cell afferent nerve fiber (IHC–ANF) ribbon synapse encodes a graded presynaptic signal based on the intensity of the auditory stimuli (i.e., the loudness of a sound). Vesicle release within the hair cells has evolved to provide a continuous, inexhaustible supply of glutamate into the synaptic cleft by pooling vesicles near the synaptic active zone. These specialized structures are known as synaptic ribbons, and are the namesake for these synapses, which are necessary for encoding high frequency stimuli, critical for hearing.

Recently we have made strides in understanding the composition of the ANFs which innervate the inner hair cells, largely thanks to innovations in transcriptomics (Petitpre et al., 2018; Shrestha et al., 2018). The ANFs, can be divided into two main groups, the type I and IIs (Meyer et al., 2009; Reijntjes and Pyott, 2016; Weisz et al., 2014; Weisz et al., 2012). Type I ANFs each selectively innervate a single inner hair cell and represent roughly 95% of all afferent neurons within the peripheral auditory circuit (Meyer *et al.*, 2009). The type II ANFs, on the other hand, innervate multiple outer hair cells and compose the remaining 5% of ANFs (Weisz *et al.*, 2014). Type I ANFs can be further divided into three categories, Ia, Ib and Ic, which innervate distinct regions along the basolateral surface of the inner hair cell (Liberman, 1982; Shrestha *et al.*, 2018; Sun et al., 2018). This innervation pattern is believed to correlate with the

excitability of the ANFs, being the highest among Ia, which innervate the pillar side of inner hair cells, and lowest in Ic, which innervate on the modiolar side (Furman et al., 2013; Liberman et al., 2011). This stereotyped positioning around the base of the inner hair cell is believed to, in part, be a result of measurable differences in the voltage dependence of Ca^{2+} influx at glutamate release sites along the modiolar-pillar axis (Ohn et al. 2016). In terms of glutamate receptor subtypes expressed by ANFs, it has been widely accepted that AMPA-type glutamate receptors are the primary drivers of afferent excitability (Glowatzki & Fuchs 2002) and while there has been evidence for the presence of N-methyl-D-aspartate (NMDA) receptors, and metabotropic glutamate receptors being expressed by type I ANFs, (Coate et al) their contributions with respect to afferent transmission is minor (Reijntjes & Pyott 2016, Glowatzki & Fuchs 2002).

Completing the PAC are cholinergic efferent neurons, originating from the brainstem, which release acetylcholine (Ach) to inhibit hair cells through activation of calcium-dependent potassium channels (Glowatzki and Fuchs, 2002). Notably, efferent neurons have only been shown to innervate outer hair cells directly, where Ach shunts and suppresses outer hair cell electromotility, reducing the amplification of basilar membrane motility ultimately depressing inner hair cell depolarization. The elegant linearity of the PAC, in conjunction with auditory brainstem response recordings described in the next section, provide a unique platform for the investigation of synaptic proteins.

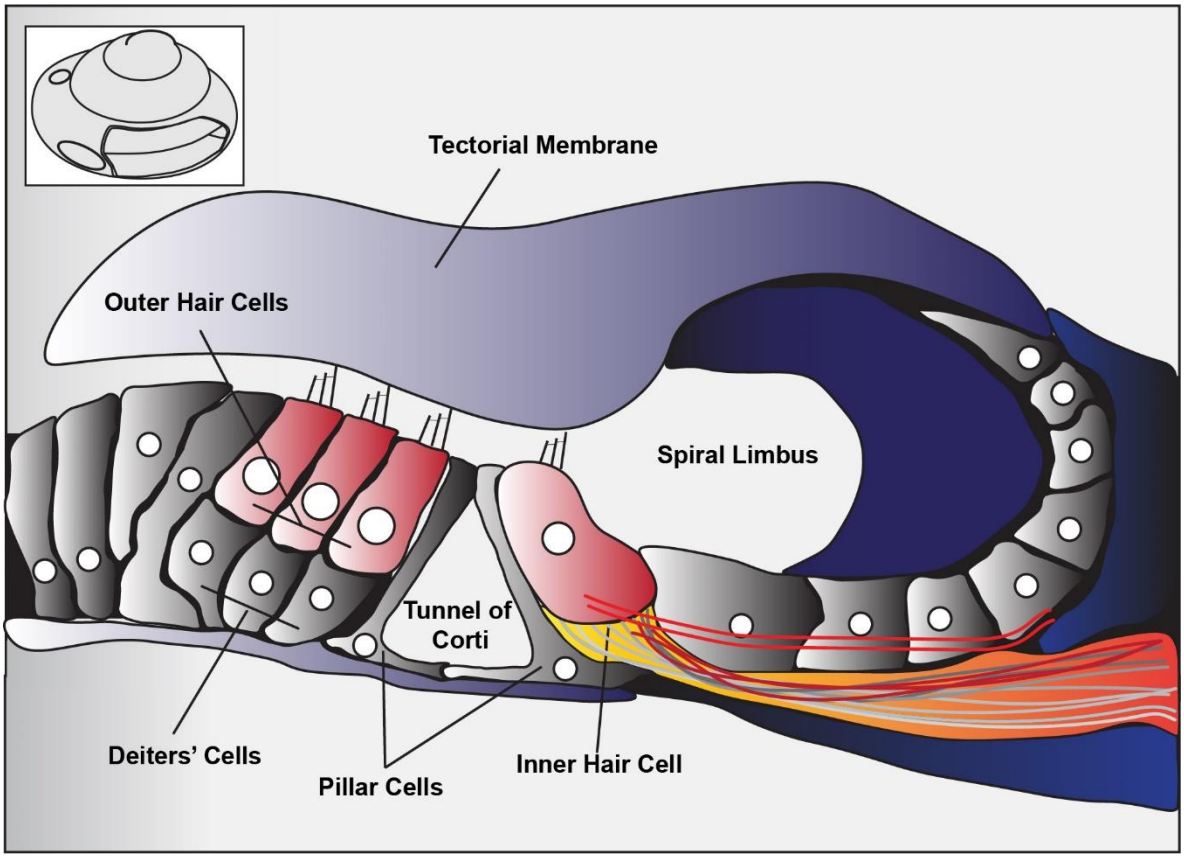
Tectorial Membrane
Outer Hair Cells
Spiral Limbus
Tunnel of Corti
Deiters' Cells
Pillar Cells
Inner Hair Cell

Figure 1. Overview of the cells within the organ of Corti. Illustration of the various cell types that reside within the organ of Corti. Inner and outer hair cells, shown in red are the mechanoreceptors within the cochlear responsible for changing the physical movement of the tectorial and basilar membranes into chemical signals. Pillar cells line the tunnel of Corti, a fluid filled pocket that runs the length of the cochlea to physically support the inner and outer hair cells. Deiters' cells are shown underneath the outer hair cells provide the support to outer hair cells.

How We Measure Hearing

As sound enters the inner ear the deflection of the cochlear fluid will stimulate hundreds of hair cells which in turn will activate groups of afferent nerve fibers. The collective electrical activity of these spiral ganglion bundles in response to the auditory stimuli, referred to as an evoked potential, can be measured via electrodes placed near the skin. These types of measurements, referred to as auditory brainstem response recordings (ABRs), are powerful tools in gaining insight into the health of the auditory pathway. The ABR generally consists of seven positive peaks which occur within 10 ms after the presentation of an auditory stimuli. Each peak is reflective of neuronal activity along the auditory nerve and different levels of the brainstem where Waves I and II are generated by the auditory nerve. Waves III-VI are believed to reflect activity deeper in the auditory brainstem. Wave III is believed to originate from the cochlear nucleus; Wave IV from the superior olivary complex; and Wave V from the lateral lemniscus and the inferior colliculus.

Typically, the characterization of Wave I, reflective of the IHC-ANF synapse is used to characterize the role of unknown proteins or mutations with respect to peripheral hearing. By quantifying aspects such as the Wave I amplitude, latency, duration we gain insights into potential roles for these proteins and mutations. For instance, an increased but homogeneous delay in the generation of Wave I, that does not affect the amplitude of the waveform, can point to conductive hearing loss, where either the threshold of the ANFs have been elevated or an impairment in the outer ear which dampens the stimuli exists. Similarly, variable delays in action potentials will drive a desynchronization of the ANFs in response to sounds and can be observed in ABRs by reductions in Wave I amplitude in addition to increases in latency. Loss of hair cell

function or a reduction in spiral ganglion neuron (SGN) population would also manifest as a decrease in Wave I amplitude but would require further investigation to accurately diagnose. Often paired with ABR analysis are distortion-product otoacoustic emission (DPOAE), which are sounds generated within the cochlea due to nonlinear interaction between two stimulus tones of slightly different frequency (Gorga et al., 1997). This measurement is key in distinguishing if a loss in hearing sensitivity is primarily due to impairments within the IHC-ANF synapses or if amplification of the auditory stimuli, by the outer hair cells, is also impaired leading to reductions in Wave I amplitude or increased threshold levels. Thus, ABRs, when paired with DPOAEs, are a robust tool for the characterization of hearing impairments.

Organizers of the cochlear ribbon synapse.

Given the linearity of the PAC, with the cochlear ribbon synapses being the first instance of chemical signaling into the central nervous system, the importance of this synapse's development and functionality can easily be appreciated. Perturbations to cochlear ribbon synapse physiology or impairments in their formation or development can result in decreased sensitivity to auditory stimuli.

For instance, Bassoon mutants are known to lack membrane-anchored ribbons and spatially diffuse voltage gated calcium channels which together are believed to be responsible for impairments in the temporal precision of sound encoding. The loss of such a critical presynaptic protein has thus been attributed to deficits in synaptic transmission, reduction in presynaptic calcium currents and impairments in synchronous auditory signaling. Similarly, Strip2 has been recently shown to be critical for the innervation of inner hair cell afferent synapses, suggesting a potential cochlear neuropathy (Pisciottano et al., 2019). Strip2 KOs were observed to alter the

normal Ctbp2 ribbon localization gradient toward the modiolar side of the inner hair cell, relative to the wild-type mice ultimately effecting auditory function. The size and organization of the cochlear ribbons is critical in the encoding of auditory stimuli, in APC KOs for instance the size distribution of the ribbons is altered in the absence of a reduction of ribbon synapse number (Breitman et al., 2008; Tran et al., 2008, Hickman et al., 2015).

Although we are beginning to understand the role of critical synaptic organizers among ribbon synapse proteins, even less is known about elements of the postsynaptic membrane which may be acting independently or in union with presynaptic organizers. To note, it has been shown that prolonged deprivation of auditory input during the critical period in auditory development led to an increase in AMPAR subunit and Shank1 density which occurred almost a week prior to remodeling of ribbons. Suggesting a post synaptic influence of presynaptic ribbon elements through an understudied retrograde transsynaptic signaling pathway in the absence of auditory input.

Trans-Synaptic Adhesion Molecules in the context of Hearing

Neurexins (Nrxns), which are trans-synaptic adhesion ligands, and their postsynaptic receptors neuroligins (Nlgns) are widely studied in the context of central nervous system (CNS) synapses, where they have been shown to influence synaptic formation, maturation, and function of CNS neurons (Sudhof, 2008; 2017; Varoqueaux et al., 2006). In brief, there are three Nrxn genes, with two separate promoters that can transcribe either an α- (long) or β- (short) forms of the protein. Nrxns, additionally, undergo extensive alternative splicing at five splice sites resulting in thousands of Nrxn isoforms (Ullrich et al., 1995). Alternative splicing of Nrxns is

regionally regulated and altered by activity in neurons leading to a great deal of promiscuity with respect to Nrxn binding partners (Sudhof, 2017).

Neuroligins are regulated by alternative splicing as well, with Nlgn1 having an additional B splice site. Nlgn1 and Nlgn3 have conserved A1, A2 or A1/A2 inserts, with the neuroligin A inserts having little effect on interaction with Nrxn or MDGA protein domains(Bolliger et al., 2008; Comoletti et al., 2006; Oku et al., 2020). Given the large number of splicing isoforms in the neuroligin and neurexin families, it is widely believed that these complex interactions underlie the molecular and synaptic diversity observed within the CNS (Comoletti *et al.*, 2006; Nam and Chen, 2005; Ullrich *et al.*, 1995). Dimerization, which is present as either neuroligin homodimers or Nlgn1/3 heterodimers, is crucial for the trans-synaptic interactions of neuroligins with neurexins and some instances can prevent the inhibition of Nlgn/Nrxn interactions (Poulopoulos et al., 2012; Shipman and Nicoll, 2012; Yoshida et al., 2021). In particular, the interactions of Nlgn1 and Nlgn3 are known to localize and influence the maturation of excitatory synapses either in tandem or alone (Blundell et al., 2010; Chih et al., 2006; Etherton et al., 2011a; Etherton et al., 2011b; Gibson et al., 2009).

To date evidence linking Nlgn1 and Nlgn3 in AMPAR recruitment, diffusion rates throughout the postsynaptic membrane, in addition to driving reductions of evoked excitatory postsynaptic potentials (eEPSPs) and smaller postsynaptic densities (PSD) in single and double KOs is substantial (Chanda et al., 2017; Haas et al., 2018; Heine et al., 2008; Shipman et al., 2011). Given that AMPARs are primary drivers of synaptic transmission at the ribbon synapses, due to their fast activation kinetics, it is likely that any disturbance to their normal localization would result in functional deficits of the ribbon synapse (Glowatzki and Fuchs, 2002; Muller and

Barr-Gillespie, 2015). However, little is known regarding how neuroligins influence synaptic formation, maturation, and function of the cochlear ribbon synapses. While in its infancy, the study of potential candidates of transynaptic ribbon organizers may provide critical insights into not only how cochlear ribbon synapses form but also how they are maintained and preserved following insult.

What is Noise and How Does it Affects Us?

Noise is a term used in the study of hearing to describe any sound that has the potential to damage components of the PAC. Intense noise, typically greater than 115 dB SPL, results in direct mechanical trauma to the tissues of the inner ear, potentially ripping cells open as a result of the sheering force applied to the membranes (Henderson and Hamernik, 1995; Le Prell et al., 2007; Liberman and Dodds, 1984). Moderately intense noise, those above 105 dB SPL, will predominantly affect the organization of the stereocilia bundles, the presynaptic hair cell ribbons, and ANF terminals (Liberman, 2017). This degree of noise also reduces cochlear blood flow, ultimately triggering hair cell death through numerous signaling pathways (Cheng et al., 2005, Le Prell et al., 2007; Strimbu et al., 2019). Although not as immediately destructive, lower levels of prolonged noise exposure are also hazardous to hearing, primarily driving the loss of synaptic connections between inner hair cells and SGNs, causing cochlear synaptopathy. This prolonged exposure, in addition to imposing a high metabolic demand on many cochleae cell types, increasing the generation of reactive oxygen species and other free radical production, can lead to excitotoxicity further contributing to noise induced hearing loss (NIHL) (Le Prell et al., 2007; Lu et al., 2014; Maulucci et al., 2014).

NIHL is categorized based on the period of post-exposure where hearing is impaired (Liberman, 2016). Exposure to moderate noise levels (e.g. rock concerts or nightclubs) bring about an acute yet transient attenuation of hearing sensitivity, referred to as a temporary threshold shift (TTS), which decreases auditory sensitivity for a period of days to weeks. In contrast, more severe auditory insults result in a permanent threshold shift (PTS) leading to partial or complete sensorineural hearing loss. In laboratory settings, threshold shifts that fail to completely recover to baseline levels after more than 2 - 4 weeks following exposure are generally considered permanent in rodents (Kujawa and Liberman, 2006; Liberman, 2016; Ryan et al., 2016). Despite these clear physiological definitions, we lack a comprehensive understanding of the complex molecular mechanisms responsible for noise induced threshold elevation and the processes responsible for hearing threshold recovery.

What is a Proteome and How Does Proteomics Further Our Understanding of Hearing?

Proteomics, as the name suggests, is the systematic study of the abundance, diversity, and modifications to proteins within specific cells or organisms, collectively referred to as the proteome (Wang et al., 2022; Yates et al., 2000; Yates et al., 1997). The composition of the proteome is constantly being remodeled in response to changes in the environment. Within the cochlea we can take advantage of this principle to gain insights into mechanisms directly involved in hearing and noise exposures by comparing the measurable changes observed to the cochlear proteome both before and after manipulation.

However, robustly measuring minute changes within the cochlear proteome poses a unique challenge. The first is the small amount of protein that can be obtained from the digestion of cochlea, roughly 1-3µg compared to the milligrams of proteins obtained from brain lysates.

The second is the complexity of cochlear lysates making the investigation of low abundance proteins particularly challenging. Pooling cochlea from multiple mice is one strategy to overcome challenge of low starting material but this also reduces the chances of detecting low abundance proteins within the cochlear proteome (Hickox et al., 2017). This is because less than 10% of the cochlear proteome comes from proteins related to the ganglion or hair cells.

To enhance the detection of hair cell specific proteins in the past, we have taken advantage of fluorescence-activated cell sorting (FACS) to purify hair cells with which we were able to characterize the hair cell proteome (Hickox *et al.*, 2017) . The challenge of this strategy, however, lies in the demand for starting material, in one experiment alone we harvested hair cells from over 100 mice. This makes the addition of an experimental manipulation, such as noise, almost impossible to achieve due to variation within the sample preparation and noise exposure consistently across 100 animals. An alternative strategy is the purification of heavy labeled proteins of interest to be used as internal standards (Gouw et al., 2010). Under this paradigm we amend cochlear lysates with known concentrations of heavy isotopic labeled protein or peptides for analysis by mass spectrometry. The power of this strategy lies in the identical properties of the heavy and light peptides, making their elution from the liquid chromatography column nearly identical. By taking advantage of this, we can then detect the signal coming from the heavy peptides and analyze regions of interest during the acquisition window to detect the endogenous "light" peptides (Liu et al., 2019; Savas et al., 2016; Savas et al., 2012). Because we amended cochlear lysates of known quantities of heavy standards, by taking the ratio of heavy to light intensities we can then calculate the absolute abundance of the endogenous proteins.

While a powerful tool, the use of heavy standards can be an expensive endeavor and is selective to specific proteins of interest, limiting the conclusions we can draw to *a priori* hypotheses. To this extent, we have used metabolic labeling of entire mice as internal standards or the use of isobaric tandem mass tagging (TMT) to directly compare shifts of the entire cochlear proteome in response to a stimulus. Metabolic labeling is done by feeding mice with ^{15}N enriched chow, effectively labeling nearly the entire proteome. Metabolically labeled cochlear lysates can then be mixed with cochlear lysates that have received a manipulation, such as drug treatment or noise, and analyzed in tandem with mass spectrometry. Comparison of the ^{15}N to ^{14}N ratios of the measurable proteins then allows us to determine the proteome directed changes in response to our manipulation (Liu *et al.*, 2019; Savas *et al.*, 2012). The limitation of using metabolically labeled tissues, however, is the inability to compare multiple experimental conditions within the same analysis, which can lead to variations in data acquisition. To this extent, TMT-multiplexing, which allows us to directly compare changes to the proteome across up to 16 conditions or among 4 biological replicates across 4 independent conditions is an appealing alternative strategy (Raso et al., 2012; Rauniyar and Yates, 2014). By analyzing each condition in tandem there is considerably less variation between biological replicates. Changes to the proteome are then assessed based on the comparison of average peak intensity for each peptide among the respective channels. Where a reduction or increase in signal intensity compared to control conditions would be representative of either a down or upregulation of that protein (Hickox *et al.*, 2017). The major flaw of TMT labeling stems from the comparison of channel intensities making the labeling efficiency critical for the interpretation of these mass spectrometry results. In comparison to metabolic labeling, where more than 99% of the proteome is labeled, TMT will label up to 95% of all peptides leading to potential discrepancies when

comparing the results from ^{15}N and TMT based experiments. While both strategies are useful in comparing alterations to the cochlear proteome, consideration must be taken when deciding which strategy is most beneficial to the scientific question.

Chapter 2: Experimental Methods

Cochlear functional assays

Waveforms used for acoustic overexposure were designed using a waveform generator (Tucker-Davis Technologies, Alachua, FL) within the frequency range of 8-16 kHz for 30 min. Noise level intensity was delivered through an exponential horn extending from compression driver (JBL, 2446H/J, Northridge, CA). The mice randomly assigned to the noise exposure groups, and exposed to ambient (65 – 70, or 70 dB SPL), moderate (94 or 100 dB SPL), or severe (105 dB SPL), 0.0355 - 0.0632, 0.0632 1.00, 2.00, 3.55 Pa SIL respectively. Noise generation stability was monitored by PicoLog system (Picoscope 2000 series) and a calibrating microphone (PCP Piezotronics, NY).

ABRs and distortion product otoacoustic emission (DPOAE) were recorded in young adult mice (P50-60). Baseline hearing measurements were recorded from 7-8 week old animal and sequentially recorded 1, 7 and 14 days after noise exposure. ABR and DPOAE recordings were obtained by Tucker Davis Technologies (TDT) System III workstation running BioSigRP in a soundproof chamber (EcKel audiometric room, Cambridge, MA). ABR stimulus were pre-amplified with a 4-channel MEDUSA pre-amp and analyzed by a real-time processor in TDT system3.

Prior to electrode placement, subcutaneous platinum needle electrodes were placed at the vertex (recording) and ipsilateral mastoid (reference), with the ground electrode placed on the lower back, animals were anesthetized by intraperitoneal injection of Ketamine and Xylazine cocktails given at a dose of 100 mg/kg and 3 mg/kg body weight, respectively. The top-up injections (quarter of the original dose) were administered as needed. Animal body temperature

was maintained at 37–38°C by an electric heating pad (Homeothermic blanket system, Harvard Apparatus).

The amplitude of ABR Wave-I was estimated by measuring the voltage difference between the wave-I peak and the trough between Wave-I and Wave-II. ABR thresholds were defined as the lowest stimulus level (dB SPL) for which recognizable ABR waves could be observed with a Wave I amplitude of 200 μVs. Similarly, the duration of Wave-I was measured as the time between Wave-I peak to the trough. ABR click stimulus was set at 0.1 millisecond of click duration with the rate of 20 Hz. The stimulus intensities were ranged from 15 dB SPL to 80 dB SPL with 5 dB increment steps. Tone ABRs were established by 20 millisecond tone pips, ranging from 8-32 kHz with 4 kHz increments and presented from 20 to 80 dB SPL stimulus level with 10 dB step. An average of 500 stimuli presentations were displayed on a PC monitor during the experiments using operating software (BioSigRP, TDT).

DPOAE recording was verified by using Etymotic low noise microphone system ER-10B+. The stimulus consists of two primary pure-tone frequencies (f_1 and f_2) differing by a factor of 1.2. The L_1 and L_2 values were varied from 15 to 75 dB SPL ($L_1 > L_2$, 5 dB) in 5 dB step across the frequency from 8-32 kHz. The spectral magnitude of the two primaries, $2f_1 - f_2$ distortion product, and the noise floor will be determined from an averaging of 500 stimuli.

Noise exposures were delivered to anesthetized (Ketamine (100 mg/kg) and xylazine (3 mg/kg) or unanesthetized animals held within small wire cages in a custom-built sound-proof chamber designed by Charles Liberman (Mass. Eye and Ear). The box is constructed of 3/4" plywood sheets. The basic principle is that no two sides are parallel. The front and back panel are the same, except that the back is truncated at a height of 42'' (rather than 48'') and has no door.

This makes the top slanted with respect to the floor. The side panels are then cut to fit. The top panel has a rectangular hole cut in it to which an exponential horn and the acoustic driver are mounted.

Quantitative PCR

RNA was isolated from dissected cochleae of postnatal day 1 (P1), P6, P12, P30 and P60 mice using TRIzol and RNeasy Kit (Qiagen). RNA was reverse transcribed using Superscript III First-Strand cDNA synthesis kit (Invitrogen). Real-time PCR was performed with StepOnePlus Real-Time PCR system (Applied Biosystems) using Power SYBR Green Master Mix (Applied Biosystems). A total of 50 ng of cDNA was used for each reaction. Cycling parameters were as follows: 95°C for 10 min; 40 cycles of 95°C for 15 s, and 60°C for 60 s. A minimum of five biological replicates were used for each target. Primers were sourced from Qiagen (QuanTitect primer assays) and were reconstituted to 10μM concentrations. All datasets were normalized to individual *NeuN* CT values to measure differences in neuronal RNA prior to comparison to WT gene expression levels.

RNAseq and transcriptomic quantification

Total RNA from cochlea were extracted using Trizol as per the manufacturer's recommended protocol, and further purified via RNeasy Plus Mini kit (Qiagen). Purified RNA was sent to Novogene (Novogene Corporation Inc, Sacramento, CA) for QC, library preparation, sequencing, and quantitation as per the in-house standard protocol for gene expression analysis. RNA degradation and contamination was monitored on 1% agarose gels. RNA purity was determined by NanoPhotometer® spectrophotometer (IMPLEN, CA, USA). RNA integrity and

quantitation were assessed using the RNA Nano 6000 Assay Kit of the Bioanalyzer 2100 system (Agilent Technologies, CA, USA). The samples passing the QC step were then used for library preparation and sequencing.

One microgram of RNA per sample was used as starting material for sequencing library generation. NEBNext® UltraTM RNA.Library Prep Kit for Illumina® (NEB, USA) was used for library generation following manufacturer's recommendations and index codes were added to attribute sequences to each sample. Briefly, mRNA was purified from total RNA using poly-T oligo-attached magnetic beads. Fragmentation was carried out using divalent cations under elevated temperature in NEBNext First Strand Synthesis Reaction Buffer (5X). First strand cDNA was synthesized using random hexamer primer and M-MuLV Reverse Transcriptase (RNase H-). Second strand cDNA synthesis was subsequently performed using DNA Polymerase I and RNase H. Remaining overhangs were converted into blunt ends via exonuclease/polymerase activities. After adenylation of 3' ends of DNA fragments, NEBNext Adaptor with hairpin loop structure were ligated to prepare for hybridization. To select cDNA fragments of preferentially 150~200 bp in length, the library fragments were purified with AMPure XP system (Beckman Coulter, Beverly, USA). Then 3 μl USER Enzyme (NEB, USA) was used with size-selected, adaptor ligated cDNA at 37 °C for 15 min followed by 5 min at 95 °C before PCR. Then PCR was performed with Phusion High-Fidelity DNA polymerase, Universal PCR primers and Index (X) Primer. At last, PCR products were purified (AMPure XP system) and library quality was assessed on the Agilent Bioanalyzer 2100 system. The clustering of the index-coded samples was performed on a cBot Cluster Generation System using PE Cluster Kit cBot-HS (Illumina) according to the manufacturer's instructions. After cluster

generation, the library preparations were sequenced on an Illumina Novaseq6000 and paired-end (150 bp) reads were generated.

Raw data (raw reads) of FASTQ format were processed through fastp. In this step, clean data (clean reads) was obtained by removing reads containing either adapter or poly-N sequences and/or reads with low quality scores. At the same time, Q20, Q30 and GC content of the clean data were calculated. Reference genome and gene model annotation files were downloaded from genome website browser (NCBI/UCSC/Ensembl) directly. Indexes of the reference genome was built using STAR and paired-end clean reads were aligned to the reference genome using STAR (v2.5). STAR utilizes the Maximal Mappable Prefix (MMP) method which can generate a precise mapping result for junction reads. HTSeq (v0.6.1) was used to count the read numbers mapped to each gene.

Read count per transcript were used for further analysis with the iGEAK program, an interactive gene expression analysis kit using the R/shiny platform. Read counts were filtered to remove very low signals (i.e. we required a minimum read count = 8 in at least 4 samples). Data were normalized using edgeR's TMM (Trimmed Mean of M-values) normalization method. EdgeR method provides statistical routines for determining differential expression in digital gene expression data, and the resulting P values were adjusted using the Benjamini and Hochberg's approach for controlling the False Discovery Rate (FDR). Genes with an adjusted P-value < 0.05 and fold change > 1.5 found by edgeR were assigned as differentially expressed genes. Principal Component Analysis (PCA) plots, Correlation (Pearson correlation) plots, and Volcano plots were also created using iGEAK program.

RNAScope and CellProfiler Analysis

Mouse cochleae were harvested and dissected as described above. Cochlea were fixed in a 4% PFA solution for 1 hour prior to decalcification with Immunocal O/N then cryoprotected O/N in 30% sucrose buffer. Once saturated, cochlea were mounted in OCT and frozen O/N at -80°C. Cochlea were then sectioned in 12 µm slices and mounted onto frosted glass slides and stored at -80°C. Slides were washed 3 times in PBS at room temperature then sequentially dehydrated with 30%, 50%, 70%, and 100% EtOH at room temperature. Slides were then incubated in 3% hydrogen peroxide at room temperature for 10 min. Then treated with RNAscope Protease III for 15 mins at 40°C prior to rinsing three times in DEPC treated water. RNAScope probes were prewarmed at 40 °C in the water bath for 10 min to dissolve precipitation. Afterwards the probes were cooled down to room temperature prior to mixing the target probes of C1, C2, and C3 in a 1.5 mL tube in a 50:1:1 ratio with a final volume of 50 µL per sample. Slides were then incubated with probe mix solution at 40 °C for 2 hours in the HybEZ™ Oven. Each channel was then amplified and hybridized to a fluorophore per manufacturer's instructions prior to staining with DAPI. Images were captured with confocal laser scanning microscopy (Leica DMI4000) with identical settings.

The maximum-intensity projection from each image stack was then filtered to remove any nuclei smaller than 7 µm in diameter or had a width that was less than a third of its length to remove supporting cells within the spiral ganglion from analysis. Resulting images were then imported into CellProfiler for further processing. Important steps in our pipeline identified the outlines of each nucleus and expanded this area 10 pixels in each direction to represent the area of the cell body. Nlgn1 and Nlgn3 were then independently overlaid onto the cell mask regions

to determine cells which express either Nlgn1 or Nlgn3. Sequential masks were then created to determine which cells express both neuroligins and which cells express only Nlgn1 or Nlgn3.

Metabolic labeling of the cochlea with ^{15}N mouse chow

12 FVB mice were metabolically labeled with ^{15}N-rich, Spirulina-based diet (Cambridge Isotopes and Harlan Laboratories) for two generations as we have previously described (Butko et al., 2013). The second generation "heavy" mice were maintained on the ^{15}N-rich, Spirulina-based diet until P40-50 at which time the cochlea were harvested and stored at -80˚C until homogenization and pooling. The ^{15}N protein enrichment was determined to be greater than 95% in the brain (MacCoss et al., 2003).

Preparation of cochlear extracts for ^{15}N based quantitation

FVB mice were randomly assigned into 5 groups (4 mice per group), ^{15}N heavy labeled control, and 4 experimental groups of normal ^{14}N diet (0 dB, 70 dB, 100 dB and 105 dB). Mice were sacrificed and the cochlea was immediately dissected from temporal bones and the bony/cartilaginous capsule and vestibular sensory organs (organ of Corti, utricular and saccular maculae, and semicircular canal ampullae) were removed by microdissection in less than ten minutes after the end of noise exposure and euthanasia. The extracts were homogenized in 4 mM HEPES, 0.32 M sucrose, that was amended with protease inhibitors.

The ^{14}N cochlear homogenate was then mixed 1:1 with ^{15}N homogenate and centrifuged at 1,000 × g for 10 min (4 °C). The pellet was discarded, and supernatant was subsequently centrifuged at 10,000 × g for 15 min (4 °C) to collect the crude protein pellet used for mass spectrometry. Protein concentration was verified, and 8 M urea was added. 100 μg of extracted

protein was taken from each sample and subsequently processed with ProteasMAX (Promega) according to manufacturer's instructions. Disulfides within the samples were selectively reduced by 5 mM Tris (2 carboxyethyl) phosphine at room temperature for 20 min, alkylated in the dark by 10 mM iodoacetamide (IAA) for 20 min, and trypsinized (Sequencing Grade Modified Trypsin, Promega) overnight at 37 °C, trypsinization was quenched by acidification.

Preparation of cochlear extracts for TMT based quantitation

FVB mice were randomly assigned to 94 dB or 105 dB noise exposure groups. Cochleae were collected either immediately or 2 weeks after noise exposure. Animals were euthanized and the cochlea was micro dissected as described prior to further homogenization via Precellys 24 (Bertin Technology, Rockville, MD) in Syn-PER (Thermo Scientific) lysis buffer amended with protease inhibitor cocktail. Protein was separated from impurities and lipids by methanol-chloroform precipitation prior to resuspension in 6M guanidine in (50 mM HEPES). Proteins were further processed via the reduction of disulfide bonds with DTT, and alkylation of cysteine residues with iodoacetamide. Proteins were then digested for 3 h with 2 µg of endoproteinase LysC (Promega) and subsequently digested overnight with 2 µg of Trypsin (Pierce). The digest was then acidified with formic acid to a pH of ~2–4 and desalted by using C18 HyperSep cartridges. The eluted peptide solution was completely dried before verifying the concentration by microBCA assay (Thermo Scientific, Rockford, IL).

Equal concentration of peptide (~100 µg) from each sample was then used for isobaric tandem mass tag (TMT) labeling. TMT-10 or 15plex labeling on peptide samples were performed according to the manufacturer's instructions (ThermoFisher Scientific). After 2 h incubation at room temperature, the reaction was quenched with hydroxylamine at a final

concentration of 0.3% (v/v). Isobaric labeled samples were then combined 1:1:1:1:1:1:1:1:1:1 or combined 1:1:1:1:1:1:1:1:1:1:1:1:1:1:1:1 and lyophilized. The combined isobaric labeled peptide samples were then fractionated by Hypersep SCX SPE column and eluted by the following gradient concentrations of NH_4AcO: 20 mM, 50 mM, 100 mM, 500 mM, 1,000 mM and 2,000 mM. Fractionated samples were then desalted by loose resin tips (ImcsTipS, RP-20mg) and the concentration was again determined by Micro BCA. Peptide solutions were dried, stored at −80 °C, and reconstituted in LC-MS buffer A (5% acetonitrile, 0.125% formic acid) until LC-MS/MS analysis.

Nanoflow LC with multinotch MS2/MS3 Orbitrap Fusion MS analysis

Three micrograms from each fraction were loaded for LC-MS analysis using a Thermo Orbitrap Fusion coupled to a Thermo EASY nLC-1200 UPLC pump and vented Acclaim Pepmap 100, 75 μm × 2 cm nanoViper trap column and nanoViper analytical column (Thermo—164570), 3 μm, 100 Å, C18, 0.075 mm, 500 mm with stainless steel emitter tip assembled on the Nanospray Flex Ion Source with a spray voltage of 2000V. The chromatographic run was performed by 4 h gradient beginning with 100% buffer A (5% acetonitrile, 0.125% formic acid), 0% B (95% acetonitrile, 0.125% formic acid) and increased to 7% B over 5 mins, then to 25% B over 160 mins, 36% B over 40 mins, 45% B over 10 mins, 95% B over 10 mins, and held at 95% B for 15 mins before terminating the scan. Multinotch MS3 method (McAlister et al., 2014) was programmed as the following parameter: Ion transfer tube temp = 300 °C, Easy-IC internal mass calibration, default charge state = 2 and cycle time = 3 s. MS1 detector set to orbitrap with 60 K resolution, wide quad isolation, mass range = normal, scan range = 300–1800 m/z, max injection time = 50 ms, AGC target = 2×10^5, microscans = 1, RF lens = 60%, without source

fragmentation, and datatype = positive and centroid. Monoisotopic precursor selection was set to included charge states 2–7 and reject unassigned. Dynamic exclusion was allowed $n = 1$ exclusion for 60 s with 10ppm tolerance for high and low. An intensity threshold was set to 5×10^3. Precursor selection decision = most intense, top speed, 3 s. MS2 settings include isolation window = 0.7, scan range = auto normal, collision energy = 35% CID, scan rate = turbo, max injection time = 50 ms, AGC target = 1×10^4, $Q = 0.25$. In MS3, the top ten precursor peptides were selected for analysis were then fragmented using 65% HCD before orbitrap detection. A precursor selection range of 400–1200 m/z was chosen with mass range tolerance. An exclusion mass width was set to 18 ppm on the low and 5 ppm on the high. Isobaric tag loss exclusion was set to TMT reagent. Additional MS3 settings include an isolation window = 2, orbitrap resolution = 60 K, scan range = 120 – 500 m/z, AGC target = $1*10^4$, max injection time = 120 ms, microscans = 1, and datatype = profile.

Absolute quantitation of peptide / protein abundance

Synthetic peptides were synthesized containing a single heavy C-terminal arginine residue (JPT Peptide Technologies GmbH, Berlin, Germany). SpikeTide TQL peptides were quantified using a proprietary Quanti-Tag. Peptides are released from tag by trypic digestion and aliquoted at nM. These peptides were spiked (0.5 nM) into cochlear peptide mixtures from three independent biological replicates (prepared as described above) each exposed to 70 dB SPL, 94 dB SPL, and 105 dB SPL and purified with C18 Ziptips. The purified peptide concentrated using a SpeedVac vacuum concentrator (Labconco Inc.), and analyzed by shotgun LC-MS/MS with a 2 or 4 hour analysis runs with an Orbitrap Fusion MS as described above. The resulting spectra was extracted, searched, and quantified as described below with Prolucid/Sequest DTASelect

and Census. We used the reconstructed MS1 chromatograms (relative area under the curves) to determine the absolute peptide quantities.

Analysis of tandem mass spectra

The Integrated Proteomics Pipeline - IP2 (Integrated Proteomics Applications, Inc., www.integratedproteomics.com/) was used to analyze the proteomic results with ProLuCID, DTASelect2, Census, and QuantCompare. Spectrum raw files were extracted into ms1 and ms2 files by using RawExtract 1.9.9 software (http://fields.scripps.edu/downloads.php) (McDonald et al., 2004). Tandem mass spectra were searched against the European Bioinformatic Institute (IPI) mouse protein database (www.ebi.ac.uk/IPI/IPImouse.html). The target/decoy database containing the reversed sequences of all proteins was used to accurately determine peptide probabilities and FDRs (Peng et al., 2003a). ProLuCID searches on an Intel Xeon cluster was used to match tandem mass spectra to peptide sequences with 50 ppm peptide mass tolerance for precursor ions and 400 ppm for fragment ions (Xu et al., 2015). The search space included fully and half-tryptic peptide candidates that matched within the mass tolerance criteria with no miscleavage constraint. Carbamidomethylation (+57.02146 Da) of cysteine was considered as a static modification. DTASelect was used to access validity of peptide/spectrum matches (PSMs) (Cociorva et al., 2007; Tabb et al., 2002) by using two SEQUEST-defined parameters (Eng et al., 1994), the cross-correlation score (XCorr), and normalized difference in cross-correlation scores (DeltaCN).

The search results were grouped by charge state (+1, +2, +3, and greater than +3) and tryptic status (fully tryptic, half-tryptic, and nontryptic), resulting in 12 distinct subgroups. The distribution of Xcorr, DeltaCN, and DeltaMass values for (a) direct and (b) decoy database PSMs

in each of these subgroups, was obtained. The direct and decoy subsets were then separated by discriminant analysis. Peptide match probabilities were calculated based on a nonparametric fit of the direct and decoy score distributions. The minimum threshold peptide confidence was set at 0.95. The FDR was then determined as the percentage of reverse decoy PSMs among all the PSMs which passed the confidence threshold. The minimum of one peptide was required for each protein identification, this peptide had to be an excellent match with an FDR less than 0.001 and at least one excellent peptide match. The quantified proteins which FDRs below 1% were estimated for each sample analysis.

For the ^{14}N / ^{15}N analysis, each of protein data set was searched twice in the light and heavy protein SEQUEST databases, respectively. The search results were then filtered using DTASelect2 and ion chromatograms were generated using an updated version of a program previously written in our laboratory (MacCoss *et al.*, 2003). This software, called "Census", is available from the authors for individual use and evaluation through an Institutional Software Transfer Agreement (see http:// fields.scripps.edu/census for details) (Park et al., 2008). First, the elemental compositions and corresponding isotopic distributions for both the unlabeled and labeled peptides were calculated. This information was then used to set an appropriate m/z range from extracted ion intensities, which included all isotopes greater than 5% of the calculated isotope cluster base peak abundance. MS1 files were used to generate chromatograms from the m/z range surrounding both the unlabeled and labeled precursor peptides. Census calculates peptide ion intensity ratios for each pair of extracted ion chromatograms. The linear least-squares correlation was used to calculate the ratio (i.e., slope of the line) and closeness of fit [i.e., correlation coefficient (r)] between the data points of the unlabeled and labeled ion

chromatograms. Finally, QuantCompare was used to analyze protein ratios which represent by log two-fold change and ANOVA p-value with BH correction to identify significant quantified proteins.

For TMT, the raw spectral raw files were extracted into MS1, MS2, and MS3 files using the in-house program RawConverter (He et al., 2015). Spectral files were then pooled from fractions for each sample and searched against the Uniprot mouse protein database and matched to sequences using the ProLuCID/SEQUEST algorithm (ProLuCID ver. 3.1) with 50 p.p.m. peptide mass tolerance for precursor ions and 600 p.p.m. for fragment ions. Fully and half-tryptic peptide candidates were included in search space, all that fell within the mass tolerance window with no miscleavage constraint, assembled and filtered with DTASelect2 (ver. 2.1.3) through the Integrated Proteomics Pipeline (IP2 v.5.0.1, Integrated Proteomics Applications, Inc., CA, USA). Static modifications at 57.02146 C and 229.162932 K and N-term were included. The target-decoy strategy was used to verify peptide probabilities and false discovery ratios (Elias and Gygi, 2007). Minimum peptide length of five was set for the process of each protein identification. Each dataset had an 1% FDR rate at the protein level based on the target-decoy strategy. Isobaric labeling analysis was established with Census 2 as previously described (Park et al., 2014). TMT channels were normalized by dividing it over the sum of all channels. No intensity threshold was applied. The fold change was then calculated as the mean of the experimental group standardized values. *p*-values were then calculated by Student's *t*-test with the B.H. adjustment.

Bioinformatic analysis with PATHER AND STRING

Protein ontologies were investigated with the protein analysis through evolutionary relationships (PANTHER) system (http://www.pantherdb.org), in complete cellular component and complete molecular function categories (Mi et al., 2016; Mi et al., 2013). The statistical overrepresentation test was calculated by using the significant proteins from each individual noise exposure experiment as the query and the aggregated total proteins identified in all three noise exposure conditions as the reference. Protein ontologies with Fisher statistical tests with false discovery rate (FRD) correction less than 0.05 were considered significant.

The Search Tool for the Retrieval of Interacting Genes (STRING) database was used to determine protein-protein interaction from significant quantified protein which found in each noise exposure condition. The STRING resource is available at http:// string-db.org (Szklarczyk et al., 2017). The corresponding protein–protein interaction networks were constructed with highest confidence of interaction score at 0.9.

Heat maps, clustering and volcano plots for the recovery period

Reporter ion intensity from the MS/MS analysis were analyzed using NCI-BRB ArrayTool software. The data was normalized using quantile normalization and differentially expressed (DE) proteins were selected based on univariate T-test with a p-value cut off 0.05 and minimum fold change on 1.5. The selected DE proteins were used to create heatmaps using the "Dynamic Heatmap Viewer" module implemented in the ArrayTool using default parameters, distance metrics of one-minus correlation and average linkage. Volcano plots were created in the

R statistical program using ggplot2 with $\log_2$ fold change on the x-axis and $-\log_{10}$ p-value on the y-axis.

TUBE pulldown western blot

Mice were randomly assigned to either the ambient, moderate, or severe noise exposure group (5 mice per group) and exposed for 30 minutes prior to the harvesting of cochlea. Cochlea from each group were then pooled respectively (total of 10 cochleae per noise exposure group) prior to homogenization via Precellys 24 in modified lysis buffer: 50 mM Tris-HCl (pH 7.5), 0.15 M NaCl, 1 mM EDTA, 1% NP-40, 10% glycerol, Ub/Ub protease inhibitors, PR-619 and 1,10-phenanthroline (o-PA). Protein concentrations were measured via micro BCA and 1.0 mg of cochlear homogenate were used for the isolation of polyubiquitylated proteins via Magnetic beads coated with Tandem Ubiquitin Binding Entities (TUBEs). Briefly, 100 µl of beads were washed with TBST and then incubated with cochlear homogenates at 4^{o}C for 4 hours. After binding, protein homogenate was removed from the beads, and the beads were washed three times with TBST. Bound ubiquitinated proteins were eluted by boiling the beads in 100 µl of SDS prior to incubation of supernatant in reducing sample buffer for 5 minutes. This solution was then centrifuged at 13,000xg for 5 minutes at 4^{o}C, 40 µl of each sample was then loaded into a 5-15% tris gel in addition to input and positive control (10.0 µl of MG132 treated HEK293T cell lysate). Following gel electrophoresis, the proteins were transferred to nitrocellulose via wet transfer method in transfer buffer with 0.02% SDS. The blots were blocked with 15 ml of 1X sigma block for 2 hours, and then incubated with primary antibody, 1:1000 anti-Ubiquitin Antibody (P4D1, sc-8017), overnight at 4^{o}C. Blots were washed three times with TBST, and then incubated with anti-mouse IgGHRP (1:5000) for 1 hour at room temperature.

Blots were washed three times with TBST, and the immune reaction was then assed using ECL, and imaged via Chemi doc gel imaging system (Bio-rad).

diGly analysis of protein ubiquitination

Mice were exposed to Noise and cochlea were harvested as described above (5 mice per condition). Cochlea were pooled (10 cochleae per condition) and soluble protein was extracted using Urea cell lysis buffer containing 20 mM HEPES (pH 8.0), 9 M Urea, 1mM Sodium orthovandate, 2.5 mM sodium pyrophosphate,1 mM β-glycerophosphate and homogenized by Percellys. Cochlear lysates were then further homogenized via needle sonication, lysates were then incubated on ice for 10 minutes prior to centrifugation at 10,000 x g for 10 minutes. Supernatant was then collected and digested for diGly peptide capture with PTMScan Ubiquitin Remnant Motif Kit (cat# 5562, Cell Signaling technology, USA) as per recommended protocol. Briefly, cochlear lysates were reduced with 5 mM DTT and alkylated with idoacetaminde solution. Urea concentration was reduced via the addition of 20 mM HEPES to a final concentration of 2 M Urea prior to protein digestion with LysC overnight at 37°C. The following day, trypsin was added at a concentration of 2 µg /100 µg and incubated overnight at 37°C. Peptides were then desalted and purified using Hypersep columns and dried down. 400 µg of purified peptides were then solubilized in 1.4 ml of Immunoaffinity Purification buffer (IAP). DiGly bead slurry was washed four times with PBS and added to the solubilized peptide solutions for overnight incubation at 4°C with end over end rotation. Beads were separated from supernatant by centrifugation and washed one time with IAP buffer and then three times with chilled DI water. Bound peptides were eluted from the beads by incubating with 40 µl of 0.15% TFA for 10 min at room temperature, this was repeated once and both elutions were

pooled. Eluted diGly peptides were desalted using spin columns and dried. Dried peptides were resolubilized in MS loading buffer contain 5% acetonitrile and 0.1% TFA and injected for MS/MS analysis.

Immunofluorescence with confocal microscopy analysis

Immediately following noise exposure, if performed, mice were anesthetized and cochleae were collected. Oval and round windows were punctured and a small hole was created near the apex of the cochleae for perfusion with 4% paraformaldehyde for 3 hours at 4°C. For the mid-modiolar sections, Cochleae were decalcified in Immunocal (Decal Chemical Corporation, Congers, NY) for 8 hours prior to cryoprotection for 2 days in 30% sucrose. Cochleae were mounted in OCT and sectioned at 12 µm for IF. Slides were rinsed three times in PBS at room temperature followed by blocking in 20% NHS 0.5% Triton-X (Cat# 1086431000, Millipore) for 1 hour at room temperature prior to primary antibody incubation (see below).

For cochlea whole mount, cochleae were decalcified in Immunocal (Decal Chemical Corporation, Congers, NY) overnight at 4°C or until cochleae became translucent. The decalcified bone, lateral wall, Reissner's membrane and tectorial membranes were dissected away from the organ of Corti. Whole mounted cochlea were then sectioned into 4 pieces and cryoprotected in 30% sucrose for 30 minutes prior to freezing on dry ice. The frozen pieces were then thawed and rinsed three times in PBS for 10 minutes at room temperature with agitation. Cochlear sections were then blocked for 1 hour in 20% NHS 1% Triton-X blocking buffer at room temperature.

Primary antibodies were diluted in blocking buffer as follows: Recombinant Anti-ARPC2 antibody (1:100, Abcam, ab133315), Human gp96/HSP90B1 90b1 (1:200, R&D Systems, MAB7606, 816803), CtBP2 (1:200, SCBT, RRID: AB_2086774), GluA2 (1:100, Millipore, MAB397, RRID:AB_2113875), Anti-LTBP4 antibody (1:100, Abcam, ab222844), Myosin-V11A (1:500, Proteus Bioscience, 25-6790, RRID:AB_1001525), Neurofilament H (1:1000, Synaptic Systems, 171 106,), Nlgn1 (1:100, R&D, AF4340), and Nlgn3 (1:100, Novus, NBP1-90080)COL9A1 Polyclonal Antibody (1:100, Invitrogen, PA5-93062), PSMC5 (1:200, Cell Signaling, 13392S), VCP (1:200, Abcam, ab111740), UBA2 (1:200, Cell Signaling, 5293) and incubated overnight at 4°C for sections and at 37°C for whole mounts. Following primary antibody incubation slides were rinsed three times with PBS for 15 minutes at room temperature. Slides were incubated in secondary antibody: 1:500 Goat Anti-Mouse IgG H&L (Alexa Fluor® 488, Abcam, ab150113), 1:500 Goat Anti-Rabbit IgG H&L (Alexa Fluor® 568, Abcam, ab150088), 1:50 Alexa Fluor™ 647 Phalloidin (Thermo Fisher, A22287) 1:1000 Goat Anti-Mouse IgG2a Cross-Adsorbed Secondary Antibody (Alexa Fluor® 488, Invitrogen, A-21131), and 1:1000 Goat Anti-Mouse IgG1 Cross-Adsorbed Secondary Antibody (Alexa Fluor® 568, Invitrogen, A-21124), Goat Anti-Rabbit H&L (1:250, Alexa Fluor® 647, Abcam, A27040), Donkey Anti-Sheep H&L (1:250, Alexa Fluor® 647, Abcam, ab150179), Donkey Anti-Sheep H&L (1:250, Alexa Fluor® 405, Abcam, ab175676) for three hours at room temperate. Slides were then rinsed three times in PBS for 15 minutes and stained with DAPI Staining Solution (Abcam, ab228549) for 5 minutes prior to mounting in Fluoromount-G (Thermo Scientific, cat. 00-4958-02). Tissues were counterstained with DAPI nucleic acid stain and/or Alexa Fluor-conjugated phalloidin actin stain. Images were captured with confocal laser scanning microscopy

(Leica DMI4000) with identical settings. Images were cropped and the brightness contrast was adjusted with ImageJ software using constant settings.

Quantification of synapse density, volume, and diversity

Images were captured with confocal laser scanning microscopy (Leica DMI4000) with identical settings. Cochlear pieces were measured from base to apex and regions corresponding to the 9-12, 12-16 and 24-28 kHz regions of the cochlea were captured for synapse density measurements. Images were cropped and the brightness contrast was adjusted with ImageJ software using constant settings. Areas in which presynaptic CtBP2 puncta overlapped with postsynaptic GluR2 puncta were then counted as a single synapse.

Synaptic coordinates and volumes were obtained from confocal stacks after deconvolution with the AMIRA FEI software suite and processing in MATLAB. Images were imported into AMIRA and islands larger than 5 pixels were removed prior to analysis. Synaptic volumes were acquired by measuring the intersection of CtBP2 and GluA2 puncta in 3-demenstional space. 3D image analysis recorded coordinates of ribbon puncta (anti-CtBP2) overlaid onto either anti-Nlgn1 or anti-Nlgn3 puncta which were then rotated using matrix transformation and centered onto the zero coordinate to orient all data points onto the same plane, only data for paired structures is presented.

To obtain positional information for paired ribbon synapses, we adapted methods previously described (Gilels et al., 2013). In brief, to analyze the distribution of synapses along the pillar-modiolar axis, rotated datasets were oriented into a cross-sectional quadrant plane representing the pillar-modiolar axis (x-axis) and basal-apical axis (z-axis) in MATLAB (N = 5

mice, 75 inner hair cells, 1306 synapses). The midpoints of both axes for each tissue sample were aligned to normalize these positions with the other data stacks of the same genotype before analysis. The population clusters were chosen using the implemented Bayesian information criterion and were constrained to the 90% quantile with two possible population clusters for each dataset.

Synapses containing only Nlgn1, only Nlgn3, or both neuroligins were then segregated and plotted for visual comparison of spatial distributions along the pillar to modiolar face of the inner hair cell. Synapses were then divided into pillar and modiolar groups based on their distance from the center point of the Z axis for comparison of spatial distributions of Nlgn1 and Nlgn3. Percentages were taken as the proportion of synapses for each group (i.e. Nlgn1 only) on either the pillar or modiolar face over the total measured synapses for that group.

Synapse distance quantification

For each image of synapse markers CtBP2 and GluA2, the two channels were separated and segmented individually using Ilastik pixel classification (Berg et al., 2019), yielding a three-dimensional segmentation of each. Within each channel, the intensity-weighted centroids of each segmented object were first found, and then the centroid-to-centroid distances between all possible CtBP2 and GluA2 pairs were calculated. For each CtBP2 punctum, the nearest GluA2 punctum was identified. The opposite was also done, generating a list the nearest CtBP2 punctum to each GluA2 punctum. Only puncta paired as nearest neighbors on both lists were classified as paired synapses. Pairs existing on only one list were discarded as mismatched lone puncta.

SEM analysis

FVB mice were euthanized and perfused with ice cold 4% paraformaldehyde in 0.1 M sodium cacodylate, pH 7.4 until exsanguinated immediately following noise exposure. All buffers were prepared and filtered using PES 0.22 micron syringe filters (Sterlitech,Kent, WA). The cochlea were then micro dissected as described above, apex was perforated and both round and oval windows were punctured. Prepared cochlea were then incubated at 4°C in 4% paraformaldehyde in 0.1 M sodium cacodylate (pH 7.4) overnight with end over end rotation. Cochlea was decalcified in 0.1 M sodium cacodylate (pH 7.4) amended with Immunocal (Decal Chemical Corporation, Congers, NY) for three hours at room temperature. Decalcified bone and tectorial membrane were then removed from the cochlea prior to overnight incubation in 2.5% glutaraldehyde in 0.1 M sodium cacodylate (pH 7.4) overnight at 4°C with agitation. Prepared specimens were then rinsed three times with 0.1 M sodium cacodylate (pH 7.4) for 30 minutes at room temperature prior to 45-minute wash with filtered HPLC grade water. Samples were dried using a Samdri-795 critical point dryer (Tousimis Research Corp, Rockville, MD) following a graded ethanol series to prevent structural damage during imaging. The dried samples were then mounted on aluminum stubs and coated with 15 nm of osmium using a SPI Filgen Osmium Coater (SPI, West Chester, PA). Scanning electron microscope imaging was performed at 3 kV on the JEOL 7900FLV high resolution microscope in the NUANCE Facility at Northwestern University. Images were taken at 2500X and 4500X magnifications for quantification of altered stereocilia morphology.

Western blot analysis

Cochlea extracts were homogenized in Syn-PER buffer (Thermo Scientific, cat. 87793) amended with 1% Triton-X (Sigma-Aldrich, cat. T8787) and 0.5% SDS by Percellys 24 (Bertin, cat. P000669-PR240-A) with three 30 second pulses at 6800 rpm at room temperature. Lysates were then incubated on ice for 10 minutes prior to needle sonication, QSonica Q700 Sonicator (M2 Scientifics, cat Q700), with amplitude set to 20 for 30 seconds. Lysates were then incubated on ice for 30 minutes, followed by centrifugation for 5 minutes at 10,000 X G at 4°C. Supernatants were collected, and protein concentrations were measured with Pierce™ BCA protein assay (Thermo Scientific, cat. 23225). Twenty-five micrograms of cochlear lysates were then amended with 6X Loading Buffer and boiled at 100°C for 5 minutes and immediately run on 4-15% gradient mini Protean TGX gel (Bio-Rad) and transferred to nitrocellulose membrane using Bio-Rad Trans-Blot Turbo transfer system (1.3A -25V-10 minute). Membranes were blocked with 1X Casein blocking solution (Sigma, cat. B6429) for two hours at room temperature and incubated with primary antibody (1:1000) overnight at 4°C. Membranes were washed three times with TBST and incubated with an anti-rabbit IgG-HRP secondary antibody (1:5000, Cell Signal, Cat. 7074S) for an hour at room temperature. Immune reaction on the membranes is captured by incubating with SuperSignal West Femto chemiluminescent substrates (Thermo cat# 34096) and imaged using the Chemidoc imaging system, Bio-Rad. Primary antibodies used for western blot were ARPC2 (Abcam, ab133315), TRIP (Cell signal, cat.13392S) and GAPDH (Abcam, ab181602).

Quantification and statistical analysis

Statistical analyses were performed using Excel (Microsoft, Seattle, WA) and GraphPad Prism. All values in figures with error bars are presented as either the mean $\pm$ SEM or $\pm$ SD.

Comparisons of averaged data were performed using the one-way ANOVA for three categories and the paired or unpaired Student's t-test (as indicated) for two categories. Tests with multiple measures at multiple points (i.e. ABR thresholds, DPOAE thresholds, and wave I amplitude) were compared by one-way ANOVA with comparative p-values between genotypes adjusted to correct for multiple comparisons using Tukey's method. P values <0.05 were considered statistically significant. Multiple test correction was performed with the Benjamini-Hochberg correction or FDR strategies as indicated. Measured synapse volumes were normalized to the median value recorded in each respective image dataset and tested for the probability of Gaussian or log normal distributions. Outliers were then identified utilizing the ROUT method in Prism based on linear regression with a false discovery rate (FDR) of 1% in each respective dataset prior to analysis by one-way ANOVA with Benjamini-Hochberg correction of 0.01.

Animal experiments

All animal experiments were conducted according to Northwestern University Institutional Animal Care and Use Committee (IACUC), Northwestern University IACUC (approved protocol numbers IS00001182). For euthanasia, pups were immediately decapitated, and adult animals were euthanized by isoflurane overdose and decapitation. In all studies, mice of both sexes were used in equal numbers.

Chapter 3: Neuroligins and Neurexins among the Cochlear Ribbon Synapses

Introduction

Chemical synapses in the central nervous system represent the most basic functional units of neuronal communication, and information processing. Since the initial discovery of long-term potentiation by Hebb in 1949, numerous protein factors and mechanisms have been discovered that influence the activities of neurons, one such group of proteins are synoptically localized cell adhesion molecules (SAMs) (Sudhof, 2017). The most well understood group of SAMs are the presynaptic neurexins (Nrxns) and their postsynaptic receptors, neuroligins (Nlgns). Neuroligins and neurexins are both single pass transmembrane proteins with long extracellular domains which interact with each other to form trans-synaptic complexes (Lise and El-Husseini, 2006). The expression of either neuroligin or neurexin is sufficient for the formation of hemi-synapses but require the formation of dimer pairs to interact in trans (Poulopoulos *et al.*, 2012; Scheiffele et al., 2000; Shipman and Nicoll, 2012). While it is generally agreed that different combinations of neurexins and neuroligins contribute to the specification of inhibitory and excitatory synapses, the detailed mechanisms by which these proteins influence synaptic transmission in mature neurons remains elusive (Craig and Kang, 2007; Sudhof, 2008; 2017; Varoqueaux *et al.*, 2006). Emerging evidence shows that Nlgn1 and Nlgn3 play partially overlapping roles in the maturation of glutamatergic synapses, even existing as heterodimers with unique binding affinities (Chanda *et al.*, 2017; Poulopoulos *et al.*, 2012; Shipman *et al.*, 2011).

Given the intimate interactions of Nlgn1 and Nlgn3, it can be appreciated the challenges associated with differentiating the roles of these proteins among excitatory synapses. Specific roles are further clouded by conflicting *in vivo* and *in vitro* findings, which likely stem from artificial interactions driven by overexpression and mis-localization (Chanda *et al.*, 2017;

Sudhof, 2008; 2017; Varoqueaux *et al.*, 2006). The artificial oversimplification of the physiological conditions and neuronal circuits *in vitro* is also a likely source of variance. Thus unique properties of the cochlear ribbon synapses lend themselves toward the characterization of synaptic proteins *in vivo*, due to the lack of efferent innervation, as the system is relatively isolated with direct functional readouts readily available.

Early in my graduate career I worked to characterize the cochlear proteome and identified Nlgn3 as a predominant synaptic adhesion protein within the cochlea (Hickox *et al.*, 2017). Moreover, *Nrxn* transcripts have been detected in transcriptomic studies of purified hair cells (Cai et al., 2015; Scheffer et al., 2015). However, given that hair cells are exclusively presynaptic, finding Nlgn3 within the purified hair cell was perplexing (Hickox *et al.*, 2017). Our initial finding of Nlgn3 within a population of FACS purified hair cells, thus, raises two possibilities: (1) that *Nlgn3* is expressed by the hair cells within the PAC, making it one of the few instances where neuroligins are present pre-synaptically or (2) Nlgn3 may have been identified as the result of a co-purification of an ANF postsynaptic density (PSD), which remained attached to the face of a hair cell during the purification process. Given that not much is known regarding how neuroligins contribute to the physiology of the cochlear ribbon synapses, much less where within the cochlea these proteins localize, further investigation was required.

In this chapter, I determined that both Nlgn1 and Nlgn3 are expressed by the spiral ganglion neurons and localize to roughly 85% of all cochlear ribbon synapses. Furthermore, in characterizing the localization patterns of both Nlgn1 and Nlgn3, I find evidence for cochlear ribbon synapses preferentially containing either Nlgn1 or Nlgn3. Lastly, I report that Nlgn3

expression gradually increases within the cochlea throughout postnatal maturation and that neither Nlgn1 nor Nlgn3 are necessary for the formation of ribbon synapses during development. These results provide the first characterization of neuroligins among cochlear ribbon synapses and support future investigations into the functional impact of these proteins with respect to cochlear ribbon function.

Results

Neuroligins are Primarily Expressed by Cochlear Spiral Ganglion Neurons.

Analysis of the cochlear transcriptome and proteome have established that neuroligins are present within the cochlear, however, we currently lack the resolution of which cell express these genes and where the resulting protein is localized. Therefore, a necessary first step into characterizing neuroligins within the cochlea was to first determine which cells within the cochlea express neuroligins. For this characterization I exclusively focused on both *Nlgn1* and *Nlgn3* as both of these proteins are known to localize to glutamatergic synapses and so would be expected to be present among the cochlear ribbon synapses (Budreck and Scheiffele, 2007; Scheiffele *et al.*, 2000; Song et al., 1999). I choose not to explore *Nlgn2* as the cell bodies of the efferent neurons are located outside of the cochlea which then project onto SGN fibers. Similarly, given the extensive alternative splicing among *NRXNs,* characterization of each isoform in detail would likely be impossible to quantify.

To visualize specific expression of *Nlgn1* and *Nlgn3* within the spiral ganglion and organ of Corti, I used multiplexed RNAScope *in situ* hybridization in 12 µm thick mid-modiolar radial sections. Positive controls were used to determine the quality and condition of the RNA present within the cochlear slices and negative controls which consisted of bacterially expressed genes

allowed for proper gauging of signal-to-noise (**Figure 2A-B**). Expression of both *Nlgn1* and *Nlgn3* was present in cells positive for *Tubb1* (i.e. *β-tub*) within the spiral bundle region (**Figure 3A**). However, expression for either *Nlgn1* or *Nlgn3* was not observed in cells positive for *MyosinVIIa* (i.e. *Myo7a*), suggesting that hair cells lack neuroligin expression (**Figure 3B**). Consistent with what is known about these postsynaptic proteins, it would then be reasonable to conclude that it is the SGNs which contribute neuroligins to the cochlear ribbon synapses and not the hair cells.

Having determined that SGNs express *Nlgn1 and Nlgn3*, I next sought to determine the proportion of SGNs which express either *Nlgn1* and/or *Nlgn*3. Within the mid modiolar section all three regions of the cochlea (i.e. apical (4-12 kHz), middle (12-32 kHz) and basal (32-64 kHz)) can be visualized. Analysis of the neuroligin expression revealed no obvious tonotopic gradient with 86 $\pm$ 5.1% of cells expressing *Nlgn1* and 85 $\pm$ 5.3% of cells expressing *Nlgn3* throughout the turns of the cochlea (**Figure 4 A-B)**. Moreover, 72 $\pm$ 10.4% of all cells within the bundle were positive for both *Nlgn1* and *Nlgn3* suggesting that *Nlgn1* and *Nlgn3* are expressed by many of the same neurons throughout the cochlea.

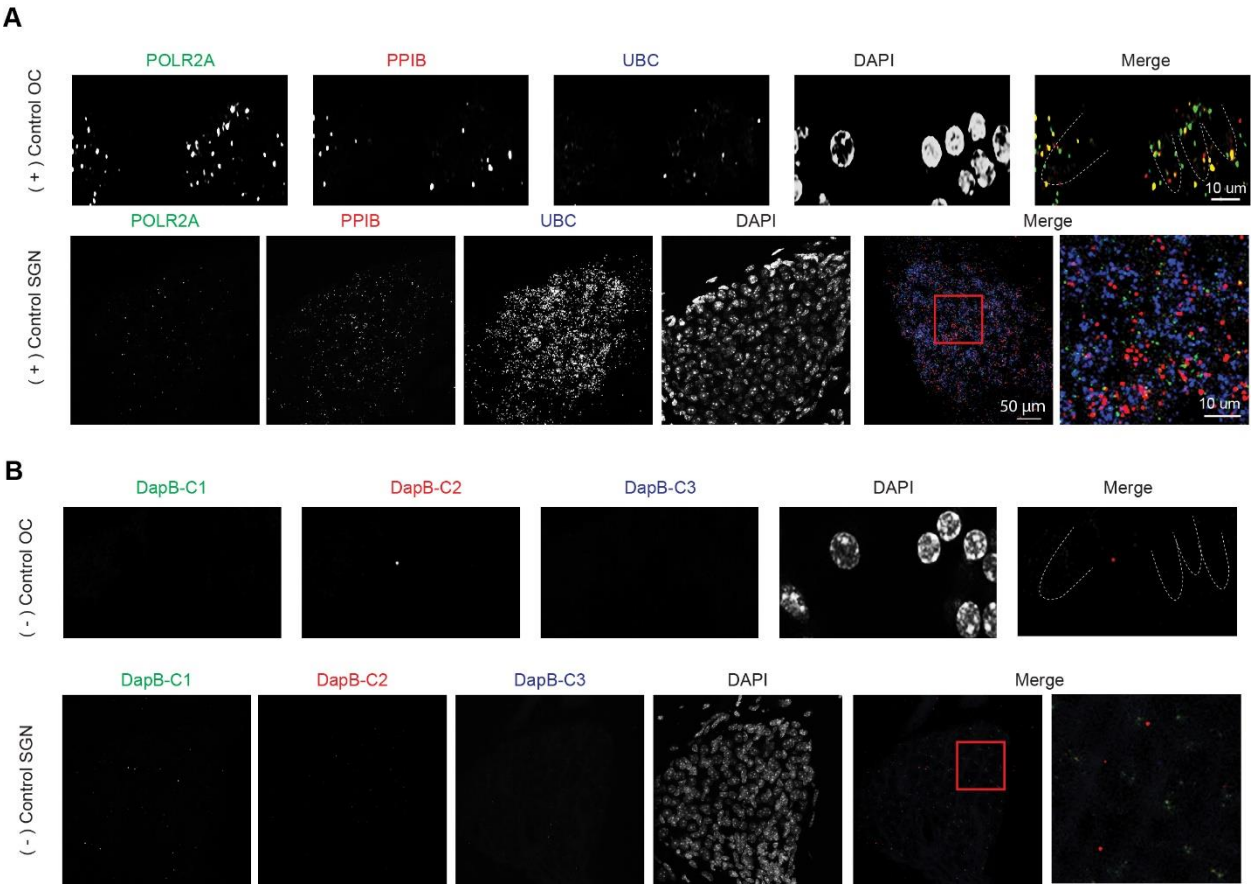
A
POLR2A
PPIB
UBC
DAPI
Merge
(+) Control OC
10 um
POLR2A
PPIB
UBC
DAPI
Merge
(+) Control SGN
50 µm
10 um
B
DapB-C1
DapB-C2
DapB-C3
DAPI
Merge
(-) Control OC
DapB-C1
DapB-C2
DapB-C3
DAPI
Merge
(-) Control SGN

Figure 2. Positive and negative controls within the cochlea used for RNAScope expression analysis. (A) Representative fluorescent images from RNAScope in situ hybridization analysis from 12 µm-thick sections of spiral ganglion in WT cochlea. Positive controls RNA Polymerase II Subunit A (*POLR2A*- green), Peptidylprolyl Isomerase B (*PPIB*- red) and Ubiquitin C (*UBC*- blue) expression was detectable among cells within both the organ of corti and spiral bundle. **(B)** Probes directed towards 4-hydroxy-tetrahydrodipicolinate reductase (DapB), which is expressed exclusively by bacteria was used as negative control. Residual fluorescence signal was used to determine the signal to noise for each channel. Scale bar = 10 µm and 50 µm.

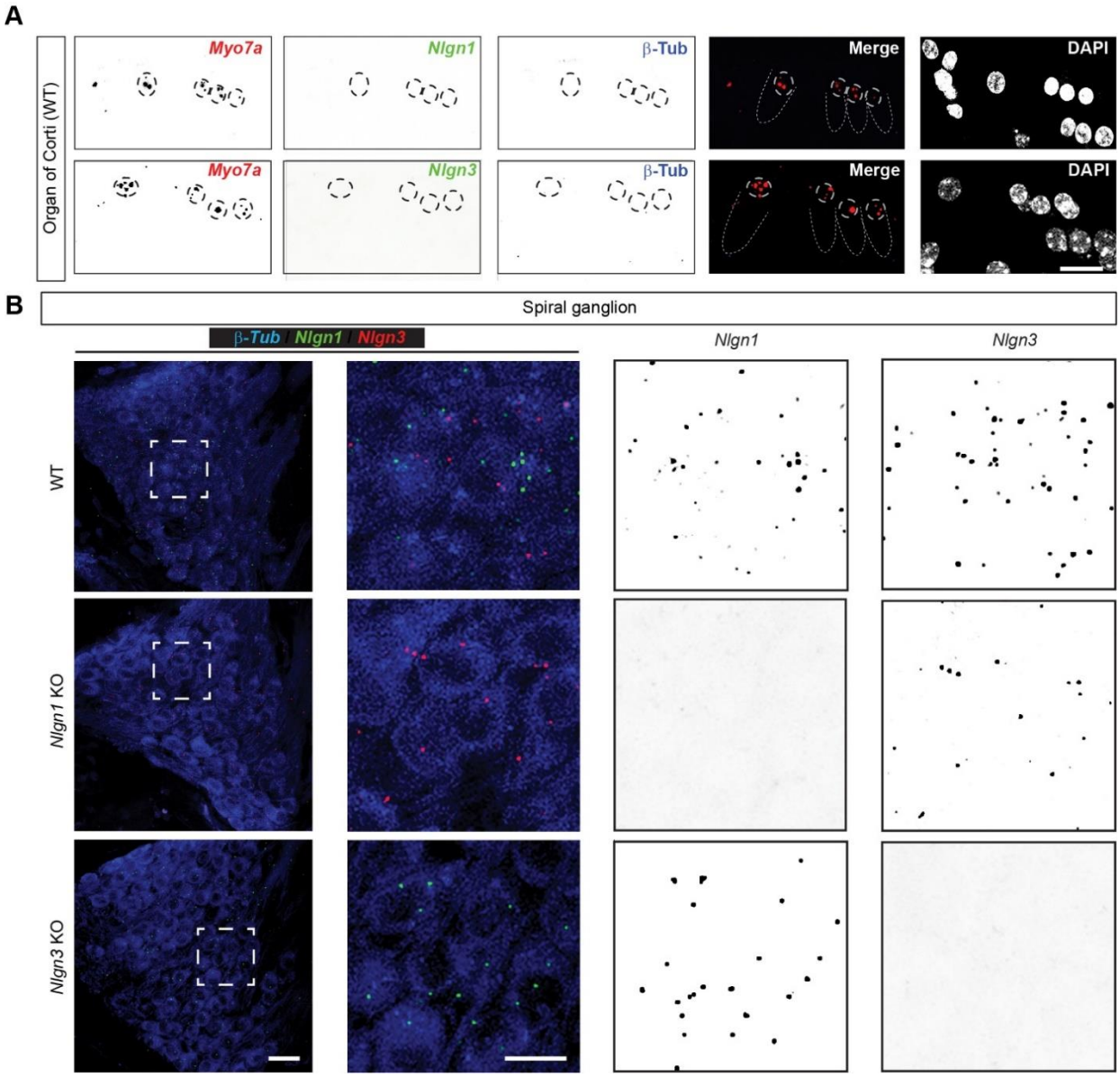
A
Organ of Corti (WT)
Myo7a
Nlgn1
β-Tub
Merge
DAPI
Myo7a
Nlgn3
β-Tub
Merge
DAPI
B
Spiral ganglion
β-Tub / Nlgn1 / Nlgn3
Nlgn1
Nlgn3
WT
Nlgn1 KO
Nlgn3 KO

Figure 3. *Nlgn1 is* expressed by spiral ganglion neurons alongside *Nlgn3*. (A) Representative fluorescent images from RNAScope in situ hybridization analysis from 12 µm-thick sections of the Organ of Corti in WT, *Nlgn1* KO, or *Nlgn3* KO cochlea. *Nlgn1* (green) and *Nlgn3* (green) were undetected in cells positive for hair cell marker Myo7a (red). **(B)** Representative fluorescent images from RNAScope in situ hybridization analysis of the spiral ganglion. *Nlgn1* (green) and *Nlgn3* (green) expression was detectable in cells positive for beta-tubulin (β-tub: blue). Probe specificity was validated in KO tissues which demonstrate little to no reactivity for *Nlgn1* or *Nlgn3* probes. Scale bar = 10 µm (D-E).

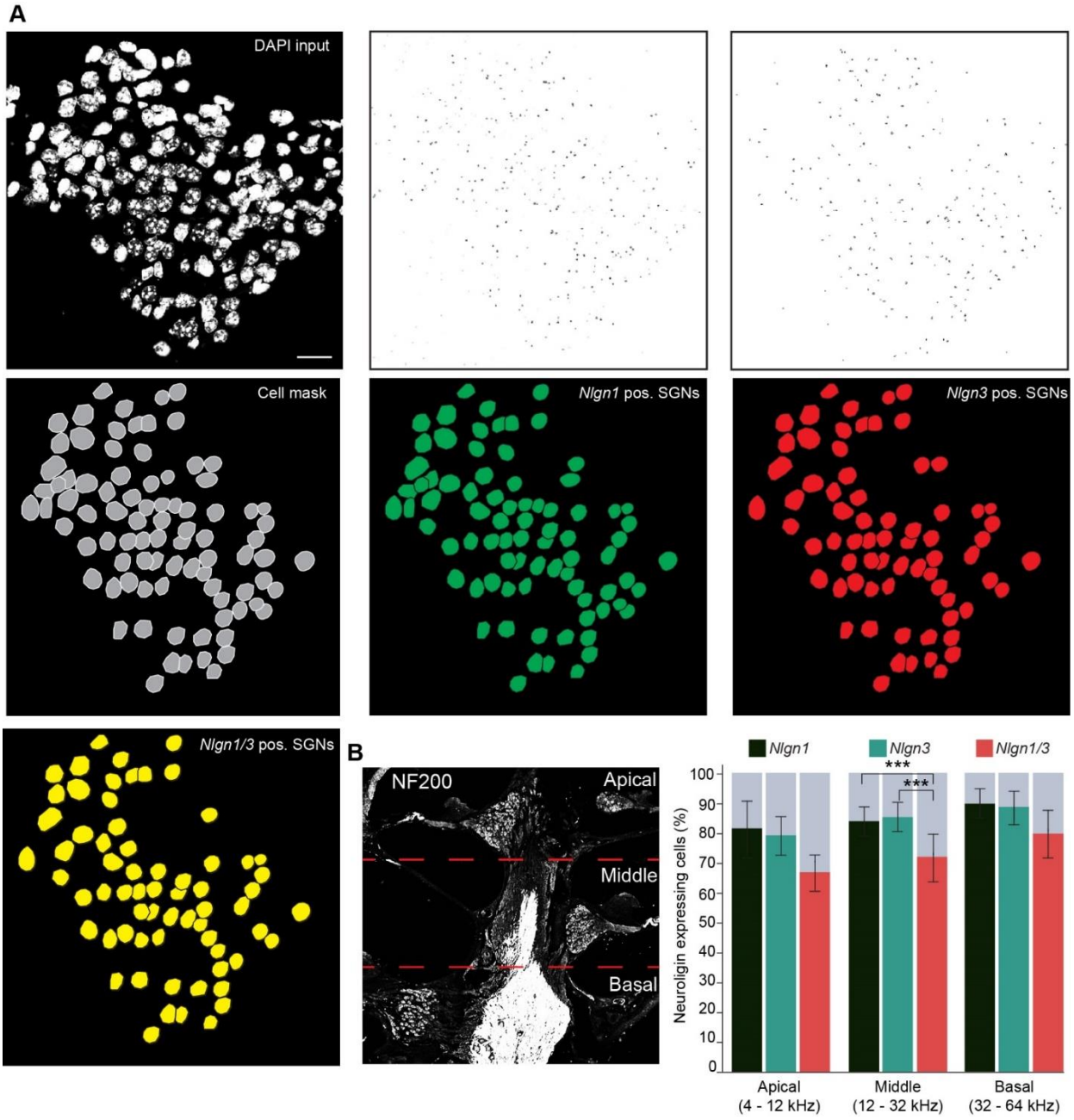
A
DAPI input
Cell mask
Nlgn1 pos. SGNs
Nlgn3 pos. SGNs
Nlgn1/3 pos. SGNs
B
NF200
Apical
Middle
Basal
Nlgn1
Nlgn3
Nlgn1/3
***
***
Neuroligin expressing cells (%)
100
90
80
70
60
50
40
30
20
10
0
Apical
(4 - 12 kHz)
Middle
(12 - 32 kHz)
Basal
(32 - 64 kHz)

Figure 4. *Nlgn1* and *Nlgn3* mRNAs are co-expressed among neurons in the cochlea.
(A) Representative images used for RNAScope-based quantification; Cell masks were created by expanding SGN DAPI signal by 10 pixels in all directions, determined to be the average distance between the perimeter of the nuclei to the edge of the cellular membrane. A cell mask was then overlayed onto *Nlgn1* or *Nlgn3* images to indicate neurons expressing *Nlgn1* (green) or *Nlgn3* (red). Cells expressing both *Nlgn1* and *Nlgn3* are shown in yellow. Scale bar = 10 µm. **(B)** Images were analyzed in apical (4-12 kHz), middle (12-32 kHz), or basal (32-64 kHz) regions. Neurons are labelled with NF200 (white). In apical regions 81.6 $\pm$ 11.2% of neurons were positive for *Nlgn1*, 78.8 $\pm$ 11.0% were positive for *Nlgn3*, and 65.6 $\pm$ 17.5% were positive for both *Nlgn1* and *Nlgn3*. In middle regions 86.1 $\pm$ 5.5% of neurons were positive for *Nlgn1*, 85.2 $\pm$ 5.5% were positive for *Nlgn3*, and 72.3 $\pm$ 8.1% were positive for both *Nlgn1* and *Nlgn3*. In basal regions 91.8 $\pm$ 4.7% of neurons were positive for *Nlgn1*, 89.2 $\pm$ 7.1% were positive for *Nlgn3*, and 79.3 $\pm$ 11.8% were positive for both *Nlgn1* and *Nlgn3*. N = 3 mice for apical, 6 mice for middle, 4 mice for basal regions at P60. Data are represented as mean $\pm$ SD. *** = p value < 0.001 by one-way ANOVA with Tukey post hoc correction.

Nlgn1 and Nlgn3 Localize to Common and Distinct Ribbon Synapses.

To confirm Nlgn1 and Nlgn3 proteins localize to ribbon synapses to a similar degree as proposed by RNAScope ISH data, I used immunofluorescence (IF) and confocal microscopy analysis of cochlear explants. To ensure the specificity of the neuroligin antibodies we obtained *Nlgn1* KO and *Nlgn3* KO mice (Varoqueaux *et al.*, 2006), and performed Western blot (WB) analyses of brain extracts, revealing no antibody reactivity among KO mice **(Figure 5)**. I next visualized Nlgn1 puncta relative to ribbon synapses determined by C-terminal binding protein 2 (CtBP2), present at the presynapse, juxtaposed to GluA2 puncta, localized within the postsynaptic SGNs, in KO and WT cochlea **(Figure 6A-B)**. Nlgn1 was present at about two-thirds of ribbon synapses (68 $\pm$ 2.1%) **(Figure 6C)**. Parallel IF analysis of Nlgn3 revealed that a slightly larger proportion of ribbon synapses contained Nlgn3 (77 $\pm$ 2.6%) **(Figure 6D-F).** Additionally, I confirmed that *Nlgn2* was not present among the cochlear ribbon synapses and that both *Nlgn1 and Nlgn3* were also present among outer hair cells in addition to the presence of Nrxns among ribbon synapses **(Figure 7A-C)**. To investigate whether neuroligins localize to cochlear ribbon synapses in other species, I confirmed synaptic localization with additional IF experiments in rat and marmoset cochlear whole mounts **(Figure 7D-E)**. The presence of neuroligins at ribbon synapses across species supports an evolutionarily conserved role among cochlear ribbon synapses, which is potentially significant for hearing.

Next, I determined whether Nlgn1 and Nlgn3 are present at common or distinct cochlear ribbon synapses. I found 40 $\pm$ 6.7% of synapses contain both Nlgn1 and Nlgn3, 17 $\pm$ 9.5% were positive for only Nlgn1, and 31 $\pm$ 4.2% only for Nlgn3, while 11 $\pm$ 8.1% had undetectable levels for both neuroligins **(Figure 8A-B)**. The presence of synapses which lack either Nlgn1 or Nlgn3

is of particular interest as this potentially lends itself towards distinct roles for these proteins within the cochlea. Recently there has been growing interest in the characterization of IHC-ANF synapse subtypes, which broadly are divided into three categories (Liberman, 1982; Shrestha *et al.*, 2018; Sun *et al.*, 2018). The type Ia-Ic SGNs are theorized to have somewhat spatially segregated innervation patterns along the pillar to modiolar inner hair cell axis, which is closely linked to their activity patterns. Generally, the type Ib fibers innervate regions closer to the modiolar face of inner hair cells and are believed to have higher thresholds compared to the type Ia and Ic fibers that localize to the pillar face (Furman *et al.*, 2013; Liberman, 1982; Shrestha *et al.*, 2018). Thus, to investigate the possibility that Nlgn1 and Nlgn3 have distinct roles among the subtypes of ribbon synapses, I quantified synapses containing either Nlgn1 or Nlgn3 or both across the pillar to modiolar axis of inner hair cell from the 16-20 kHz region of the cochlea **(Figure 8C)**. A larger proportion of Nlgn1 exclusive synapses (43 $\pm$ 5.4%) were present on the modiolar face compared to Nlgn3 exclusive (29 $\pm$ 4.8%) synapses **(Figure 8D)**. Conversely, on the pillar face the opposite was found, the majority of synapses were populated with Nlgn3 (Nlgn1 exclusive: 18 $\pm$ 0.51%, Nlgn3 exclusive: 49 $\pm$ 1.3%, and Nlgn1 and Nlgn3: 33 $\pm$ 1.0%) **(Figure 8E-F)**. Consistent with our findings, two labs have independently published databases which determined that *Nlgn3* is expressed to a similar degree among type Ia, Ib and Ic whereas *Nlgn1* was seen to be expressed only among type Ia and Ic SGNs (Petitpre *et al.*, 2018; Shrestha *et al.*, 2018). Together supporting that neuroligins, while potentially overlapping in function within the same synapses, may hold specific roles among a subset of synapses along the pillar-modiolar axis.

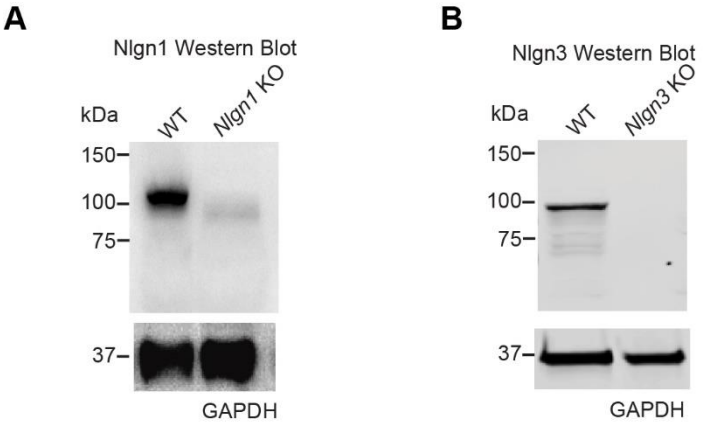
A
Nlgn1 Western Blot
kDa
WT
Nlgn1 KO
150
100
75
37
GAPDH
B
Nlgn3 Western Blot
kDa
WT
Nlgn3 KO
150
100
75
37
GAPDH

Figure 5. Western blot analysis of brain lysates validates Nlgn1 and Nlgn3 KO. (A) Western blot from *Nlgn1* KO brain lysates validating the specificity of our Nlgn1antibody. **(B)** Similarly, Western blot from *Nlgn3* KO brain lysates validating the specificity of our Nlgn3 antibody.

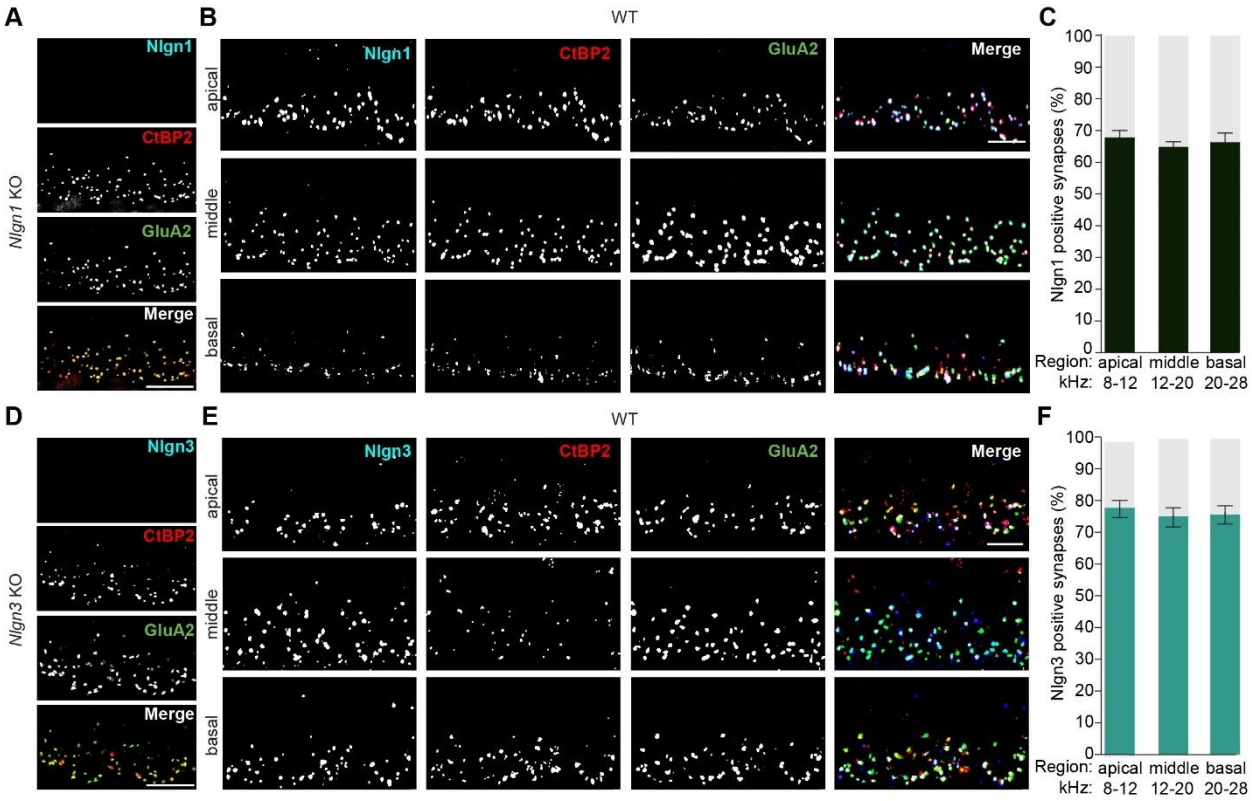
A
B
WT
C
Nlgn1
CtBP2
GluA2
Merge
Nlgn1 KO
apical
middle
basal
Nlgn1 positive synapses (%)
Region: apical middle basal
kHz: 8-12 12-20 20-28
D
E
WT
F
Nlgn3
Nlgn3 KO
Nlgn3 positive synapses (%)

Figure 6. Nlgn1 and Nlgn3 localize to cochlear ribbon synapses throughout the turns of the cochlea. (A) Representative immunofluorescent images from *Nlgn1* KO cochlear whole mounts demonstrating the absence of Nlgn1 at ribbon synapse (CtBP2 = red, GluA2 = green). **(B)** Representative images from apical (8-12 kHz), middle (12-20 kHz), and basal (20-28 kHz) regions of the cochlea immunostained with antibodies for Nlgn1 (blue) and inner hair cell ribbon synapse markers CtBP2 (red) and GluA2 (green). **(C)** Quantification of (B) reveals that on average Nlgn1 is present at greater than 65% of all inner hair cell ribbon synapses within the cochlea. **(D)** Representative immunofluorescent images from *Nlgn3* KO cochlear whole mounts demonstrating the absence of Nlgn3 at ribbon synapse (CtBP2 = red, GluA2 = green). **(E)** Representative images from apical (8-12 kHz), middle (12-20 kHz), and basal (20-28 kHz) regions of the cochlea immunostained with antibodies for Nlgn3 (blue), CtBP2 (red), and GluA2 (green). **(F)** Quantification of (E) reveals that on average Nlgn3 is present at greater than 78% of inner hair cell ribbon synapses within the cochlea.

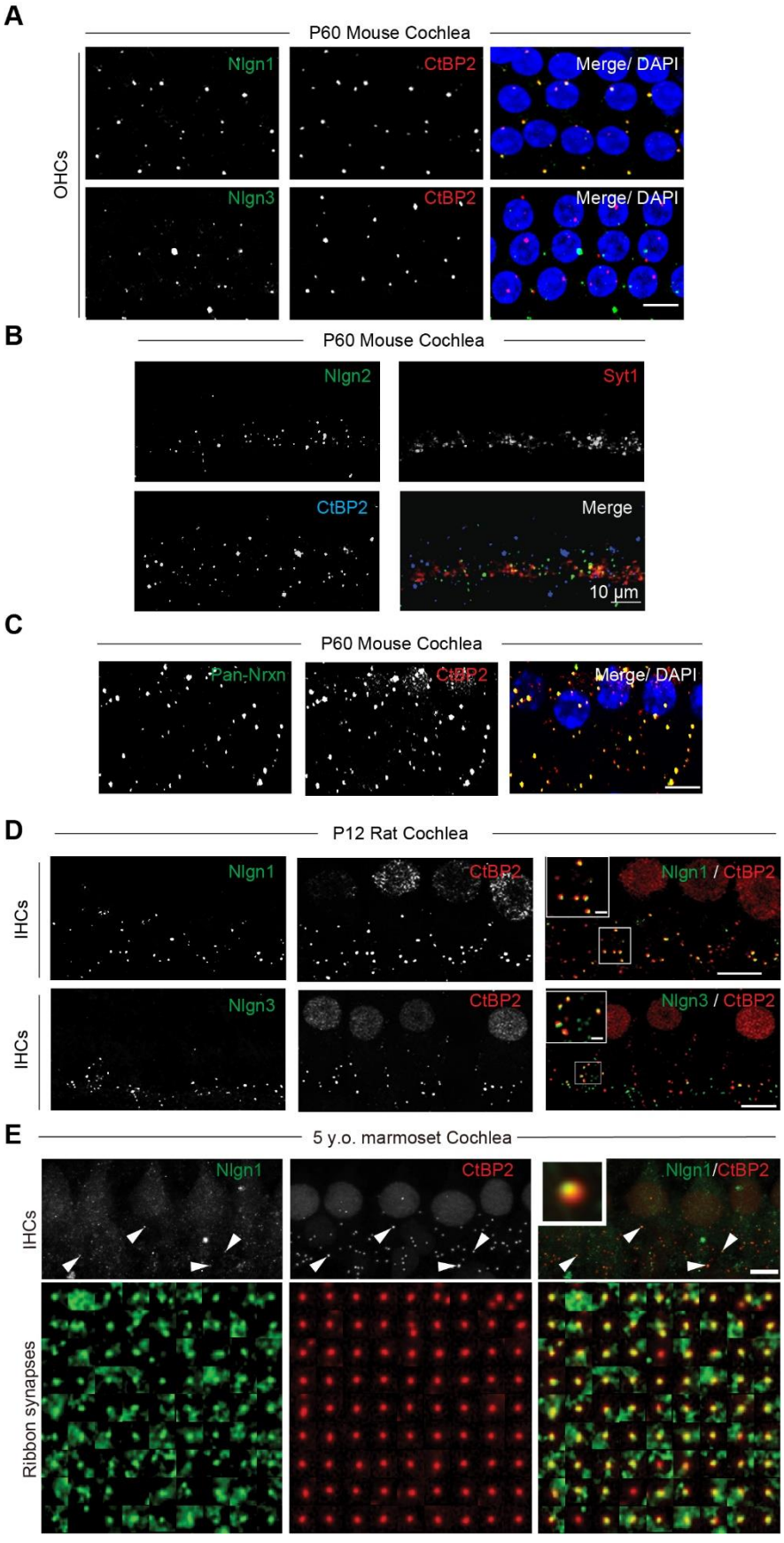
A
P60 Mouse Cochlea
Nlgn1
CtBP2
Merge/ DAPI
OHCs
Nlgn3
CtBP2
Merge/ DAPI
B
P60 Mouse Cochlea
Nlgn2
Syt1
CtBP2
Merge
10 µm
C
P60 Mouse Cochlea
Pan-Nrxn
CtBP2
Merge/ DAPI
D
P12 Rat Cochlea
IHCs
Nlgn1
CtBP2
Nlgn1 / CtBP2
IHCs
Nlgn3
CtBP2
Nlgn3 / CtBP2
E
5 y.o. marmoset Cochlea
IHCs
Nlgn1
CtBP2
Nlgn1/CtBP2
Ribbon synapses

Figure 7. The presence of Nlgn1 and Nlgn3 at cochlear ribbon synapses is conserved across species and position dependent along the modiolar-pillar axis in mice. (A) Representative images from P60 mice demonstrating the presence of both Nlgn1 and Nlgn3 within the region of the outer hair cells (OHC). **(B)** Representative images of cochlear wholemounts from P60 mice immunostained for Nlgn2 (green), synaptotagmin1 (Syt1-red), and ribbon marker CtBP2 (red). **(C)** cochlear wholemounts from P60 mice demonstrating the colocalization of pan-Nrxn antibody (green) with CtBP2 (red). **(D)** Representative images from P12 rat cochlear wholemounts immunostained with CtBP2 (red) and either Nlgn1 (top) or Nlgn3 (bottom). Inserts highlight synapses where colocalization of CtBP2 with either Nlgn1 or Nlgn3 is evident. **(E)** Representative images from five-year-old marmoset cochlear wholemounts immunostained with ribbon marker CtBP2 (red) and Nlgn1 (green). Bottom panel highlights 81 synapses, where colocalization of Nlgn1 with CtBP2 was evident. Scale bar = 10 µm.

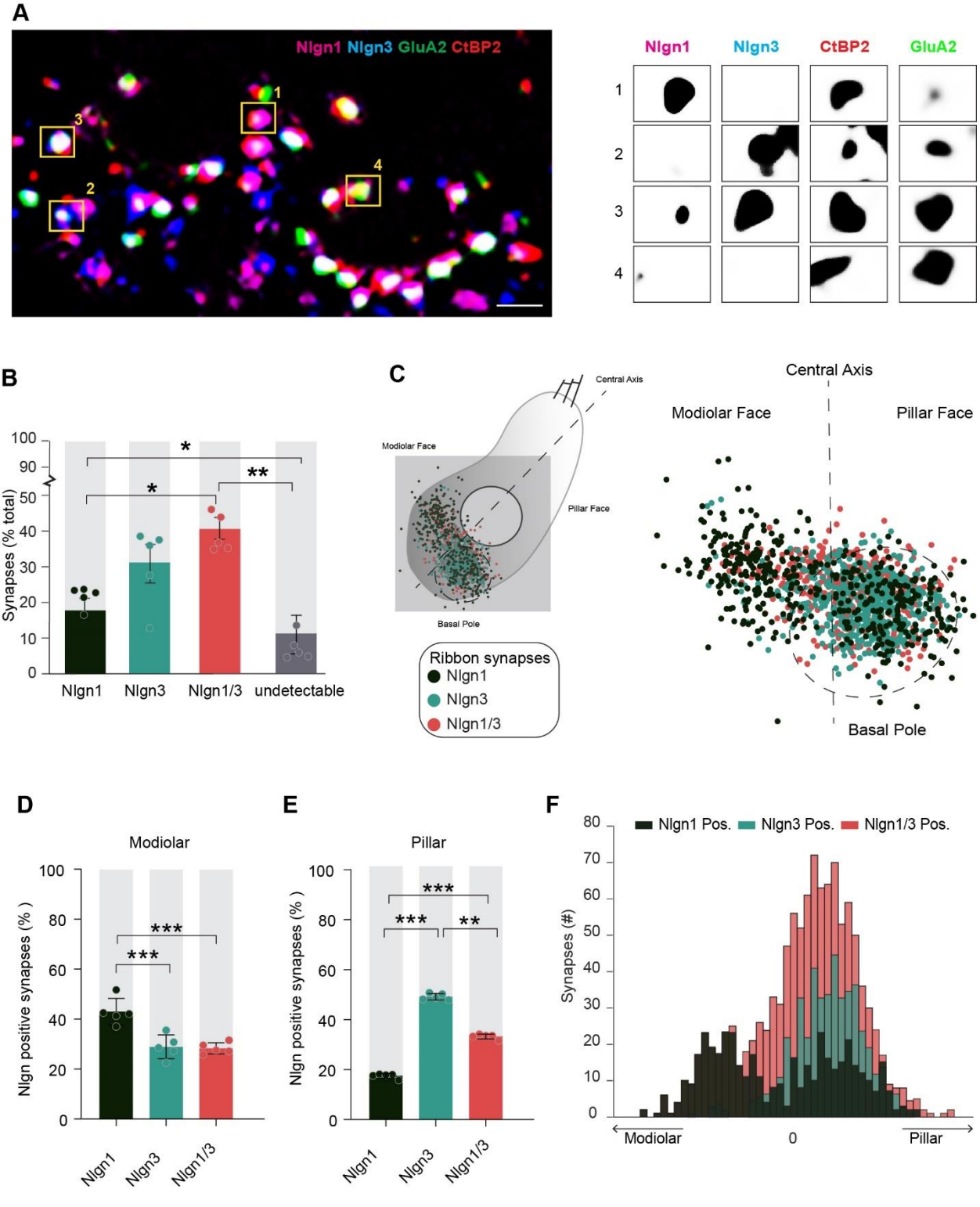
A
Nlgn1 Nlgn3 GluA2 CtBP2
1
2
3
4
Nlgn1
Nlgn3
CtBP2
GluA2
B
Synapses (% total)
Nlgn1
Nlgn3
Nlgn1/3
undetectable
C
Central Axis
Modiolar Face
Pillar Face
Basal Pole
Ribbon synapses
Nlgn1
Nlgn3
Nlgn1/3
D
Modiolar
Nlgn positive synapses (%)
E
Pillar
F
Nlgn1 Pos.
Nlgn3 Pos.
Nlgn1/3 Pos.
Synapses (#)
Modiolar
0
Pillar

Figure 8. Cochlear ribbon synapses demonstrate a modiolar-pillar dependent pattern for *Nlgn1* and *Nlgn3*. (A) Representative images of ribbon synapses immunostained with antibodies for Nlgn1 (magenta), Nlgn3 (blue), CtBP2 (red), and GluA2 (green); subpanels 1-4 are enlargements of 4 individual synapses. Data from 16-20 kHz region of the cochlea **(B)** Quantification of (A) revealed that 40 $\pm$ 6.7% of all ribbon synapses contain both Nlgn1 and 3, 17 $\pm$ 9.5% were positive for only Nlgn1, 31 $\pm$ 4.2% were positive for only Nlgn3, and 11 $\pm$ 8.1% of ribbon synapses had undetectable levels of either Nlgn1 or Nlgn3 (n= 1306 synapses). **(C)** Nlgn1 and Nlgn3 positive synapse coordinates plotted according to the inner hair cell pillar-to-modiolar axis from the 16-20 kHz region of the cochlea. Dotted lines represent the basal pole and the line demarcating the pillar to modiolar boarder used for analysis. **(D)** Quantification of (C) reveals that on the modiolar side a larger proportion of ribbon synapses contained exclusively Nlgn1 (42 $\pm$ 5.4%) compared to exclusively Nlgn3 (29 $\pm$ 4.8). **(E)** Quantification of (C) revealed that on the pillar face the majority of synapses were populated with Nlgn3 (Nlgn1 exclusive: 18 $\pm$ 5.4%, Nlgn3 exclusive: 49 $\pm$ 1.3%, and Nlgn1 and Nlgn3: 33 $\pm$ 1.0%). **(F)** Histogram showing the number and distribution of Nlgn1 (black), Nlgn3 (light blue) and Nlgn1/3 (salmon) positive synapses across the pillar to modiolar axis of WT inner hair cells. n= 1306 quantified synapses from 5 mice. Data are represented as mean $\pm$ SD. * = p value < 0.05, *** = p value < 0.001 by one-way ANOVA with Tukey post hoc correction for pairwise comparison. Scale bar = 2 µm (A). N = 5 mice per genotype aged P60-65.

Nlgn3 is Predominantly Expressed Throughout Cochlear Ribbon Synapse Maturation but neither Nlgn1 nor Nlgn3 are Necessary for Synapse Formation.

To delineate whether Nlgn1 or Nlgn3 are required for formation of the cochlear ribbon synapses during development, I quantified *Nlgn1, 2,* and *3* gene expression and synapse density at major milestones in cochlear maturation such as the onset of hearing at P12 (Takahashi et al., 2018). Although previous research has shown neuroligin expression in the cochlea, little is known regarding the patterns of expression throughout postnatal cochlear maturation (Petitpre *et al.*, 2018; Shrestha *et al.*, 2018). Thus, I compared *Nlgn1, 2, 3* mRNA levels at P6 (postnatal day 6), P12, and P30 to P1 **(Figure 9A)**. *Nlgn1* mRNA levels are significantly higher at P1 compared to all other ages. In contrast, *Nlgn3* expression progressively increased throughout maturation. Cochlear synapse refinement occurs from P12 to about P30. To determine if synapse density is reduced prior to the onset of hearing (i.e. P12), I analyzed the number of ribbon synapses among inner hair cell at P12 and P30 in single KO cochlea compared to WT **(Figure 9B)**. Synapse density at P12 was unaltered in *Nlgn1* and *Nlgn3* KOs compared to WT mice (*Nlgn1* KO 13 $\pm$ 0.8, *Nlgn3* KO 13 $\pm$ 1.1, WT 14 $\pm$ 0.7 synapses per inner hair cell). However, synaptic density was significantly reduced among neuroligin KOs at P30 compared to age mathced WT mice (*Nlgn1* KO 15 $\pm$ 0.9, *Nlgn3* KO 14 $\pm$ 1.2, WT 16 $\pm$ 0.7 synapses per inner hair cell) **(Figure 9C)**. Together suggesting that neuroligins influence the maturation of synapses after the onset of hearing rather than the formation of synapse formation pre-hearing.

Given the promiscuity of NRXN interactions, it is likely that another synaptic adhesion molecule may be acting to compensate for the loss of both Nlgn1 and Nlgn3 resulting in the formation of synapses throughout development. Likely compensatory candidates are LRRTM1

and LRRTM3, which have previously been shown to be expressed by SGNS and are known to influence glutamatergic synapse formation (de Wit et al., 2013; de Wit et al., 2009; Shrestha *et al.*, 2018). Together supporting a role for neuroligin more closely related to the organization and maturation of cochlear ribbon synapses rather than the initial formation of these synapses. Indeed, the presence of cochlear ribbon synapses within adult *Nlgn1/3* dKO cochlea further supports a role for these proteins extending past the initial formation of synapses.

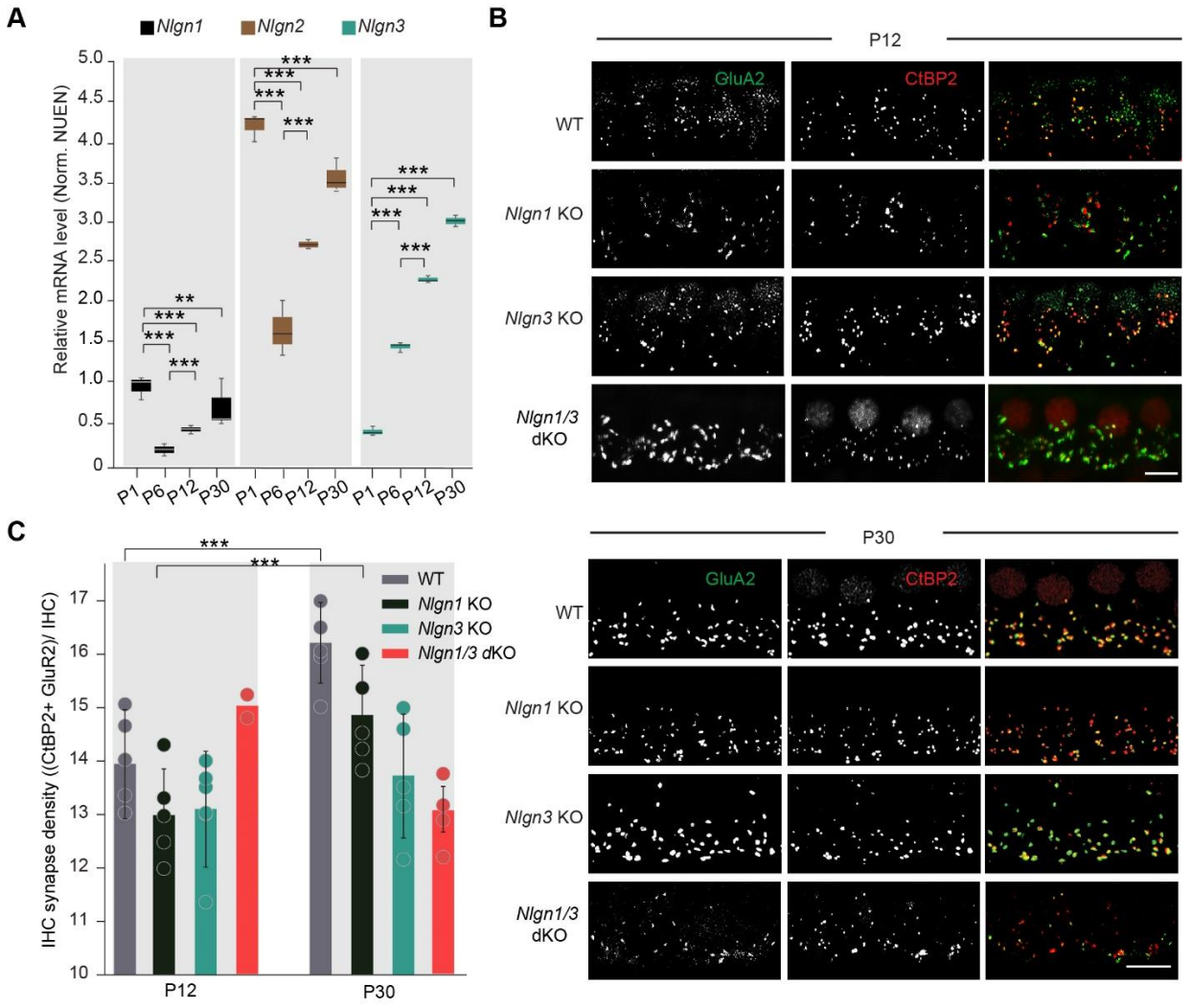
A
Nlgn1
Nlgn2
Nlgn3
Relative mRNA level (Norm. NUEN)
P1 P6 P12 P30
B
P12
GluA2
CtBP2
WT
Nlgn1 KO
Nlgn3 KO
Nlgn1/3 dKO
P30
C
IHC synapse density ((CtBP2+ GluR2)/ IHC)
WT
Nlgn1 KO
Nlgn3 KO
Nlgn1/3 dKO
P12
P30

Figure 9. Neuroligins are expressed throughout cochlear development but are not required for synapse formation. (A) Expression of *Nlgn1*, *2,* and *3* mRNA were measured in cochlea extracts from P1, P6, P12 and P30 WT mice. *Nlgn3* is expressed about 3-fold higher at P30 compared to P1. *Nlgn1* is expressed at significantly higher levels at P1 compared to all other ages *(Nlgn1*: P1 = 0.94 $\pm$ 0.13, P6 = 0.19 $\pm$ 0.11, P12 = 0.45 $\pm$ 0.04, P30 = 0.74 $\pm$ 0.31). *Nlgn3* expression levels progressively increased throughout development (*Nlgn3*: P1 = 0.43 $\pm$ 0.05, P6 = 1.45 $\pm$ 0.05, P12 = 2.27 $\pm$ 0.04, P30 = 2.97 $\pm$ 0.06) N = 4 mice per age, mean $\pm$ SD * = p value <0.05, ** = p value < 0.01, *** = p value < 0.001 by one-way ANOVA with Bonferroni correction. **(B)** Representative images from P12 and P30 cochlear wholemounts from *Nlgn1* KO, *Nlgn3* KO and WT mice immunostained with antibodies for ribbon synapses. Scale bar = 10 µm. **(C)** Quantification of (B) demonstrating no significant change in synaptic density across IHCs at P12 among *Nlgn1* KO (13.06 $\pm$ 1.06), *Nlgn3* KO (12.92 $\pm$ 0.83) and WT (13.66 $\pm$ 0.71) cochlear wholemounts. By P30 synaptic density was already reduced among single KOs compared to WT cochlea (*Nlgn1* KO = 14.77 $\pm$ 0.89, *Nlgn3* KO = 13.68 $\pm$ 1.15, WT = 16.1 $\pm$ 0.74). N= 8 mice per age per genotype. *** = p value < 0.001 by one-way ANOVA with Tukey post hoc correction.

Chapter 4: Maturation of Cochlear Ribbon Synapses is dependent on Neuroligins 1 and 3

Introduction

Hearing requires high-fidelity cochlear ribbon synapses linking mechanosensitive inner hair cells and SGN dendrites. The graded release of glutamate from synaptic vesicles near inner hair cell ribbons drives synaptic transmission primarily through AMPA receptors on SGN postsynaptic terminals. Although significant progress has been made in elucidating the presynaptic release machinery and the identity of the postsynaptic glutamate receptors, very little is known about synaptic organizing proteins within the cochlea.

The diversity among cochlear neurons within the PAC, lend themselves to the presence of some type of synaptic code within the cochlea (Meyer *et al.*, 2009; Reijntjes and Pyott, 2016; Weisz *et al.*, 2014; Weisz *et al.*, 2012). The type I ANFs alone can be further classified into 3 subpopulations based on their spontaneous activity and excitability (Liberman *et al.*, 2011; Liberman, 1978; 1982; Shrestha *et al.*, 2018; Sun *et al.*, 2018). The more than 1000 splice isoforms of NRXN, each with unique and promiscuous binding affinities, are theorized to contribute to the diversity of synapses within the brain and likely to the diversity observed within the cochlea as well (Sudhof, 2017). Synaptic cell adhesion proteins are critical organizers of the pre- and post-synaptic proteome and play key roles in synapse formation, specification, maturation, and function in the brain (Craig and Kang, 2007; Sudhof, 2008; 2017; Varoqueaux *et al.*, 2006). However, given the vast number of neurexin isoforms in existence, to systematically characterize the expression of each within the cochlea alone would be a herculean task.

Therefore, characterizing the influence of canonical neurexin binding partners, neuroligins (Nlgns), with respect to hearing is a more manageable task (Chanda *et al.*, 2017; Choi et al., 2011; Craig and Kang, 2007; Heine *et al.*, 2008; Kim et al., 2017; Sudhof, 2017;

Ullrich *et al.*, 1995). Moreover, there are only 3 neuroligins expressed in mice, with only *Nlgn1* and *Nlgn3* localizing to excitatory synapses, further focusing the scope of this study (Ko et al., 2009; Song *et al.*, 1999; Sudhof, 2008; 2017; Varoqueaux *et al.*, 2006). Additionally, there is substantial evidence for both *Nlgn1* and *Nlgn3* playing partially overlapping roles in the maturation of glutamatergic synapses (Chanda *et al.*, 2017; Shipman *et al.*, 2011). In brief, ablation of *Nlgn1* expression in cultured neurons results in a decrease of both NMDAR- and AMPAR-mediated excitatory synaptic responses, with a greater effect on NMDAR responses (Chanda *et al.*, 2017). Similarly, *Nlgn3* mutations and deletions drive milder phenotypes more closely related to impairments in AMPAR responses, which are generally exacerbated when paired with *Nlgn1* deletions (Chanda *et al.*, 2017; Shipman *et al.*, 2011; Zhang et al., 2017). Given the influence of *Nlgn1* and Nlgn3 on AMPAR activity and localization, and the dependence of AMPAR functions with respect to hearing. It is then reasonable to hypothesize that ablation of either *Nlgn1* and/or *Nlgn3* would result in functional deficits at the ribbon synapse. Further motivating the characterization of *Nlgn1* and *Nlgn3* with respect to cochlear ribbon synapse physiology and hearing.

In this chapter I report that *Nlgn1* and *Nlgn3* single gene KOs have reduced ribbon synapse size and number. This phenotype is exacerbated in mice lacking both Nlgn1 and Nlgn3 in a way consistent with these proteins having partially redundant roles. *Nlgn1* and *Nlgn3* KO mice have compromised cochlear function and trans-synaptic coordination, which are additively impaired in the dKOs based on ABRs and synapse anatomy. Proteomic analysis of cochlear extracts from dKO mice revealed reduced abundance of several postsynaptic scaffolding proteins, consistent with reduced synapse number and volume. *Nlgn3* KOs were also shown to

have impaired recovery after noise exposures from which WT mice fully recover. These results provide a pioneering description of the essential roles of Nlgn1 and Nlgn3 proteins in cochlear synapse structure and function.

Results

Ribbon synapses are significantly fewer and smaller in Nlgn1, 3 dKO mice

To investigate if Nlgn1 or Nlgn3 are required for ribbon synapse maintenance, I performed IF analysis of cochlear whole mounts from *Nlgn1* KO, *Nlgn3* KO, and *Nlgn1/3* dKO mice **(Figure 10A-D)**. Across the base, middle, and apical regions of the cochlea, loss of Nlgn1 or Nlgn3 resulted in about a 10% reduction in synapse density (i.e., synapse number per inner hair cell: *Nlgn1* KO: 92 $\pm$ 2.4%, *Nlgn3* KO: 93 $\pm$ 3.8%). Markedly, the dKO mice had a more pronounced 25% reduction in ribbon synapse density compared to WT (*Nlgn1/3* dKO: 76 $\pm$ 2.2%) **(Figure 11A)**. I then quantified the number of orphan ribbons (i.e. CtBP2 puncta without colocalized GluA2 puncta) in KO and dKO cochleae relative to WT controls. Notably, *Nlgn1* KO mice had a significantly greater number of orphan ribbons compared to WT or *Nlgn3* KO mice (*Nlgn1* KO: 1.4 $\pm$ 0.61, *Nlgn3* KO: 0.31 $\pm$ 0.10, WT: 0.30 $\pm$ 0.20 orphans per inner hair cell) **(Figure 11B)**. Strikingly, mice lacking both Nlgn1 and 3 had a dramatic increase in the number of orphan ribbons, which far exceeded the additive synaptic phenotype observed in the single gene KOs (*Nlgn1/3* dKO: 5.7 $\pm$ 1.5 orphans per inner hair cell) **(Figure 11B)**. Suggesting *Nlgn1* has a more prominent role in physically linking pre- and postsynaptic elements in the cochlea.

Next, I determined if disruption of the ribbon synapse organizer would result in smaller or larger synapses. Utilizing Amira, I measured the synaptic volumes across each genotype and

revealed a significant ~ 50% decrease in *Nlgn1* and *Nlgn3* KOs synaptic volumes compared to WT. The absence of both neuroligins resulted in greater than a five-fold reduction in ribbon synapse volume **(Figure 11C)**. To further investigate this finding, I then asked if this reduction in volume was due to smaller clusters of AMPARs or if the ribbons were smaller among the single and double KOs. Notably, I found that in the absence of *Nlgn1* and *Nlgn3* resulted in larger GluA2 puncta volumes **(Figure 11D)**. The larger GluA2 puncta may be the result of an impairment in the concentration of AMPAR clusters into tightly packed pockets. Evidence for higher diffusion coefficient among the AMPARs in the absence of Nlgn1 has been previously reported and would be supportive of the larger puncta I observe (Letellier et al., 2018; Mondin et al., 2011). Surprisingly, I also found that the ribbons were significantly larger among *Nlgn1* and *Nlgn1/3* dKO inner hair cells **(Figure 11E)**. At odds with reduced synaptic volumes, it was curious to see that both pre- and post-synaptic elements are enlarged across the single and double KOs. To address this disparity, we next determined whether the distance between paired CtBP2 and GluA2 puncta in neuroligin KOs, dKOs was larger than those recorded in WT cochlea **(Figure 11F)**. The results of this analysis determined that the average distance between pre and postsynaptic elements was significantly greater in *Nlgn1,* and *Nlgn3* KO cochlea compared to WT **(Figure 11G)**. This finding is consistent with previous findings demonstrating that *Nlgn1* aids in the alignment of AMPAR nanodomains with pre-synaptic release sites through transsynaptic interactions within CNS neurons (Haas, 2018). Suggesting that the reduced volumes recorded in the single KOs are a result of an increase in the distance of the pre-postsynaptic elements rather than the reduction of AMPAR clusters or reduced ribbon volumes. The distance between paired puncta at the remaining synapses in the dKOs was not significantly different from WT controls, perhaps a caveat of the increased volumes of GluA2 and CtBP2

puncta recorded in the dKO. This would result in shorter centroid-to-centroid distances between possible CtBP2 and GluR2 puncta despite an reduction of the overlapping areas of these puncta observed in the smaller synaptic volumes recorded in the dKO.

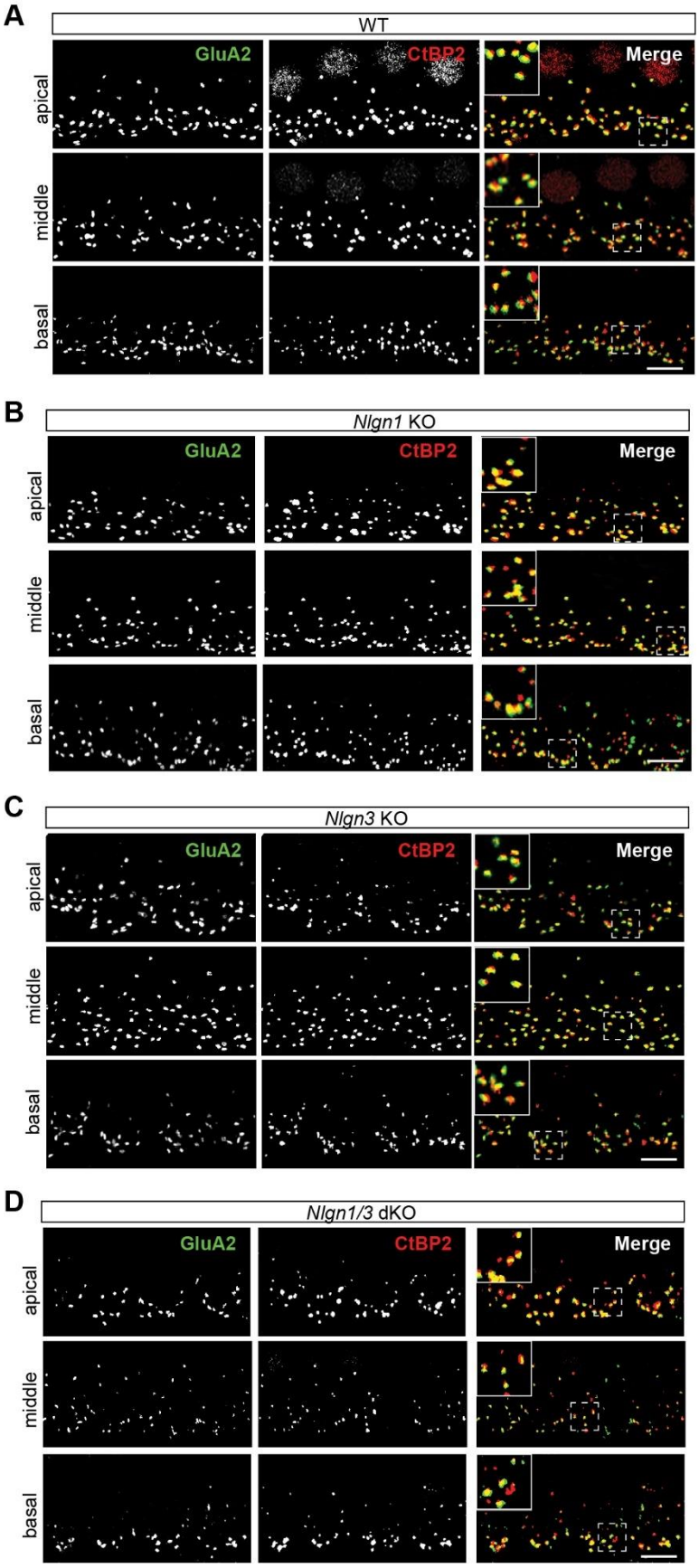
A
WT
GluA2
CtBP2
Merge
apical
middle
basal
B
Nlgn1 KO
GluA2
CtBP2
Merge
apical
middle
basal
C
Nlgn3 KO
GluA2
CtBP2
Merge
apical
middle
basal
D
Nlgn1/3 dKO
GluA2
CtBP2
Merge
apical
middle
basal

Figure 10. Visualization of cochlear ribbon synapses across single and double neuroligin knock-outs compared to WT. (A-D) Representative images from WT, *Nlgn1* KO, *Nlgn3* KO and *Nlgn1/3* dKO cochlear wholemounts from P60-65 mice immunostained with antibodies for ribbon synapses. Scale bar = 10µm.

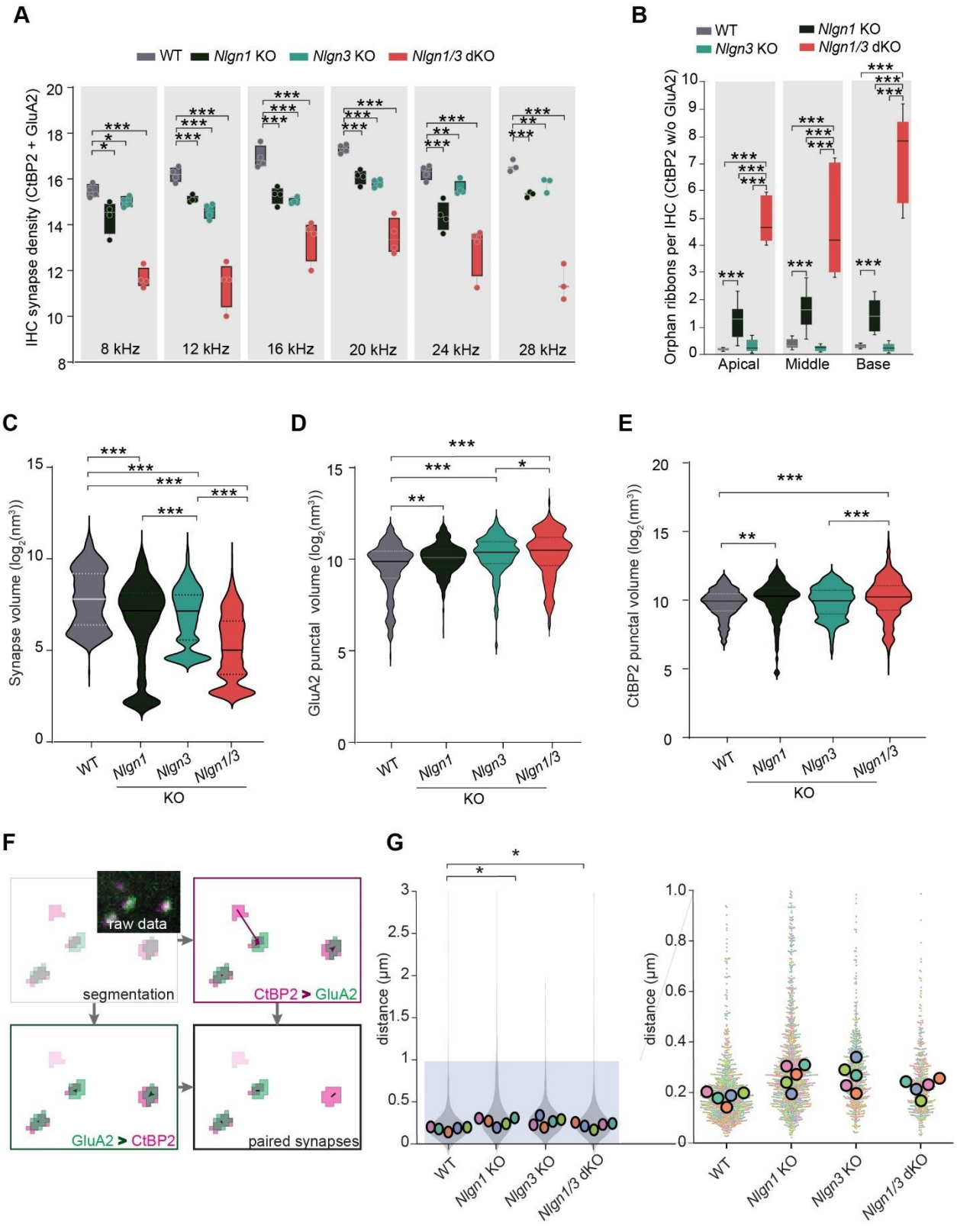
A
WT
Nlgn1 KO
Nlgn3 KO
Nlgn1/3 dKO
IHC synapse density (CtBP2 + GluA2)
8 kHz
12 kHz
16 kHz
20 kHz
24 kHz
28 kHz
B
Orphan ribbons per IHC (CtBP2 w/o GluA2)
Apical
Middle
Base
C
Synapse volume (log2(nm3))
D
GluA2 punctal volume (log2(nm3))
E
CtBP2 punctal volume (log2(nm3))
KO
F
raw data
segmentation
CtBP2 > GluA2
GluA2 > CtBP2
paired synapses
G
distance (µm)

Figure 11. Nlgn1 and 3 are required for cochlear ribbon synapse maturation. (A) Summary of synaptic density measured across the 8-28 kHz region of the cochlea in WT, *Nlgn1* KO, *Nlgn3* KO and *Nlgn1/3* dKO cochlea. Synaptic density was significantly reduced at all measured regions: **8 kHz**- WT 15.5 ± 0.28 , *Nlgn1* KO 14.4 ± 0.72, *Nlgn3* KO 15 ± 0.22, *Nlgn1/3* dKO 11.7 ± 0.45 ; **12 kHz**- WT 16.2 ± 0.32 , *Nlgn1* KO 15.1 ± 0.14, *Nlgn3* KO 14.6 ± 0.33, *Nlgn1/3* dKO 11.4 ± 1.0; **16 kHz**- WT 17.0 ± 0.49 , *Nlgn1* KO 15.3 ± 0.37, *Nlgn3* KO 15 ± 0.13, *Nlgn1/3* dKO 13.3 ± 0.93; **20 kHz**- WT 17.3 ± 0.19 , *Nlgn1* KO 16 ± 0.31, *Nlgn3* KO 15.8 ± 0.17, *Nlgn1/3* dKO 13.5 ± 0.79; **24 kHz**- WT 16.6 ± 0.26 , *Nlgn1* KO 15.3 ± 0.12, *Nlgn3* KO 15.8 ± 0.32, *Nlgn1/3* dKO 11.6 ± 0.79; **28 kHz**- WT 16.5 ± 0.64 , *Nlgn1* KO 15.1 ± 0.66, *Nlgn3* KO 15.3 ± 0.5, *Nlgn1/3* dKO 12.4 ± 0.98. **(B)** The number of orphan ribbons per inner hair cells was elevated in both *Nlgn1* KO and dKO mice compared to WT in the apical (WT: 0.23 ± 0.04; *Nlgn1* KO: 1.2 ± 0.61; *Nlgn1/3* dKO: 4.9 ± .85), middle (WT: 0.41 ± 0.16; *Nlgn1* KO: 1.7 ± 0.69; *Nlgn1/3* dKO: 4.8 ± 2.0) and basal (WT: 0.31 ± 0.09; *Nlgn1* KO: 1.5 ± 0.54; *Nlgn1/3* dKO: 7.2 ± 1.6) regions of the cochlea. Box and whisker plot highlighting the 25th-75th quartile distribution middle line is the median of the distribution. **(C)** Single gene KO cochlea had significantly reduced afferent synapse volume, on average, compared to WT (*Nlgn1* KO: 0.21 ± 0.05 μm^3, *Nlgn3* KO: 0.19 ± 0.04 μm^3, WT: 0.40 ± 0.19 μm^3). Analysis of the *Nlgn1/3* dKO cochlea reveal an exacerbated phenotype (0.07 ± 0.01 μm^3). **(D)** Analysis of GluA2 puncta volumes determined significantly larger puncta among single and double KOs compared to WT controls (*Nlgn1* KO: 10.03 ± .68 μm^3, *Nlgn3* KO: 10.22 ± 1.13 μm^3, *Nlgn1/3* dKO: 10.26 ± 1.66 μm^3, WT: 9.51 ± 2.01 μm^3). **(E)** Analysis of CtBP2 puncta volumes revealed significantly larger ribbon among Nlgn1 and Nlgn1/3 dKO inner hair cells compared to WT (*Nlgn1* KO: 10.00 ± 1.1 μm^3, *Nlgn3* KO: 9.82 ± 1.3 μm^3, *Nlgn1/3* dKO: 9.82 ± 1.66 μm^3, WT: 10.12 ± 2.23 μm^3). **(F)**

Schematic representation of how distances between pre- and postsynaptic elements were measured to identify nearest neighbors. Distances were measured from the center of each CtBP2 punctum to its nearest neighboring GluA2 punctum to generate a list of nearest neighbors from CtBP2, and vice versa. Lists were then compared to keep only the closest pairs common to both lists, thus eliminating mismatched lone puncta. **(G)** Quantification demonstrating a lengthening with respect to the average distance between presynaptic CtBP2 and postsynaptic GluA2 in *Nlgn1* KO cochlea (0.26 $\pm$ 0.05 µm) and *Nlgn3* KO cochlea (0.26 $\pm$ 0.06 µm) compared to WT (0.18 $\pm$ 0.02 µm) and *Nlgn1/3* dKO (0.21 $\pm$ 0.03 µm) cochlea. Data are represented as mean $\pm$ SD. * = p value < 0.05, ** = p value < 0.01, *** = p value < 0.001 by one-way ANOVA with Tukey post hoc correction. N = 4 mice for all genotypes (A-E). N= 5 mice per genotype (F-G). * = p value < 0.05, ** = p value < 0.01, *** = p value < 0.001 by one-way ANOVA with Tukey post hoc correction.

Nlgn1 and Nlgn3 are required for cochlear ribbon synapse proteome maintenance.

To investigate how the cochlear proteome is remodeled in the absence of Nlgn1 and Nlgn3, I performed quantitative mass spectrometry (MS)-based proteomic analysis of inner ear extracts from dKO mice. To confidently measure the changes in cochlear protein abundance in the dKO relative to WT mice, 6-plex TMT analysis was utilized. In total I quantified more than 3,000 proteins across the biological replicates. I assessed the dataset by graphing the reporter ion intensities and found they were similar between WT and dKO cochlea **(Figure 12A)**, additionally, biological replicates were also seen to cluster based on genotype **(Figure 12B)**. To visualize the cochlear proteome dataset, I graphed our results using a volcano plot **(Figure 12C)**. I observed more proteins with significantly reduced versus elevated fold change (194 versus 127, Adj. P value < 0.01). To further investigate the significant proteins, we performed gene ontology cellular component (GO:CC) enrichment analysis with PANTHER (Thomas et al., 2006). Among the significant terms, we found the term "anchored component of postsynaptic density membrane, GO:0099031", was the most enriched **(Figure 12D)**. This observation is consistent with the previous evidence in the CNS showing that neuroligins are key postsynaptic membrane organizers (Sudhof, 2008). Given that cochlear afferent synapses are glutamatergic, we focused on the proteins associated with the GO term "glutamatergic synapse, GO:0098978". For example, PSD95, homer3, and cortactin all had significantly reduced fold change **(Figure 12C)**. Thus, consistent with reduced synapse number and size, our proteomic analysis suggests that a reduction in synaptic scaffolding proteins in the absence of Nlgn1 and Nlgn3 may destabilizes ribbon synapses resulting in fewer, and smaller synapses.

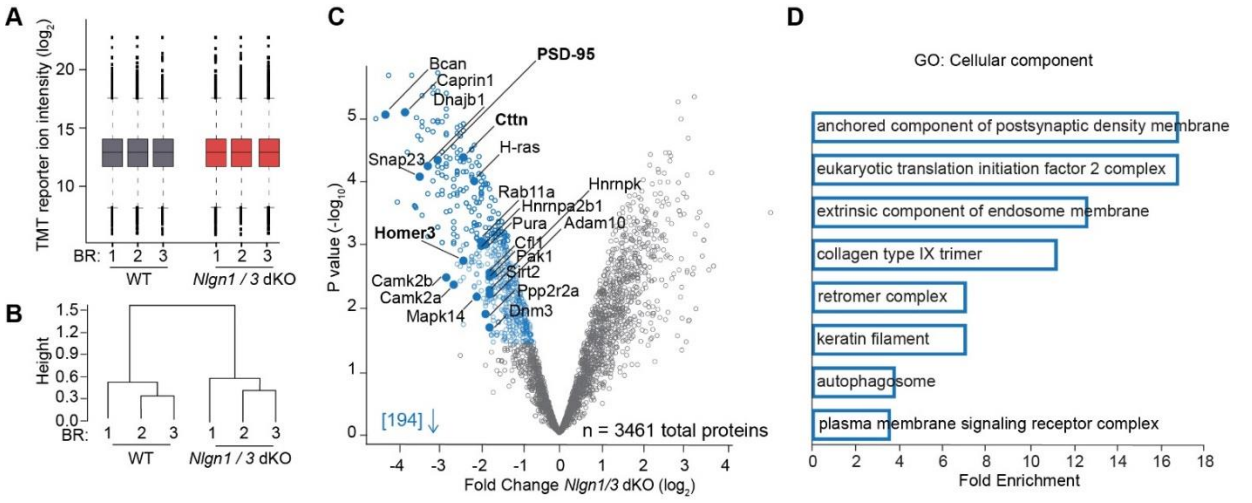
A
TMT reporter ion intensity (log2)
20
15
10
BR: 1 2 3 1 2 3
WT
Nlgn1 / 3 dKO
B
Height
1.5
1.2
0.9
0.6
0.3
0.0
BR: 1 2 3 1 2 3
WT
Nlgn1 / 3 dKO
C
P value (-log10)
5
4
3
2
1
0
PSD-95
Bcan
Caprin1
Dnajb1
Cttn
H-ras
Snap23
Rab11a
Hnrnpk
Hnrnpa2b1
Pura
Adam10
Homer3
Cfl1
Pak1
Sirt2
Camk2b
Camk2a
Ppp2r2a
Mapk14
Dnm3
[194]↓
n = 3461 total proteins
-4 -3 -2 -1 0 1 2 3 4
Fold Change Nlgn1/3 dKO (log2)
D
GO: Cellular component
anchored component of postsynaptic density membrane
eukaryotic translation initiation factor 2 complex
extrinsic component of endosome membrane
collagen type IX trimer
retromer complex
keratin filament
autophagosome
plasma membrane signaling receptor complex
0 2 4 6 8 10 12 14 16 18
Fold Enrichment

Figure 12. *Nlgn1/3* dKO cochlea have reduced levels of synaptic scaffolding proteins. (A) Assessment of overall TMT reporter ion intensities showed the biological replicates and genotypes were similar. N = 3 mice at P60-65 per genotype. **(B)** Biological replicates cluster based on genotype. **(C)** Volcano plot depicting protein fold change (*Nlgn1/3* dKO / WT) versus adjusted p value from multiplexed quantitative proteomic analysis. Blue indicates significantly reduced proteins (adj. P value < 0.01) with reduced fold change. All proteins with reduced fold change associated with the GO term "glutamatergic synapse, GO:0098978" are labeled in the volcano plot. n= 3461 total quantified proteins **(D)** "Anchored component of postsynaptic density membrane GO:0099031", is the most significantly enriched GO: cellular component term among the significantly reduced proteins (blue features from C) compared to all quantified proteins.

Absence of Nlgn1 or Nlgn3 impairs hearing

To assess the functional role of Nlgn1 or Nlgn3 in hearing, I performed ABR hearing measurements. ABR recordings are sound evoked field potentials recorded from the ascending auditory pathway in response to sound onset. Comparison of ABR thresholds (i.e. the minimum auditory stimuli needed to evoke an ABR response above the noise floor of 180 μv) in WT littermates of *Nlgn1* and *Nlgn3* single KOs demonstrated no significant differences across the background strains **(Figure 13A-B)**. Distortion product otoacoustic emissions were alike WT responses in *Nlgn1* KOs, *Nlgn3* KOs, and *Nlgn1/3* dKOs suggesting outer hair cell function is unaffected **(Figure 13C)**. ABR responses from *Nlgn3* KOs displayed a significant elevation in threshold only at 28 kHz compared to WT **(Figure 14A)**. In contrast, *Nlgn1/3* dKOs had robustly elevated threshold levels, which on average were 12 $\pm$ 3.0 dB higher than both WT and single KOs at all tested frequencies **(Figure 14B)**. Next, I assessed Wave I amplitude, which reflect the number of activated SGNs at increasing levels of sound stimulation. *Nlgn1* KO had significantly reduced Wave I amplitude at 8 kHz with 80 dB SPL stimuli compared to WT. *Nlgn3* KO and *Nlgn1/3* dKOs Wave I amplitudes at 80 dB SPL were significantly reduced by 31 $\pm$ 12% and 32 $\pm$ 14%, respectively across all frequencies compared to WT **(Figure 14C)**. Analysis of the overall I/O curves, calculated as the increase in Wave I amplitude across the 20-80 dB SPL stimulus range, for *Nlgn3* and *Nlgn1/3* (d)KOs demonstrated a global decrease in neuronal activity, given the significantly reduced Wave I amplitudes observed at most tested intensities **(Figure 14D)**. This similar reduction in ABR amplitudes across all stimulus intensities suggests that neuroligins contribute to synaptic function of high- and low-threshold SGNs. Given the reduction in ABR Wave I responses, I next investigated response latencies. Analysis at 8, 16 and

24 kHz revealed an increase in the duration and onset-latency of Wave I at both 60- and 80-dB SPL stimuli in dKOs compared to WT **(Figure 14E-F)**. Given the absence of a robust reduction in Wave I amplitude phenotype among *Nlgn1* KO mice, I investigated the possibility of compensatory *Nlgn3* gene expression. Notably, I found that Nlgn3 gene expression was indeed upregulated in *Nlgn1* KO cochlea while Nlgn1 expression was comparable to WT in *Nlgn3* KO cochlea **(Figure 15A)**. Utilizing immunohistochemistry, I validated this finding by comparing the average volume of Nlgn3 puncta among Nlgn1 KO synapses and found a significant increase in puncta volume. Together suggesting that the mild hearing phenotype observed in *Nlgn1* KO mice may be mitigated in part by Nlgn3 compensation.

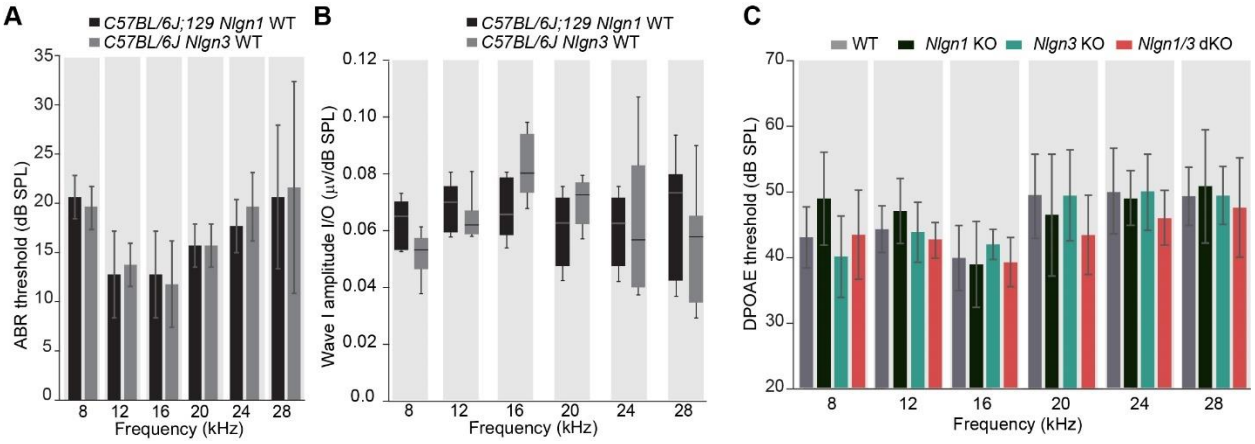
A
C57BL/6J;129 Nlgn1 WT
C57BL/6J Nlgn3 WT
ABR threshold (dB SPL)
Frequency (kHz)
B
C57BL/6J;129 Nlgn1 WT
C57BL/6J Nlgn3 WT
Wave I amplitude I/O (μv/dB SPL)
Frequency (kHz)
C
WT
Nlgn1 KO
Nlgn3 KO
Nlgn1/3 dKO
DPOAE threshold (dB SPL)
Frequency (kHz)

Figure 13. Comparison of *Nlgn1* KO and *Nlgn3* KO background strains observed comparable ABR responses. (A-B) Comparison of ABR responses from WT littermates of *Nlgn1* and *Nlgn3* KO mice showed no significant difference with respect to either threshold level or strength of synaptic response at each tested frequency **(C)** DPOAEs from the 8-28 kHz regions were unaffected in all genotypes compared to WT. N = 5 P60-65 mice per background strain (A-B). N = 8 P60-65 mice per genotype (C).

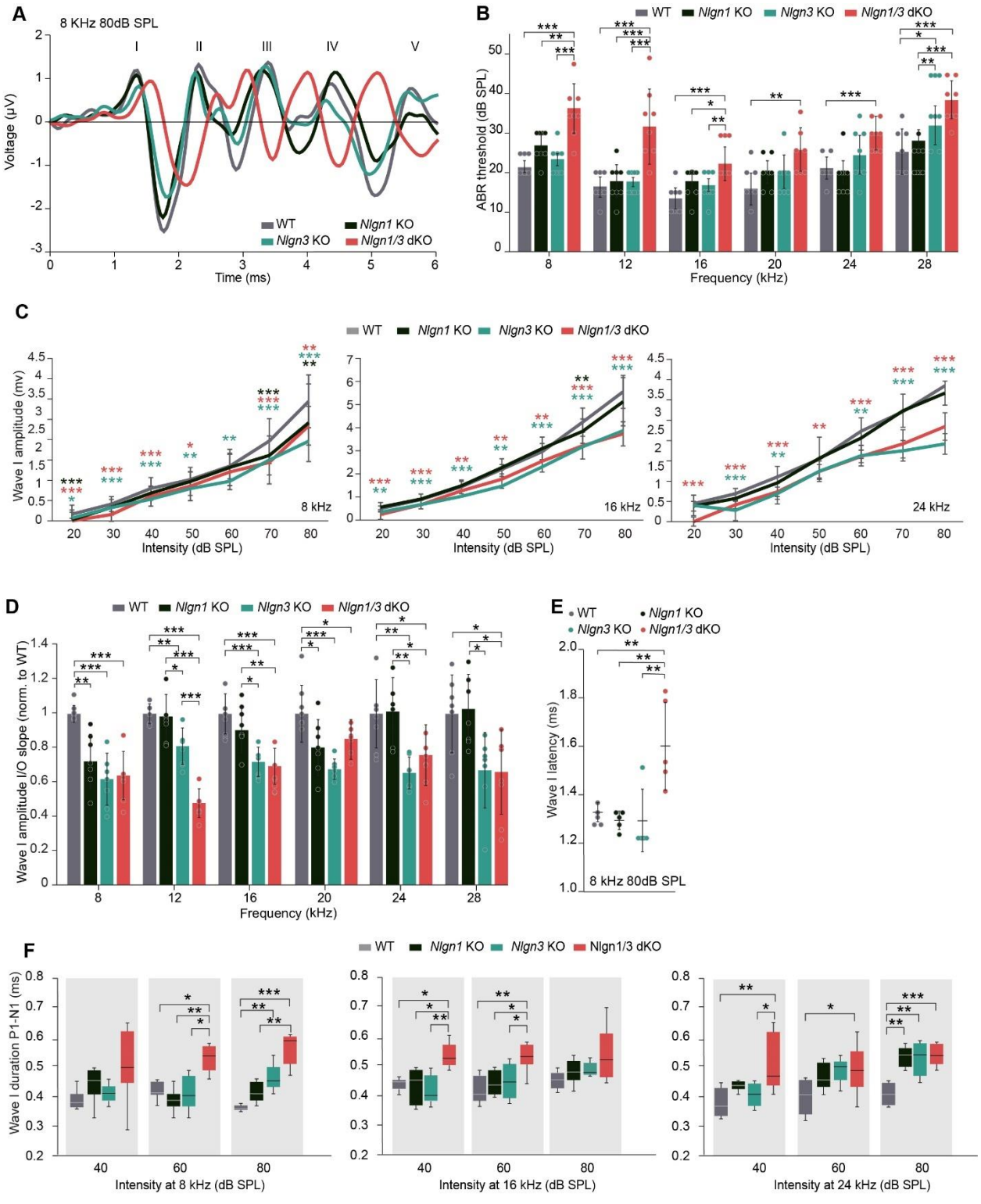
A
8 KHz 80dB SPL
I
II
III
IV
V
Voltage (μV)
Time (ms)
WT
Nlgn1 KO
Nlgn3 KO
Nlgn1/3 dKO
B
ABR threshold (dB SPL)
Frequency (kHz)
C
Wave I amplitude (mv)
Intensity (dB SPL)
8 kHz
16 kHz
24 kHz
D
Wave I amplitude I/O slope (norm. to WT)
Frequency (kHz)
E
Wave I latency (ms)
8 kHz 80dB SPL
F
Nlgn1/3 dKO
Wave I duration P1-N1 (ms)
Intensity at 8 kHz (dB SPL)
Intensity at 16 kHz (dB SPL)
Intensity at 24 kHz (dB SPL)

Figure 14. Nlgn1 and 3 are required for cochlear function. (A) Representative ABR waveforms at 8 kHz and 80 dB SPL by genotype. Wave-I amplitude was measured peak to trough; latency was measured from sound onset to peak-I; duration was measured as time from peak-I to trough-I. **(B)** Quantification reveals ABR thresholds were largely unaffected in either *Nlgn1* or *Nlgn3* KOs compared to WT. *Nlgn3* KOs had elevated threshold levels only at 28 kHz (WT: 25 ± 6.0 dB SPL, *Nlgn3* KO: 33 ± 6.6 dB SPL). *Nlgn1/3* dKO mice had significantly elevated thresholds at all tested frequencies. **(C)** Growth response curves for 8, 16, and 24 kHz from 20-80 dB SPL show significant reduction in ABR responses predominantly between *Nlgn3* KO and *Nlgn1/3* dKOs compared to WT. Wave I amplitude at **8 kHz** 80 dB SPL: WT 3.6 ± 0.31 μv, *Nlgn1* KO 2.9 ± 0.66 μv, *Nlgn3* KO 2.2 ± 0.45 μv, *Nlgn1/3* dKO 2.71 ± 0.73 μv. Wave I amplitude at **16 kHz** 80 dB SPL: WT 6.0 ± 0.58 μv, *Nlgn1* KO 5.4 ± 1.01 μv, *Nlgn3* KO 3.9 ± 0.25 μv, *Nlgn1/3* dKO 3.8 ± 0.53 μv. Wave I amplitude at **24 kHz** 80 dB SPL: WT 3.7 ± 0.38 μv, *Nlgn*1 KO 3.5 ± 0.55 μv, *Nlgn3* KO 2.1 ± 0.33 μv, *Nlgn1/3* dKO 2.6 ± 0.43 μv **(D)** Quantification of the ABR Wave-I I/O slope functions across 20-80 dB SPL stimuli range demonstrated reduced synaptic responses in *Nlgn3* KO and *Nlgn1/3* dKO mice, which were reduced on average across the tested frequencies by 30.9 ± 12.0% and 32 ± 14% respectively. *Nlgn1* KO mice have reduced responses only at the 8 kHz region by 28 ± 16%. **(E)** Wave-I latency was significantly increased in dKO mice compared to *Nlgn1* KO, *Nlgn3* KO, or WT mice (*Nlgn1/3* dKO: 1.6 ± 0.18 ms, WT: 1.3 ± 0.04 ms, *Nlgn1* KO: 1.3 ± 0.13 ms, *Nlgn3* KO: 1.3 ± 0.13 ms). **(F)** Wave-I durations at 80 dB SPL for 8 and 28 kHz are lengthened in *Nlgn1/3* dKO compared to WT mice (8 kHz: WT 0.37 ± 0.01 ms, *Nlgn1* KO 0.42 ± 0.04 ms, *Nlgn3* KO 0.47 ± 0.05 ms, *Nlgn1/3* dKO 0.53 ± 0.14 ms; 24 kHz: WT 0.41 ± 0.04 ms, *Nlgn1* KO 0.53 ± 0.03 ms, *Nlgn3* KO 0.53 ± 0.06 ms, *Nlgn1/3* dKO 0.56 ± 0.03 ms). Data are represented as mean ± SD. *

= p value < 0.05, ** = p value < 0.01, *** = p value < 0.001 by one-way ANOVA with Tukey post hoc correction. (* WT vs dKO, * WT vs *Nlgn1*, and * WT vs *Nlgn3*). N = 8 mice for (A-D), 5 mice for (E-F) at P60-65 per genotype. (mean ± SD).

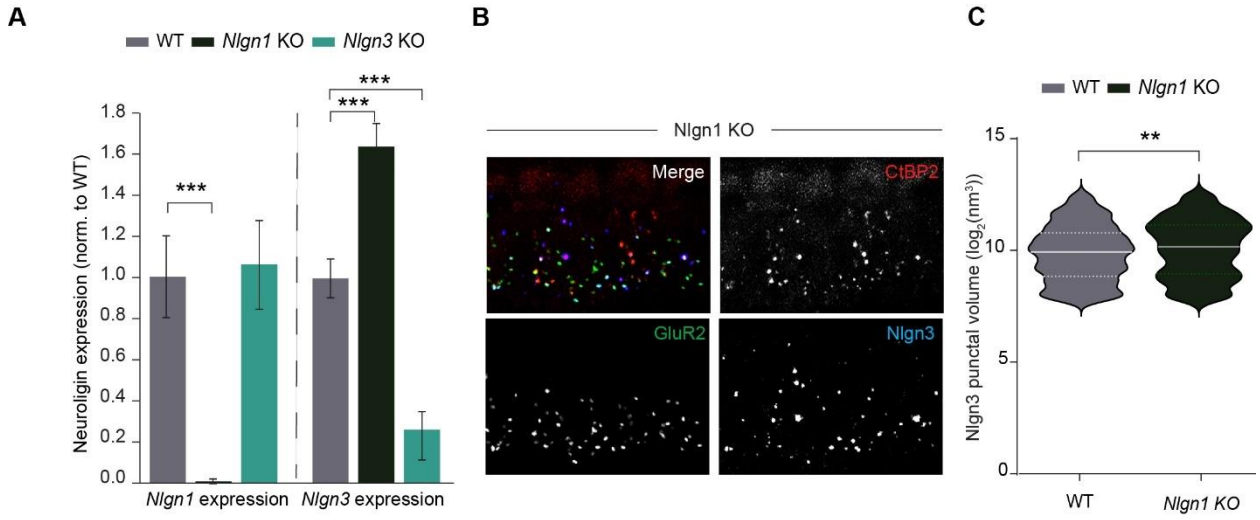
A
WT
Nlgn1 KO
Nlgn3 KO
Neuroligin expression (norm. to WT)
1.8
1.6
1.4
1.2
1.0
0.8
0.6
0.4
0.2
0.0
***
***
***
Nlgn1 expression
Nlgn3 expression
B
Nlgn1 KO
Merge
CtBP2
GluR2
Nlgn3
C
WT
Nlgn1 KO
Nlgn3 punctal volume (log2(nm3))
15
10
5
0
**
WT
Nlgn1 KO

Figure 15. *Nlgn3* is overexpressed in *Nlgn1* KO cochlea. (A) qPCR analysis of *Nlgn1* and *Nlgn3* gene expression from *Nlgn1* and *Nlgn3* KO cochlea normalized to WT. Left: *Nlgn1* gene expression levels were unaltered in *Nlgn3* KO cochlea (1.08 $\pm$ 0.22) and significantly reduced in *Nlgn1* KO cochlea (0.007 $\pm$ 0.005). Right: *Nlgn3* gene expression was significantly elevated in *Nlgn1* KO cochlea (1.7 $\pm$ 0.02) and significantly reduced in *Nlgn3* KO cochlea (0.026 $\pm$ 0.31). N = 8 mice at P60 per genotype. **(B)** Representative images of cochlear wholemounts stained with Nlgn3 colocalized with cochlear ribbon markers CtBP2 (red) and GluA2 (green) collected from *Nlgn1* KO cochlea. **(C)** Quantification of (B) demonstrated that Nlgn3 puncta are generally larger in *Nlgn1* KO cochlea compared to WT cochlea (9.877 $\pm$ 1.57μm^3 WT vs 10.09 $\pm$ 1.71μm^3 *Nlgn1* KO). Data is represented as mean $\pm$ SD, *** = p value < 0.001 by one-way ANOVA with Tukey post hoc correction.

Mice lacking Nlgn1 or Nlgn3 are highly sensitive to loud noise

Given that neuroligins function as trans-synaptic adhesion proteins, I hypothesized that *Nlgn1* or *Nlgn3* KO cochlea would be more sensitive to acoustic trauma compared to WT controls. Young adult mice were exposed to band-pass-filtered white noise (6–18 kHz) for 30 min at 94 dB SPL (Jongkamonwiwat et al., 2020). ABR were measured before and 1, 7, and 14 days after noise exposure (DAN). Notably, comparison of background strains demonstrated no significant differences with respect to sensitivity to noise induce hearing loss at this intensity **(Figure 16 A-B).** As expected, this noise insult resulted in a significant threshold shift of ~20–30 dB at 16 and 24 kHz but only a 2 dB shift at 8 kHz 1 DAN in WT mice. However, at 14 DAN ABR thresholds fully recovered to pre-noise exposure levels at 8, 16, and 24 kHz **(Figure 17A)**. Both *Nlgn1* and *Nlgn3* KOs had significant threshold shifts 1DAN compared to WT at 8 kHz **(Figure 17A-C)**. Strikingly, *Nlgn3* KOs failed to generate a Wave I response at 80 dB SPL above 24 kHz and on average exhibited a 43 $\pm$ 12 dB shift at 16 kHz **(Figure 17C)**. At 14 DAN *Nlgn1* KO thresholds fully recovered with a non-significant 6.7 $\pm$ 5.1 dB residual shift **(Figure 17B)**. Contrarily, *Nlgn3* KOs had only a very limited recovery at 24 kHz 14 DAN with an average threshold shift of 29 $\pm$17 dB.

To determine if cochleae lacking Nlgn1 or Nlgn3 have hampered Wave I amplitudes 14 DAN relative to before noise. Comparison of Wave I amplitudes (80 dB SPL stimuli) relative to before noise revealed a gradual recovery of cochlear output in WT mice, which largely recovered to baseline levels 14 DAN at 8, 16 and 24 kHz **(Figure 17D)**. For *Nlgn1* KO, the only frequency range that failed to fully recover was 8 kHz which on average had a 22 $\pm$ 11% reduction in synaptic strength compared to before noise **(Figure 17E)**. Consistent with the dramatic threshold

shifts in *Nlgn3* KO mice **(Figure 17C)**, Wave I amplitudes failed to recover at 16 kHz and 24 kHz even 14 DAN, while at 8 kHz amplitudes fully recovered **(Figure 17F)**. Next, I performed IF analysis across the 20-24 kHz region 14 DAN to determine if a reduction in synapse density underlies the weakening of Wave I response in *Nlgn3* KO **(Figure 17G)**. On average, WT inner hair cell contained 15 $\pm$ 0.84 ribbon synapses compared to 14 $\pm$ 0.51 ribbon synapses in *Nlgn1* KOs. Synaptic density across this region of the cochlea was significantly reduced in *Nlgn3* KOs, on average inner hair cells contained only 4.2 $\pm$ 1.4 ribbon synapses **(Figure 17H)**. Taken together, Nlgn3 plays a far more critical role in maintaining cochlear ribbon synapse structure and function following exposure to loud noise compared to Nlgn1.

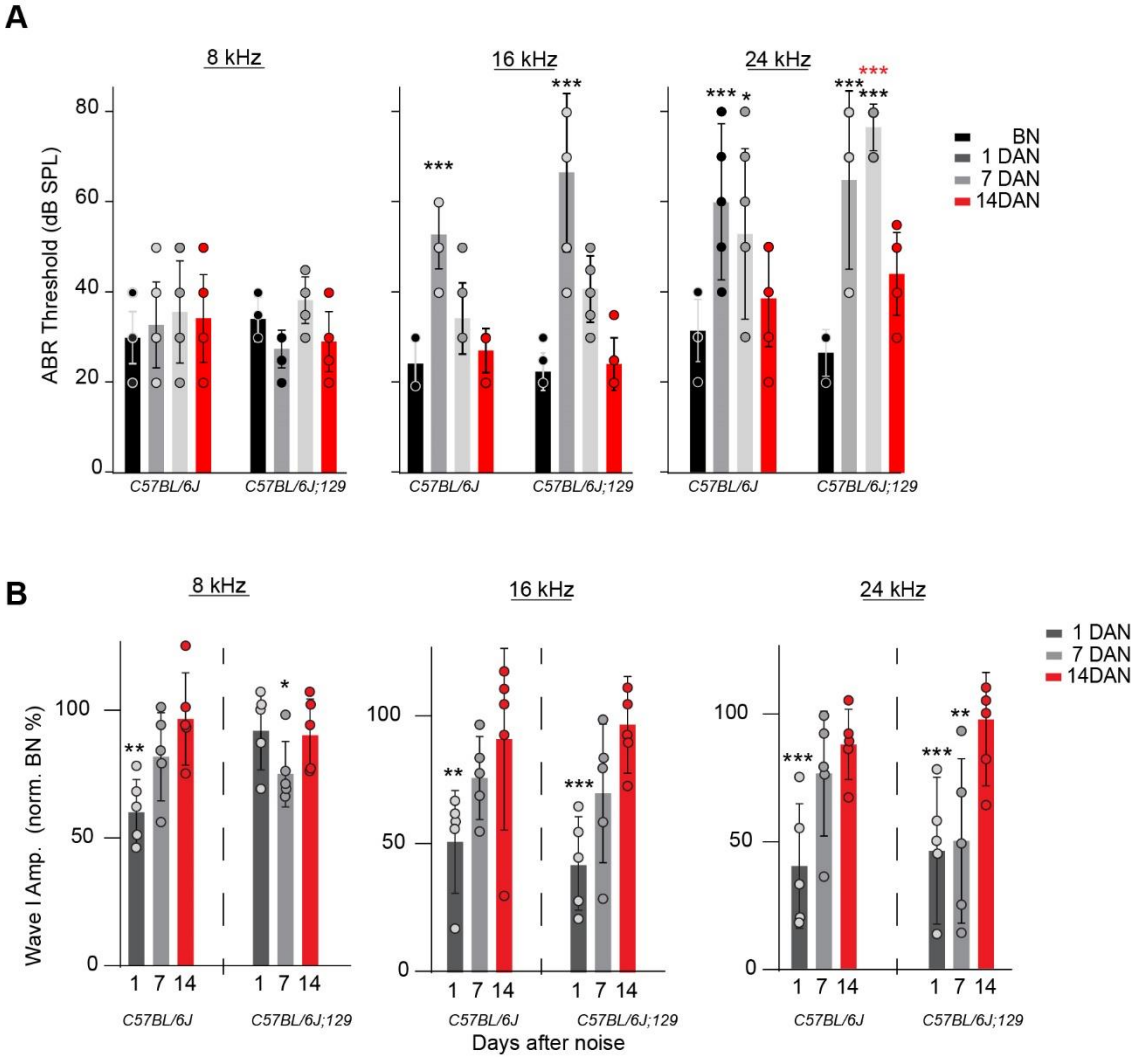
A
8 kHz
16 kHz
24 kHz
ABR Threshold (dB SPL)
0
20
40
60
80
BN
1 DAN
7 DAN
14DAN
C57BL/6J
C57BL/6J;129
B
Wave I Amp. (norm. BN %)
0
50
100
1 7 14
Days after noise

Figure 16. Nlgn1 KO and Nlgn3 KO background strains observe comparable susceptibility to noise and recovery. (A) ABR thresholds fully recovered to before noise (BN) threshold levels by 14 DAN at **8 kHz** (**C57BL/6J**: BN= 30 ± 7.0 dB SPL, 1 DAN= 32 ± 11.0 dB SPL, 7 DAN= 36 ± 13.4 dB SPL, 14 DAN= 30 ± 7.1 dB SPL; **C57BL/6J; 129**: BN= 27 ± 4.2 dB SPL, 1 DAN= 34 ± 5.0 dB SPL, 7 DAN= 38 ± 5.7 dB SPL, 14 DAN= 29 ± 6.6 dB SPL), **16 kHz** (**C57BL/6J**: BN= 26 ± 5.5 dB SPL, 1 DAN= 56 ± 5.5 dB SPL, 7 DAN= 36 ± 8.9 dB SPL, 14 DAN= 30 ± 0.1 dB SPL; **C57BL/6J; 129**: BN= 23 ± 4.2 dB SPL, 1 DAN= 66 ± 17.5 dB SPL, 7 DAN= 43 ± 5.7 dB SPL, 14 DAN= 24 ± 5.8 dB SPL), and **24 kHz** (**C57BL/6J**: BN= 32 ± 11.4 dB SPL, 1 DAN= 68 ± 13.0 dB SPL, 7 DAN= 54 ± 13.4 dB SPL, 14 DAN= 36 ± 18.2 dB SPL; **C57BL/6J; 129**: BN= 27 ± 5.2 dB SPL, 1 DAN= 65 ± 20.0 dB SPL, 7 DAN= 78 ± 4.4 dB SPL, 14 DAN= 44 ±9.2 dB SPL) after 30 minute exposure to 94 dB SPL in both background strains. **(B)** Wave I amplitudes in response to 80 dB SPL stimulation fully recovered to BN amplitudes across WT mice 14 DAN (**8 kHz**: 97 ± 3.4% vs 92 ± 15.1%, **16kHz**: 92 + 16 vs 98 ± 8%, **24 kHz**: 88 ± 5.3% vs 98 ± 12%). Data are represented as mean ± SEM. * = p value < 0.05, ** = p value < 0.01, *** = p value < 0.001 by one-way ANOVA with Tukey post hoc correction.

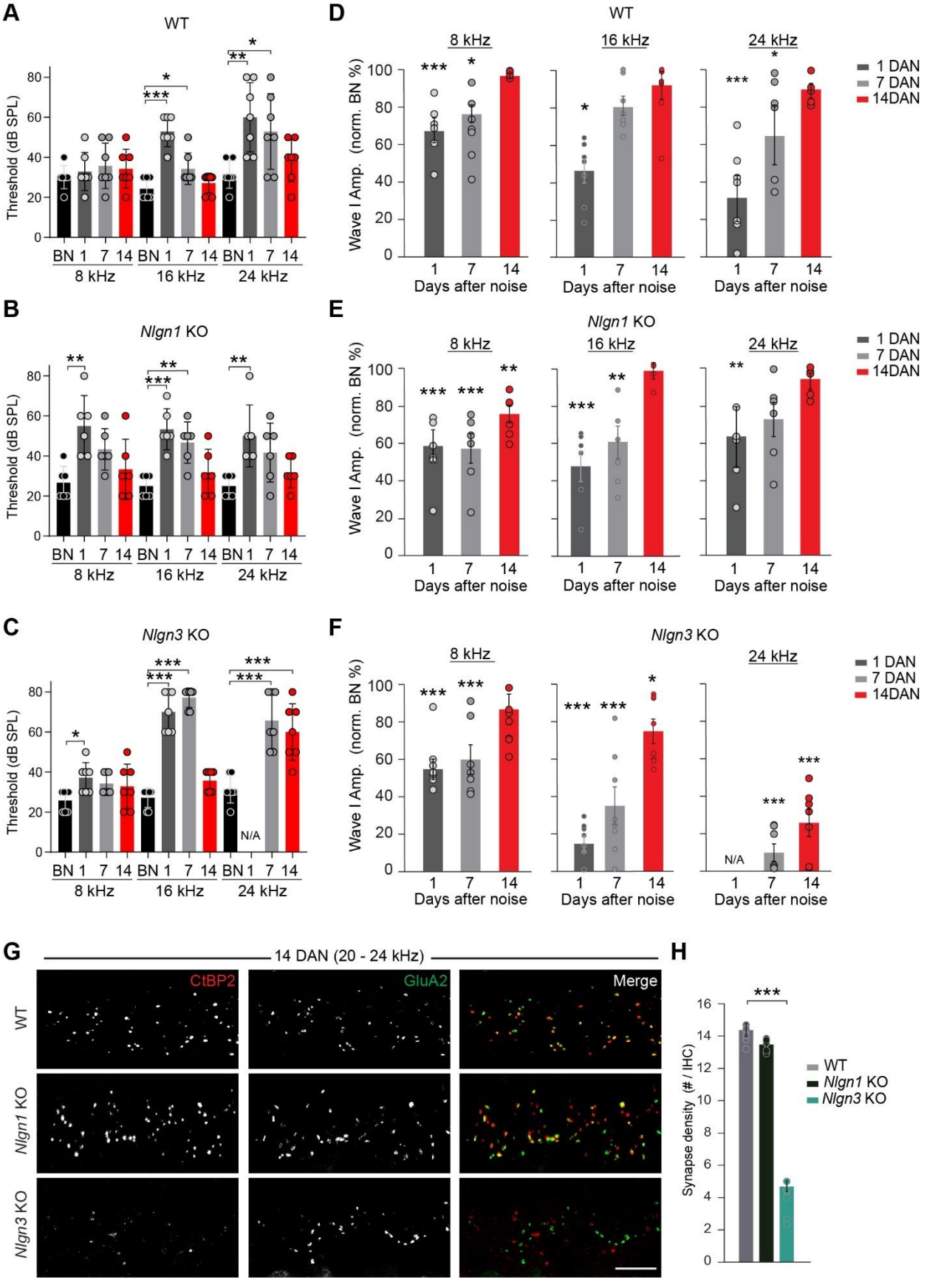
A
WT
Threshold (dB SPL)
BN 1 7 14 BN 1 7 14 BN 1 7 14
8 kHz
16 kHz
24 kHz
B
Nlgn1 KO
C
Nlgn3 KO
N/A
D
WT
8 kHz
16 kHz
24 kHz
Wave I Amp. (norm. BN %)
1 7 14
Days after noise
1 DAN
7 DAN
14DAN
E
Nlgn1 KO
F
Nlgn3 KO
G
14 DAN (20 - 24 kHz)
CtBP2
GluA2
Merge
WT
Nlgn1 KO
Nlgn3 KO
H
Synapse density (# / IHC)
WT
Nlgn1 KO
Nlgn3 KO

Figure 17. *Nlgn3* KOs have increased sensitivity to noise. (A) In WT mice: ABR thresholds fully recovered to before noise threshold levels by 14 DAN at 8 kHz (BN= 30 ± 5.8 dB SPL, 1 DAN= 33 ± 9.5 dB SPL, 7 DAN= 36 ± 11 dB SPL, 14 DAN= 34 ± 9.8 dB SPL), 16 kHz (BN= 24 ± 5.3 dB SPL, 1 DAN= 52 ± 7.5 dB SPL, 7 DAN= 34 ± 7.9 dB SPL, 14 DAN= 27 ± 4.8 dB SPL), and 24 kHz (BN= 31 ± 6.8 dB SPL, 1 DAN= 60 ± 17.3 dB SPL, 7 DAN= 52 ± 18.9 dB SPL, 14 DAN= 38 ± 10.7 dB SPL) after 30 minute exposure to 94 dB SPL. **(B)** In *Nlgn1* KO mice: ABR thresholds fully recovered to before noise threshold levels by 14 DAN at 8 kHz (BN= 26 ± 8.16 dB SPL, 1 DAN= 55 ± 15.2 dB SPL, 7 DAN= 43 ± 10.3 dB SPL, 14 DAN= 32 ± 15.0 dB SPL), 16 kHz (BN= 25 ± 5.47 dB SPL, 1 DAN= 53 ± 10.3 dB SPL, 7 DAN= 47 ± 10.3 dB SPL, 14 DAN= 32 ± 7.5 dB SPL), and 24 kHz (BN= 25 ± 5.47 dB SPL, 1 DAN= 50 ± 15.5 dB SPL, 7 DAN= 42 ± 14.7 dB SPL, 14 DAN= 31 ± 7.5 dB SPL). **(C)** In *Nlgn3* KO mice: ABR thresholds fully recovered to before noise threshold levels by 14 DAN at 8 kHz (BN= 27 ± 4.9 dB SPL, 1 DAN= 56 ± 16 dB SPL, 7 DAN= 34 ± 5.3 dB SPL, 14 DAN= 60 ± 11 dB SPL) and 16 kHz (BN= 27 ± 4.9 dB SPL, 1 DAN= 70 ± 10.0 dB SPL, 7 DAN= 66 ± 14 dB SPL, 14 DAN= 35 ± 5.3 dB SPL) but failed to recover to BN thresholds at 24 kHz (BN= 31 ± 6.9 dB SPL, 1 DAN= N/A, 7 DAN= 77 ± 4.9 dB SPL, 14 DAN= 60 ± 14 dB SPL). **(D-F)** Wave I amplitudes in response to 80 dB SPL stimulation fully recovered to BN amplitudes across WT mice 14 DAN (8 kHz = 97 + 3.4%, 24 kHz = 88 ± 5.3%). Conversely, *Nlgn1* KOs remained dramatically reduced and never recovered to baseline levels 14 DAN at 8 kHz (77 ± 11%) and *Nlgn3* KOs failed to recover at 24 kHz (26 ± 20%). **(G)** Representative images from WT, *Nlgn1* KO, and *Nlgn3* KO cochlear wholemounts from P60-65 mice 14 DAN, immunostained with antibodies for ribbon synapses. **(H)** Quantification of (G) revealed *Nlgn3* KOs had significantly disorganized pre- and postsynaptic elements with a relative reduction of 75 ± 1.4% compared to

synapse density before noise exposure. Synaptic density in WT and *Nlgn1* KO cochlea had no significant difference 14 DAN. Data are represented as mean ± SD. * = p value < 0.05, ** = p value < 0.01, *** = p value < 0.001 by one-way ANOVA with Tukey post hoc correction. N = 7 mice for (A-F), 5 mice for (G-H) at P60-65 per genotype.

Chapter 5: Cochlear Proteome Remodeling After Noise

Disclaimer: This chapter has been adapted from "Noise Exposures Causing Hearing Loss Generate Proteotoxic Stress and Activate the Proteostasis Network" by Jongkamonwiwat and Ramirez et al, published in Cell Reports with permission from co-first author Nopporn Jongkamonwiwat. Cell Reports is an open-source publisher where authors retain copyrights to their own work.

Citation: Jongkamonwiwat N, Ramirez MA, Edassery S, Wong ACY, Yu J, Abbott T, Pak K, Ryan AF, Savas JN. Noise Exposures Causing Hearing Loss Generate Proteotoxic Stress and Activate the Proteostasis Network. Cell Rep. 2020 Nov 24;33(8):108431. doi: 10.1016/j.celrep.2020.108431. PMID: 33238128; PMCID: PMC7722268.

Introduction

Exposure to moderately loud noises for extended periods of time hamper synaptic communication between hair cells and SGN, collectively referred to as ribbon synapses, which drives feedback inhibition through olivocochlear efferent nerve fibers (Kujawa and Liberman, 2009; Lin et al., 2011). During noise exposure the SGN terminals dramatically swell as a preventative measure against further damage. The physical uncoupling of the presynaptic hair cell ribbon from the postsynaptic terminal impairs hearing but protects the neuron against overstimulation and excitotoxicity (Shi et al., 2016). Moreover, this swelling is reversible and subsides within a few days after exposure (Robertson, 1983). However, following exposure to higher intensity noises cochlea synaptopathy has been shown to occur, leading to a permanent loss of up to half of inner hair cell ribbon synapses (Kujawa and Liberman, 2009; Ruel et al., 2007).

Synapse loss is often seen as the culmination of various cellular mechanisms responsible for noise induced hearing loss, but it is not always driven by the same underlying pathway following noise. For example, overstimulation can trigger metabolic decompensation resulting in the swelling of nuclei and mitochondria and cytoplasmic vesiculation (Kim et al., 2014). Moderately intense noise, namely those above 105 dB SPL, will predominantly affect the organization of the stereocilia bundles, the presynaptic hair cell ribbons, and ANF terminals (Liberman, 2017). Furthermore, this level of exposure can reduce cochlear blood flow, ultimately triggering anoxia and eventually cell death (Cheng et al., 2005; Le Prell et al., 2007; Strimbu et al., 2019). Although not as immediately destructive, the prolonged exposure to lower intensity noise exposures is also hazardous to hearing, due to the loss of synapses which results from the high metabolic demand associated with continued signaling, generation of free radicals and

eventual excitotoxicity (Le Prell *et al.*, 2007; Lu et al., 2014; Maulucci et al., 2014). Given that noise induced hearing loss (NIHL) is the primary cause of acquired hearing loss in the industrialized world (Carter et al., 2014; Saunders and Griest, 2009). It is critical that we gain further insight into the cellular mechanisms underlying noise induced trauma and more importantly how the cochlear proteome is altered under conditions where recovery is possible.

To this end, the following chapter will outline our investigation of noise induced changes to the cochlear proteome. In brief, we found that noise exposure drives the accumulation of hundreds of proteins in an intensity dependent manner. Notably, we revealed one of the first instances of a dose dependent elevation of proteostasis factors, including nearly the entire proteasome, and many protein chaperones in response to noise. Independent proteomic and biochemical analysis confirmed that exposure to intense noise triggers a cochlear protein quality control response. Utilizing Immunofluorescence (IF), we determined that a panel of proteins, which are altered after noise exposure, are expressed by HCs, SGNs, and additional cochlear cells. RNA sequencing (RNA-Seq) analysis revealed that a subset of genes encoding proteins with elevated fold change also have increased expression after exposure to moderate or severe intensity noise. Proteome-wide analysis of cochlear protein ubiquitylation revealed several proteins which were selectively modified on lysine residues following exposures to moderate and severe levels of noise exposure. Finally, we measured the cochlear proteome after two weeks of recovery and found that nearly the entire ribosome had elevated fold change after exposure to moderate intensity noise. Indicating that protein synthesis is a contributor to threshold recovery and suggesting that noise exposures causing hearing loss accelerates protein turnover.

Results

Short-Term Noise Exposure Result in Temporary and Permanent Hearing Loss in Mice

Damage accumulated after noise exposures is largely dependent on the level and duration of the exposure. Additionally, resistance to NIHL is not uniform across mouse lines, to this extent we first needed to determine the degree of hearing loss that would results from our exposure intensities in FVB mice. Broadly, noise exposure brings about an acute yet transient attenuation of hearing sensitivity, referred to as a temporary threshold shift (TTS), this decrease in auditory sensitivity lasts for a period of days to weeks. In contrast, more severe auditory insults result in a permanent threshold shift (PTS) leading to partial or complete sensorineural hearing loss. In laboratory settings, threshold shifts that fail to completely recover to pre-noise levels after 2 - 4 weeks are generally considered permanent in rodents (Kujawa and Liberman, 2006; Liberman, 2016; Ryan et al., 2016).

Considering this, we set out to advance our understanding of how auditory overstimulation drives cochlear synaptopathy by first using cochlear functional assays to determine the degree of temporary and permanent hearing loss that results following noise exposures. Young adult FVB mice were exposed to 6-18 kHz octave noise for 30 minutes at three intensity levels, ambient (65-70 dB SPL), moderate (94 dB SPL), or severe (105 dB SPL), respectively **(Figure 18)**. ABR for tone and click, as well as DPOAE were performed before noise, and then 1, 7, and 14 days after noise exposure to determine the overall health of the cochlea and degree of hearing recovery. We found that mice exposed to ambient noise had only a slight increase in ABR thresholds one-day after noise exposure **(Figure 18A-B**). Wave I amplitude, indicative of synaptic strength between inner hair cells and SGNs, was also

unaffected after this level of noise **(Figure 18D)**. Moreover, we determined that mice in the moderate noise exposures condition demonstrated significant recovery after seven days with near-complete recovery of hearing thresholds after two weeks **(Figure 18E-H)**. The severe noise exposure condition caused significant elevations in threshold levels by both DPOAE and ABR analyses **(Figure 18I-L)**. Wave I amplitudes were also significantly reduced, with minimal recovery after two weeks, suggesting a high degree of permanent damage. In summary, 30-minute exposures at ambient noise (70 dB SPL) cause negligible hearing impairments, exposure to moderate noise (94 dB SPL) result in an almost exclusively TTS, while exposure to severe noise (105 dB SPL) results in predominantly a PTS.

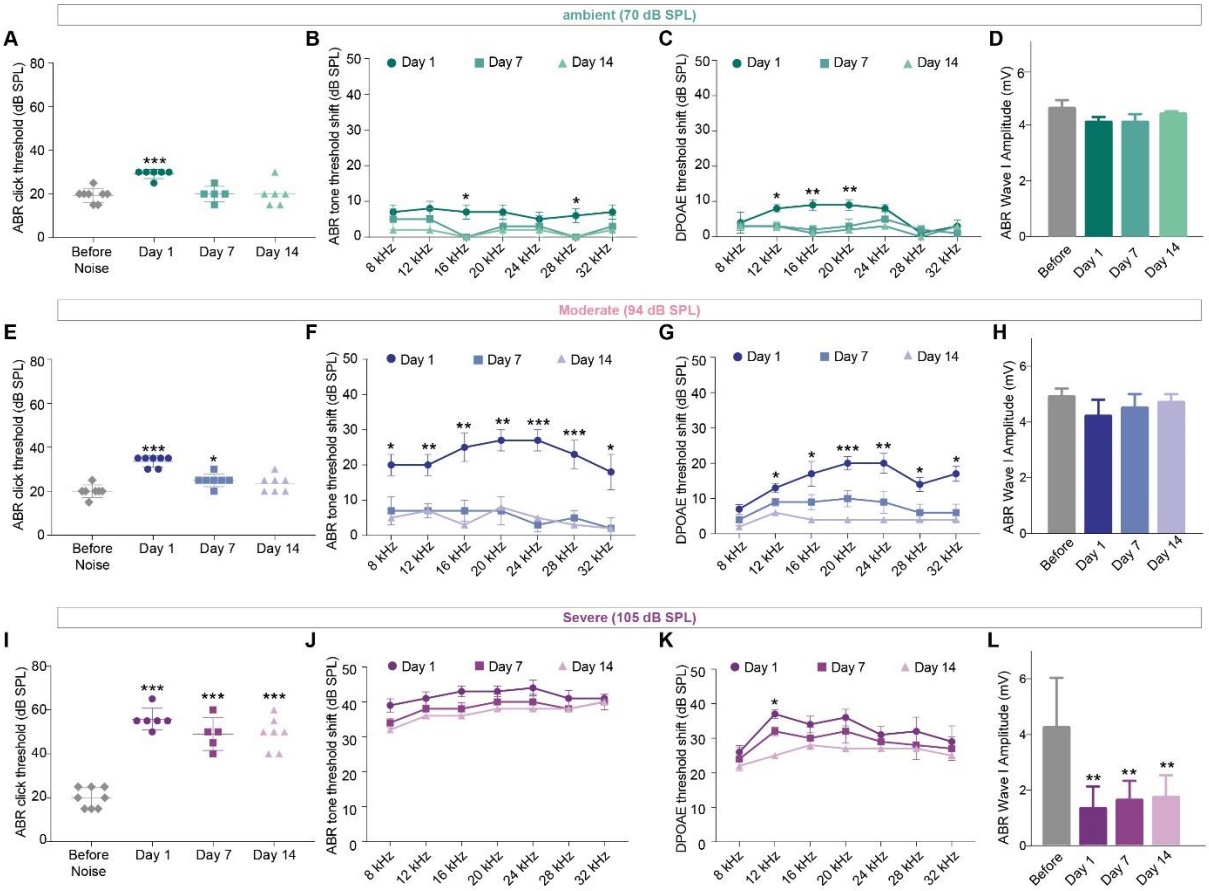
ambient (70 dB SPL)
A
B
C
D
ABR click threshold (dB SPL)
ABR tone threshold shift (dB SPL)
DPOAE threshold shift (dB SPL)
ABR Wave I Amplitude (mV)
Before Noise
Day 1
Day 7
Day 14
8 kHz
12 kHz
16 kHz
20 kHz
24 kHz
28 kHz
32 kHz
Before
Moderate (94 dB SPL)
E
F
G
H
Severe (105 dB SPL)
I
J
K
L

Figure 18. ABR and DPOAE cochlear functional assays to determine responses in FVB mice after 30 minutes of exposure to ambient, moderate, or severe noise (8-16 kHz). (A) ABR click **(B)** ABR tone **(C)** DPOAE and **(D)** Wave I amplitude of ABR click at 80 dB SPL stimulus after indicated recovery periods after noise exposure at 70 dB SPL level. The measurements show minimal shifts from baseline recordings most apparently one day after noise exposure with a return to baseline at day 7. **(E)** After 94 dB SPL noise exposure, level of ABR click threshold was significantly higher than before noise exposure. However, threshold shifts fully recovered to baseline levels by day 7. **(F)** ABR tone and **(G)** DPOAE threshold shifts had similar recovery patterns to ABR click. **(H)** ABR click wave I amplitude is not significantly reduced. **(I)** At 105 dB SPL, our highest level of noise exposure, there was a dramatic increase in the threshold level of up to 50 dB in ABR click. **(J)** ABR tone and **(K)** DPOAE also revealed a strong threshold shift with a limited recovery capacity even 14 days after noise exposure, especially in the high frequency range. **(L)** Wave I amplitude was significantly reduced more than 50% compared to before noise exposure, with limited recovery that failed to reach the before noise levels. * = p value < 0.05, ** = p value < 0.01, *** = p value < 0.001 by one-way ANOVA with Bonferroni correction.

Confirmation that noise exposure unbalances the cochlear proteome

To assess how the abundance of cochlea proteins are modulated by exposures to moderate or severe noise, relative to ambient conditions, we performed two 10-plex TMT experiments (Rauniyar and Yates, 2014) **(Figure 19A)**. In each experiment we exposed three mice to moderate noise (94 dB SPL), three mice to severe noise (105 dB SPL), and four mice to ambient noise (65-70 dB SPL). TMT channel peak intensities were assessed and determined similar levels across the 10 channels in both experiments, demonstrating efficient and reproducible chemical labeling, thus allowing for the comparison of relative protein abundances to be made **(Figure 19B)**. Similarly, we determined that experimental conditions tended to group with likewise experimental conditions based on protein abundance correlation plots **(Figure 19C)**. In both TMT experiments we quantified more than 3,500 proteins across the biological replicates. The relative distribution of protein abundance was significantly elevated in cochlear lysates collected from mice exposed to moderate versus ambient levels of noise **(Figure 19D)**. Furthermore, the global fold change (i.e. moderate or severe relative to the ambient controls) of the significantly altered proteins, was skewed towards proteins with higher ratios **(Figure 19E-F)**. Among the proteins with significantly elevated fold changes were cytoskeletal, heat shock, and proteasome protein subunits. Conversely, multiple collagen proteins we found to have reduced fold change **(Figure 20A)**.

Next, we plotted the relative protein fold change for the 147 proteins found significantly altered in our TMT experiments with those found significantly regulated in an independent ^{15}N analyses of noise dependent cochlear remodeling **(Figure 20B)**. Out of the 147 proteins found significantly altered by both quantitative proteomic strategies, three-quarters of the proteins with

elevated levels and two-thirds of those with reduced levels followed the same fold change trends in both the TMT and ^{15}N analyses **(Figure 20C)**. To further validate the trends observed by our proteomic analysis we next assessed the absolute abundance of actin binding protein Tpm1 and the fibrillary protein Col1a1, which were shown to have elevated and reduced fold changes, respectively. We obtained chemically synthesized peptides containing heavy labeled C-terminal arginine residues that were quantified with spectrophotometry (Li et al., 2015). The digested peptides were then spiked into digested cochlear extracts from mice exposed to ambient, moderate, or severe levels of noise for LC-MS/MS analysis. Indeed, these experiments supported our previous findings, confirming elevated or reduced levels for Tpm1 and Col1a1, respectively **(Figure 20D)**.

Given the intensity dependent changes to relative protein abundance, we next asked how the cochlear proteome differs after moderate exposures compared to severe exposures via TMT **(Figure 21A)**. Within this analysis we quantified more than 2,300 proteins and found a majority of the significantly quantified proteins had elevated rather than reduced fold changes (i.e. the ratio of severe / moderate levels > 1 compared to proteins with ratios < 1) **(Figure 21B)**. Among significantly regulated proteins with fold change ratios less than one (severe / moderate), indicative of enrichment in the moderate exposure condition, were Ckm, Tnni2, Tnnc2, and Myh8 **(Figure 21C)**. Interestingly, creatine kinase actively mitigates the consumption of ATP by damping its hydrolysis with elevated levels of Ckm being indicative of inflammation and underlying injury (Hettling and van Beek, 2011). Tnni2, Tnnc2, and Myh8 are all involved in force regulation, suggesting the need to mitigate force generations during moderate exposures, which are curiously not observed under severe exposures **(Figure 21C)**. Pvalb, a calcium-

binding albumin protein, which has been seen to accumulate in swollen terminals after noise exposure, was also shown to have a significant fold change ratio less than one (severe / moderate) (Kujawa and Liberman, 2009). Together potentially highlighting damage mitigating processes associated with moderate exposures which are either absent or downregulated under severe noise exposure conditions. Numerous heat shock chaperones (e.g. Dnajb9, Dnajb1, Dnajc7, Dnaja2, Dnajc3, Hspb1, and Hspg2) and proteasome subunits (e.g. Psma2, Psmb4, Psmb7, Psmb8, Psmd9, Psmd14, and Psme3) were seen to be enriched within the severe exposure condition, i.e. having significant fold change ratios greater than one (severe / moderate), suggesting a greater need for protein stability and removal under severe conditions **(Figure 21D)**. Moreover, these findings provide independent confirmation that the cochlear proteostasis network is activated in a noise intensity dependent manner.

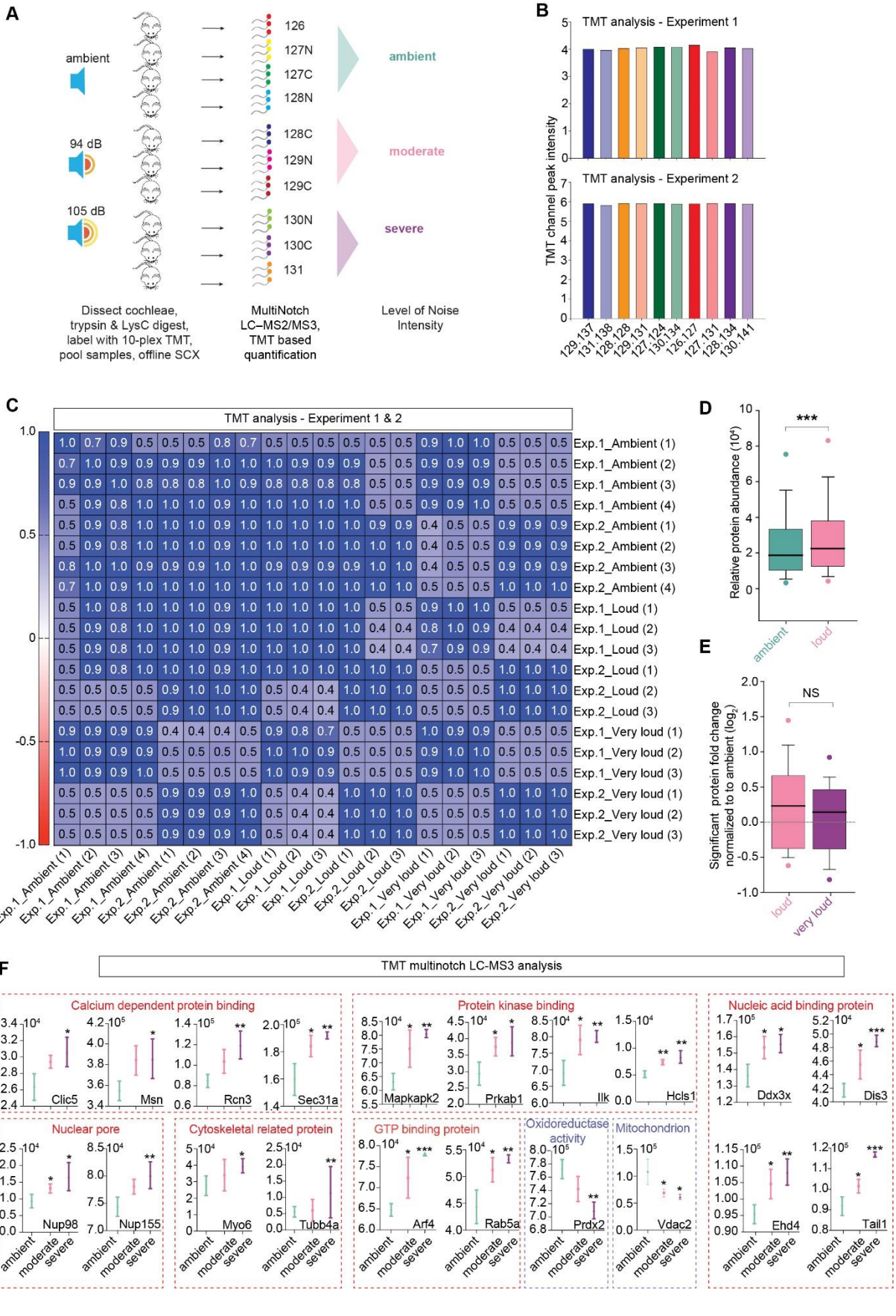
A
ambient
94 dB
105 dB
126
127N
127C
128N
128C
129N
129C
130N
130C
131
ambient
moderate
severe
Dissect cochleae, trypsin & LysC digest, label with 10-plex TMT, pool samples, offline SCX
MultiNotch LC–MS2/MS3, TMT based quantification
Level of Noise Intensity
B
TMT analysis - Experiment 1
TMT analysis - Experiment 2
TMT channel peak intensity
129.137
131.138
128.128
129.131
127.124
130.134
126.127
127.131
128.134
130.141
C
TMT analysis - Experiment 1 & 2
Exp.1_Ambient (1)
Exp.1_Ambient (2)
Exp.1_Ambient (3)
Exp.1_Ambient (4)
Exp.2_Ambient (1)
Exp.2_Ambient (2)
Exp.2_Ambient (3)
Exp.2_Ambient (4)
Exp.1_Loud (1)
Exp.1_Loud (2)
Exp.1_Loud (3)
Exp.2_Loud (1)
Exp.2_Loud (2)
Exp.2_Loud (3)
Exp.1_Very loud (1)
Exp.1_Very loud (2)
Exp.1_Very loud (3)
Exp.2_Very loud (1)
Exp.2_Very loud (2)
Exp.2_Very loud (3)
D
***
Relative protein abundance (10^4)
ambient
loud
E
NS
Significant protein fold change normalized to to ambient (log_2)
loud
very loud
F
TMT multinotch LC-MS3 analysis
Calcium dependent protein binding
Clic5
Msn
Rcn3
Sec31a
Protein kinase binding
Mapkapk2
Prkab1
Ilk
Hcls1
Nucleic acid binding protein
Ddx3x
Dis3
Nuclear pore
Nup98
Nup155
Cytoskeletal related protein
Myo6
Tubb4a
GTP binding protein
Arf4
Rab5a
Oxidoreductase activity
Prdx2
Mitochondrion
Vdac2
Ehd4
Tail1
Protein intensity
ambient
moderate
severe

Figure 19. Assessment of significantly altered proteins from TMT analyses. (A) Analysis scheme to investigate noise exposures causing hearing loss acutely influence cochleae protein levels using 9 or 10plex TMT relative quantitative proteomic analysis of mouse cochlear extracts. **(B)** Summary of individual TMT 10plex channel peak intensities prior to normalization. **(C)** Protein abundance correlation plots based on TMT ratios from 2 - 3 biological replicates exposed to ambient, moderate, or severe noise (65 – 70, 94, or 105 dB SPL). Each representative pair from ambient, moderate, or severe noise exposures were analyzed by linear regression. The correlation graphs were plotted and determined R-squared. **(D)** Summary box plot analysis for all quantified proteins from the ambient and moderate noise exposure datasets (n = 3,691 proteins). The relative protein abundance on average was significantly elevated after exposure to noise at moderate compared to ambient levels (2.87E4 $\pm$ 6.68E4, 3.28E4 $\pm$ 5.78E4, mean $\pm$ SD). Black bars indicate median. **(E)** Summary box plot analysis of significantly altered proteins (B.H. *p* value < 0.05) based on FC between moderate and severe noise exposure datasets normalized to ambient. The relative abundance of the significantly altered proteins was not significantly different between moderate and severe datasets relative to ambient (0.198 $\pm$ 0.665, 0.0437 $\pm$ 0.531, mean $\pm$ SD). Dotted line indicates protein FC = 0.0. **(F)** Selected TMT abundance plots for cytoskeletal, calcium dependant protein binding, nuclear pore, nucleic acid binding, protein kinase binding, GTP binding, oxidoreductase, and mitochondrion associated proteins with significantly elevated or reduced levels across noise exposure for 30 minutes. *** = *p* value < 0.001 by Mann-Whitney (F), * = *p* value < 0.05, ** = *p* value < 0.01, *** = *p* value < 0.001 by one-way ANOVA with Bonferroni post hoc test (F). N = 3-4 mice per group.

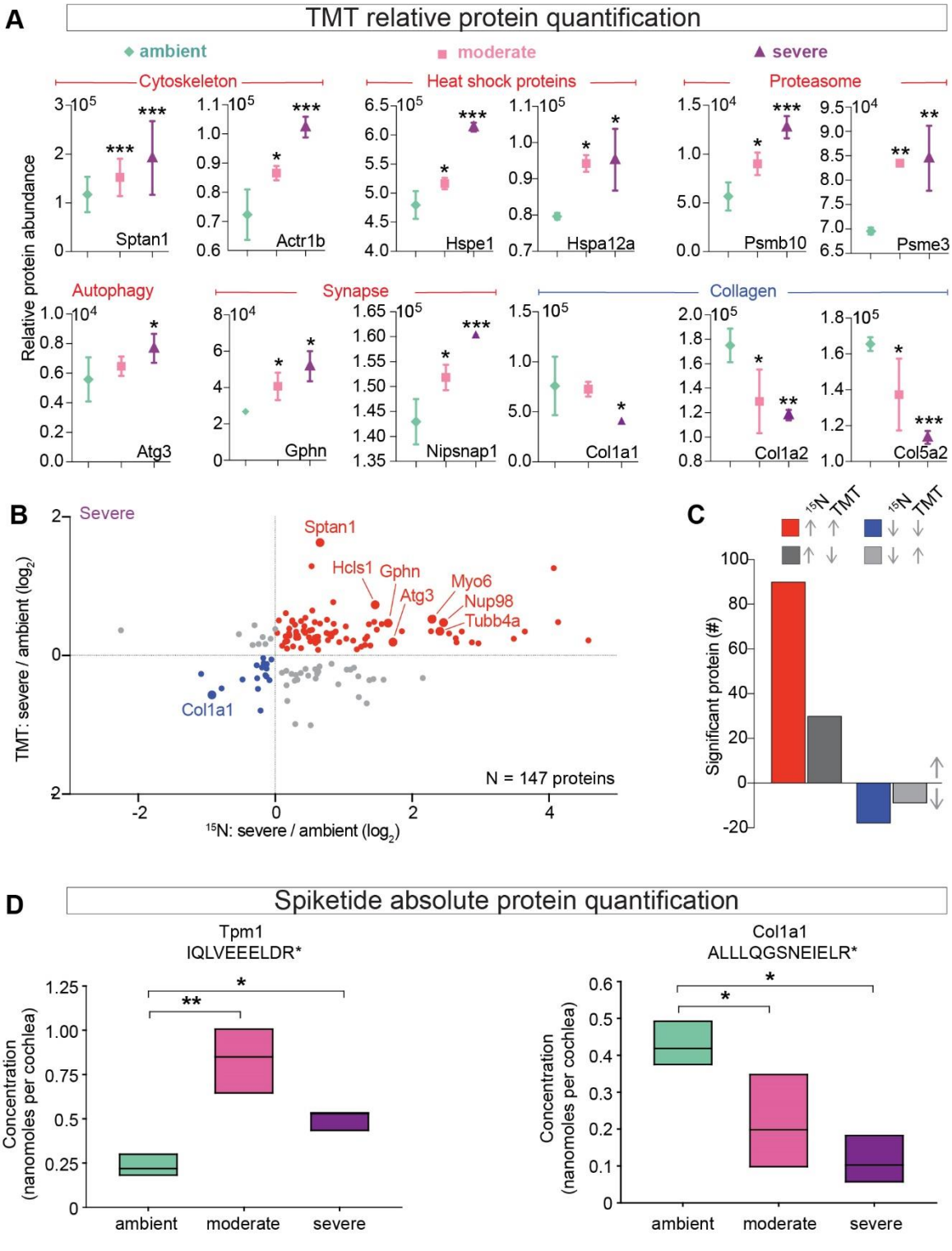
A
TMT relative protein quantification
ambient
moderate
severe
Cytoskeleton
Heat shock proteins
Proteasome
Relative protein abundance
Sptan1
Actr1b
Hspe1
Hspa12a
Psmb10
Psme3
Autophagy
Synapse
Collagen
Atg3
Gphn
Nipsnap1
Col1a1
Col1a2
Col5a2
B
Severe
Sptan1
Hcls1
Gphn
Atg3
Myo6
Nup98
Tubb4a
Col1a1
N = 147 proteins
TMT: severe / ambient (log2)
15N: severe / ambient (log2)
C
15N
TMT
Significant protein (#)
D
Spiketide absolute protein quantification
Tpm1
IQLVEEELDR*
Col1a1
ALLLQGSNEIELR*
Concentration (nanomoles per cochlea)
ambient
moderate
severe

Figure 20. Confirmation that noise exposures causing hearing loss unbalance the cochlea proteome. (A) Selected abundance plots for cytoskeletal, heat shock, proteasome, autophagy, synaptic, and collagen proteins with significantly elevated or reduced levels across noise exposures. **(B)** Comparison of individual proteins with significantly altered FC in severe ^{15}N and TMT datasets. **(C)** Summary of protein FC trends for proteins significantly altered in both ^{15}N and TMT severe datasets. Out of the 140 proteins found significantly altered by^{15}N, 66.6% proteins with reduced and 75.0% proteins with elevated levels were verified in TMT. **(D)** Absolute quantification of Tpm1 (IQLVEEELDR) and Col1a1 (ALLLQGSNEIELR) based on the ratio of light and heavy (Arg+10) peptide reconstructed MS1 chromatograms. The absolute abundance of Tpm1 was significantly elevated between moderate versus ambient and severe versus ambient (ambient = 0.233 $\pm$ 0.011, moderate = 0.834 $\pm$ 0.0417, and severe = 0.499 $\pm$ 0.0249 mean $\pm$ SD). The absolute abundance of Tpm1 was significantly reduced between moderate versus ambient and severe versus ambient (Col1a1 = ambient = 0.428 $\pm$ 0.0214, moderate = 0.215 $\pm$ 0.0107, and severe = 0.114 $\pm$ 0.00570 mean $\pm$ SD nMols / cochlea). n = 3 mice per noise exposure condition. * = p value < 0.05, ** = p value < 0.01, *** = p value < 0.001 by one-way ANOVA with Bonferroni correction (A), * = p value < 0.05, ** = p value < 0.01, by one-way ANOVA with Holm-Sidak (D).

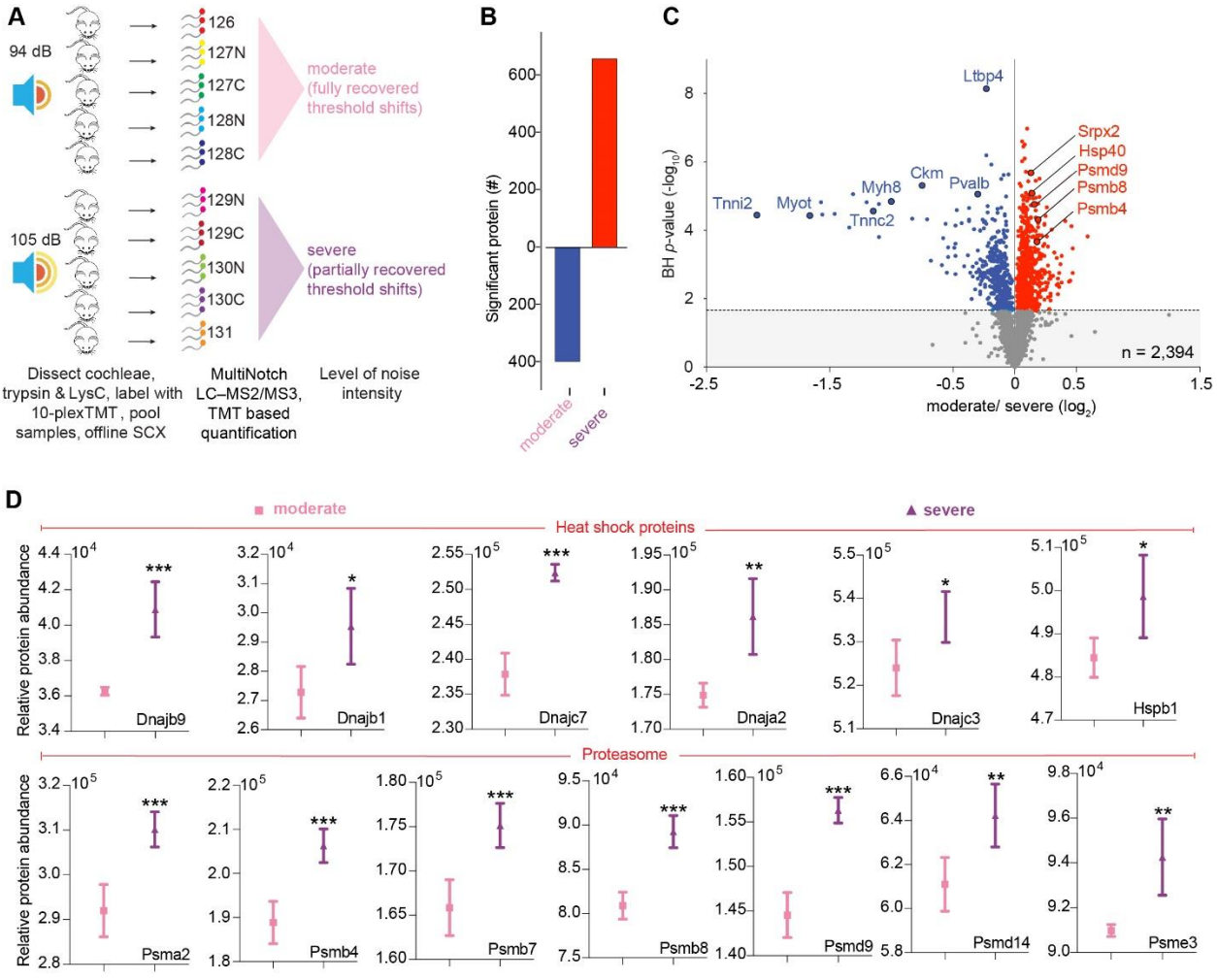
A
94 dB
105 dB
126
127N
127C
128N
128C
129N
129C
130N
130C
131
moderate (fully recovered threshold shifts)
severe (partially recovered threshold shifts)
Dissect cochleae, trypsin & LysC, label with 10-plexTMT , pool samples, offline SCX
MultiNotch LC–MS2/MS3, TMT based quantification
Level of noise intensity
B
Significant protein (#)
moderate
severe
C
BH p-value (-log10)
moderate/ severe (log2)
n = 2,394
Ltbp4
Srpx2
Hsp40
Psmd9
Psmb8
Psmb4
Tnni2
Myot
Myh8
Tnnc2
Ckm
Pvalb
D
moderate
severe
Heat shock proteins
Proteasome
Relative protein abundance
Dnajb9
Dnajb1
Dnajc7
Dnaja2
Dnajc3
Hspb1
Psma2
Psmb4
Psmb7
Psmb8
Psmd9
Psmd14
Psme3

Figure 21. Direct comparison of the cochlear proteome after 30-minute noise exposures causing temporary or permeant hearing loss. (A) Experimental scheme to determine how cochlear protein levels are acutely altered by noise exposures causing a TTS or a PTS with 10plex TMT. **(B)** Number of proteins with significantly (B.H. *p* value < 0.05) altered fold change. **(C)** Volcano plot depicting cochlear proteome remodeling after noise exposures causing TTS compared to PTS. Proteins meeting the statistical cutoff (B.H. *p* value < 0.05) are above the grey dotted line. Selected proteins with elevated levels are in red and reduced are in blue. **(D)** Selected TMT abundance plots for heat shock proteins and proteasome with significantly elevated or reduced levels between severe and moderate noise exposure for 30 minutes. Data plotted as the mean $\pm$ SD, * = *p* value < 0.05, ** = *p* value < 0.01, *** = *p* value < 0.001 by t test. N = 5 mice per group (B-D).

Exposure to moderate intensity noise leads to reduced ribbon synapse density, modest damage to the mechanotransduction machinery, but not cell death

Our ABR and DPOAE analysis allowed for generalized characterization of functional impairments following moderate and severe intensity noise exposures but do not provide robust assessment of potential structural damages. In the next set of experiments, we assessed potential damage to the stereocilia, alterations in ribbon synapse density, and hair cell viability across each noise exposure condition. Scanning electron microscopy (SEM) was used to assess any physical damage to the outer hair cell stereocilia following ambient, moderate, or severe intensity noise exposures **(Figure 22A)**. The stereocilia bundles throughout the cochlea generally appeared normal in mice exposed to ambient noise. However, we observed significantly more frayed outer hair cell bundles in the middle regions (12- 16 kHz) following severe noise exposures compared to moderate or ambient levels of noise (ambient = 7.48% $\pm$ 4.84, moderate = 10.70% $\pm$ 5.59, severe = 49.35% $\pm$ 8.21, p value < 0.001) **(Figure 22B)**. The base showed particular vulnerability as we observed significantly more damaged stereocilia bundles across moderate and severe exposures compared to ambient (ambient = 3.54% $\pm$ 3.35, moderate 15.95% $\pm$ 5.26, severe 26.48% $\pm$ 5.03, p value < 0.001) **(Figure 22B)**. Overall, SEM based characterization of stereocilia bundle damage was consistent with our DPOAE results, demonstrating the severity of hearing impairments being well correlated with the intensity of the noise exposure.

Next, we analyzed cochlear ribbon synapse density after noise exposure **(Figure 22C-H)**. In the apical region (8-12 kHz) of the cochlea, we found that ribbon synapse density was significantly reduced after exposure to severe, but not moderate, exposures compared to ambient controls (ambient = 14.20 $\pm$ 0.37, and severe = 12.00 $\pm$ 2.44 mean $\pm$ SD, p value < 0.05).

Synapse density in the middle region of the cochlea (12-16 kHz) was significantly reduced after exposure to moderate and severe intensity noise compared to ambient controls (ambient = 17.51 $\pm$ 0.92, moderate = 9.71 $\pm$ 1.90 severe = 9.20 $\pm$ 1.82 mean $\pm$ SD, p value < 0.001). The base of the cochlea (24-28 kHz) also observed significant reductions in synapse density after exposure to moderate and severe noise (ambient = 13.97 $\pm$ 0.44, moderate = 10.56 $\pm$ 0.74 severe = 7.95 $\pm$ 1.98 mean $\pm$ SD, p value < 0.001).

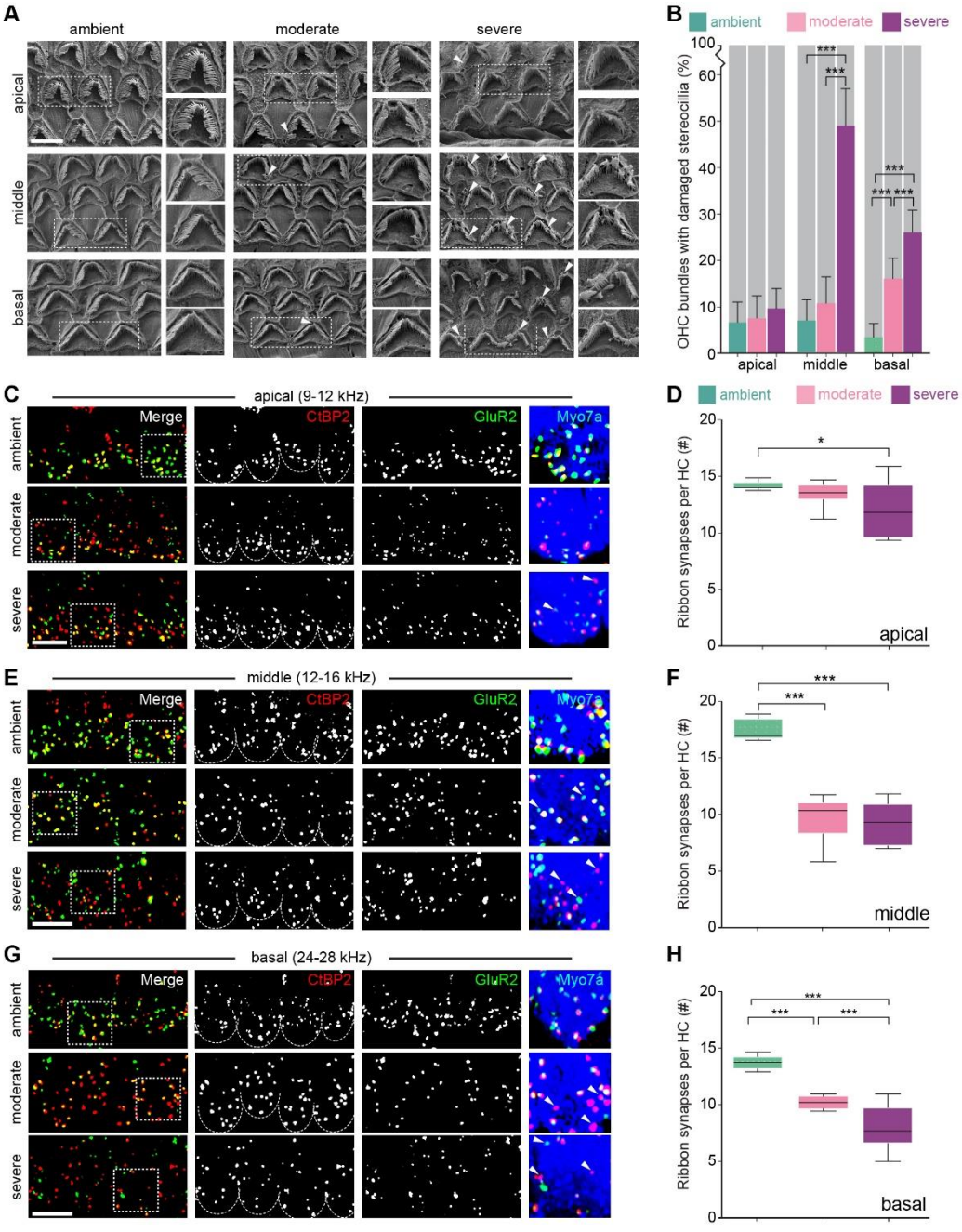
A
ambient
moderate
severe
apical
middle
basal
B
ambient
moderate
severe
OHC bundles with damaged stereocilia (%)
apical
middle
basal
C
apical (9-12 kHz)
Merge
CtBP2
GluR2
Myo7a
ambient
moderate
severe
D
Ribbon synapses per HC (#)
apical
E
middle (12-16 kHz)
middle
F
middle
G
basal (24-28 kHz)
basal
H
basal

Figure 22. Exposure to moderate and severe intensity noise alter stereocilia morphology and reduce synaptic density across the middle and base of the cochlea. (A) Representative SEM images of stereocilia bundles from cochlea whole mounts prepared immediately after noise exposure in regions corresponding to the apex (8 – 12 kHz), middle (12 – 16 kHz), and base (28 – 32 kHz). **(B)** Comparison of the degree of stereocilia fraying across the three regions of the cochlea after 30-minute exposure to either 70, 94 or 105 dB SPL (n = 3 mice per group). The percentage of stereocilia bundles with visible fraying was significantly elevated following exposure to increasingly intense noise across the middle (ambient = 7.48 $\pm$ 4.84, moderate = 10.70 $\pm$ 5.59, and severe = 49.35 $\pm$ 8.21 mean $\pm$ SD) and base (ambient = 3.54 $\pm$ 3.35, moderate = 15.95 $\pm$ 5.26, and severe = 26.48 $\pm$ 5.03 mean $\pm$ SD) of the cochlea. The apex was largely unaffected by the intensity of the exposure (70 dB = 6.76 $\pm$ 4.64, 94 dB = 7.31 $\pm$ 4.78, and 105 dB = 9.58 $\pm$ 4.40 mean $\pm$ SD). **(C-H)** Representative images form apical (9 – 12 kHz), middle (12 – 16 kHz), and base regions (24 – 28 kHz). Cochlear synaptic density (synapse per IHC) within the apex was significantly reduced in the severe versus ambient groups (ambient = 14.20 $\pm$ 0.37, moderate = 13.45 $\pm$ 1.04, and severe = 12.00 $\pm$ 2.44 mean $\pm$ SD). Cochlear synapse density was significantly reduced in the middle and base regions following exposures to both moderate and severe noise compared to ambient (middle: ambient =17.52 $\pm$ 0.93, moderate = 9.71 $\pm$ 1.90, and severe = 9.18 $\pm$ 1.82; base: ambient = 13.97 $\pm$ 0.44, moderate = $\pm$ 0.74, severe = $\pm$ 1.98 mean $\pm$ SD). Scale bar = 5 µm (A), 10 µm (B-D), and 20 µm (C, E, G). * = *p* value 0.05, *** = *p* value < 0.001 by one-way ANOVA with Bonferroni correction.

Hair cells, spiral ganglion neurons, and additional cochlear cell types express proteins with altered fold change after noise exposure

A major caveat in assessing the global changes to the cochlear proteome following noise exposure is the loss of cell type resolution. Thus, to begin to identify which proteins with altered fold changes are enriched in hair cells, we used our previous proteomic analysis of GFP expressing hair cells isolated with fluorescence-activated cell sorting as a reference (Hickox *et al.*, 2017) **(Figure 23A)**. We compared proteins enriched in hair cells to those found with significantly altered fold change after exposure to moderate or severe intensity noise from ^{15}N or TMT- based quantitative proteomics or vice versa. Interestingly, we identified 84 and 109 hair cell enriched proteins with significantly altered fold changes, in our ^{15}N and TMT experiments, respectively **(Figure 23B)**. This indicates that a modest proportion (17.0% or 22.1%) of hair cell enriched proteins are also significantly altered following damaging levels of noise exposure. However, this population of hair cell enriched proteins is only a small fraction of total proteins found to have significantly altered levels in noise exposed cochlea extracts (3.5% or 4.6%, ^{15}N or TMT respectively).

To better asses the localization of proteins we found to have altered fold change following noise, we performed IF of cochlea acutely following exposure to ambient, moderate or severe noise **(Figure 24A)**. Initially, we assessed Col9a1 patterns under whole mount and mid-modiolar sections. Interestingly, we observed prominent signal in the region between the inner and outer hair cells near the top of tunnel of Corti that became disorganized and less prominent the more severe the intensity of noise exposure **(Figure 24B)**. We then examined Hsp90b1, a molecular chaperone which functions within the endoplasmic reticulum associated degradation

(ERAD) pathway. Hsp90b1 levels were elevated in both inner and outer hair cells after exposure to moderate and severe conditions compared to ambient controls **(Figure 24C)**. We also found that the levels of proteasome subunit Psmc5 were increased in inner hair cells after moderate and severe noise exposure **(Figure 24D)**. Further investigation into the proteostasis factor VCP, which is part of the ubiquitin-proteasome system, found increases in signal among hair cells in addition to SGNs, in a noise intensity dependent manner, consistent with ^{15}N analysis **(Figure 24E)**. Finally, the actin binding protein Arpc2 and Uba2 (E1 for SUMO1-4), were also found be progressively elevated in SGNs after noise exposure, while the Latent-transforming growth factor beta-binding protein 4 (Ltbp4) signal was reduced among SGN bundles with increasing severity of noise exposure **(Figure 24F)**.

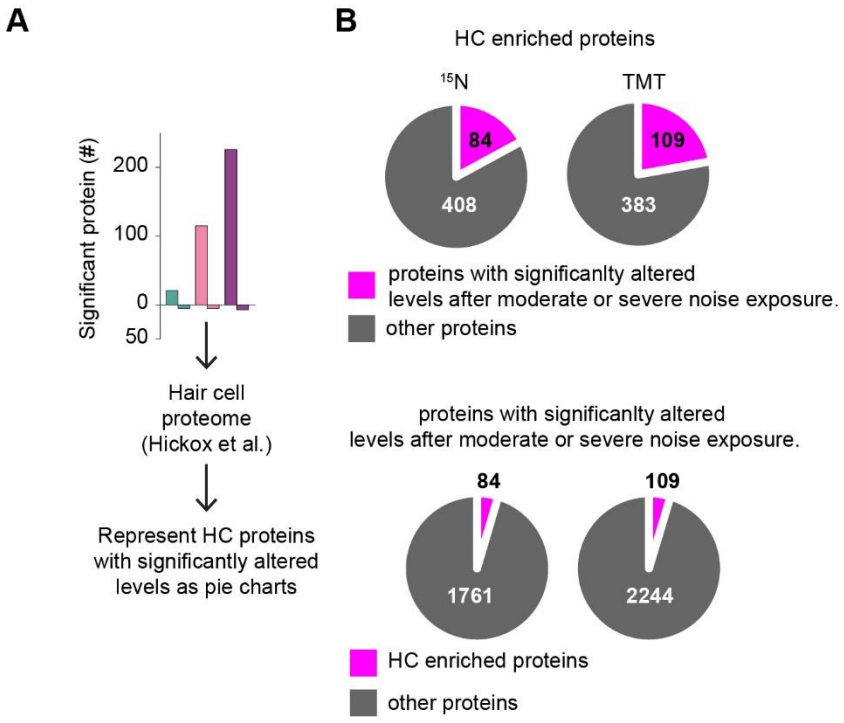
A
Significant protein (#)
200
100
0
50
Hair cell proteome (Hickox et al.)
Represent HC proteins with significantly altered levels as pie charts
B
HC enriched proteins
15N
TMT
84
408
109
383
proteins with significanlty altered levels after moderate or severe noise exposure.
other proteins
proteins with significanlty altered levels after moderate or severe noise exposure.
84
1761
109
2244
HC enriched proteins
other proteins

Figure 23. A proportion of hair cell enriched proteins are also significantly altered following damaging levels of noise exposure. (A) Identified proteins enriched in HCs by using our previous proteomic analysis of GFP expressing HCs isolated with fluorescence-activated cell sorting as a reference. **(B)** The comparison of proteins enriched in HCs to those found with significantly altered fold change after exposure to moderate or severe intensity noise from ^{15}N or TMT-based quantitative proteomics.

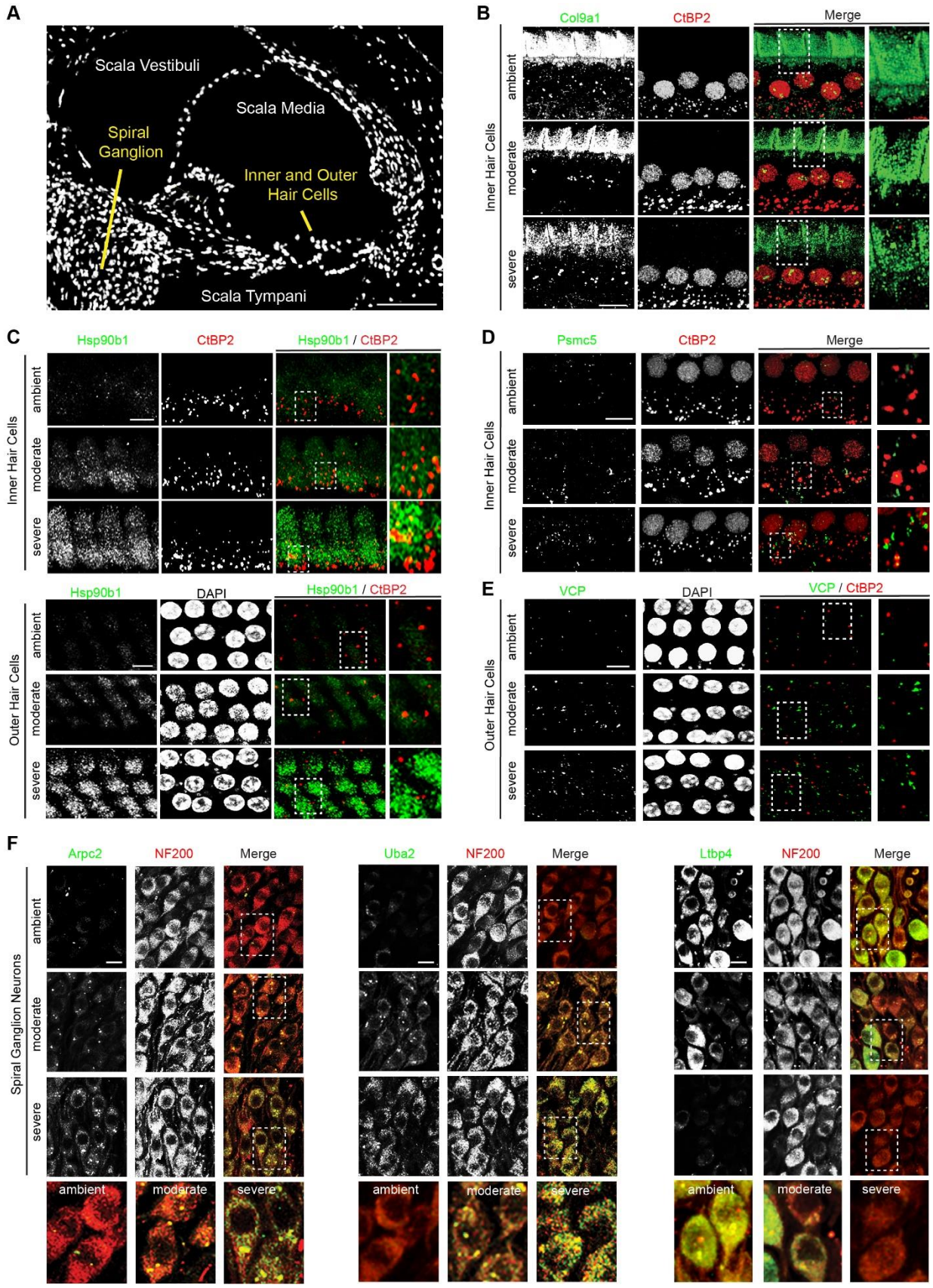
A
Scala Vestibuli
Scala Media
Spiral Ganglion
Inner and Outer Hair Cells
Scala Tympani
B
Col9a1
CtBP2
Merge
Inner Hair Cells
ambient
moderate
severe
C
Hsp90b1
CtBP2
Hsp90b1 / CtBP2
Inner Hair Cells
ambient
moderate
severe
Hsp90b1
DAPI
Hsp90b1 / CtBP2
Outer Hair Cells
ambient
moderate
severe
D
Psmc5
CtBP2
Merge
Inner Hair Cells
ambient
moderate
severe
E
VCP
DAPI
VCP / CtBP2
Outer Hair Cells
ambient
moderate
severe
F
Arpc2
NF200
Merge
Uba2
NF200
Merge
Ltbp4
NF200
Merge
Spiral Ganglion Neurons
ambient
moderate
severe
ambient
moderate
severe
ambient
moderate
severe
ambient
moderate
severe

Figure 24. Proteins regulated during noise exposure are expressed by HCs, SGNs, and supporting cells within the cochlea. (A) DAPI stained mid-modiolar cochlear section illustrating regions analyzed by IF. **(B)** Col9a1 signal becomes disorganized and decreases in the area above the Tunnel of Coti following noise exposure. Green = Col9a1 and red = CtBP2. **(C)** Hsp90b1 levels are elevated in both inner and outer hair cells after exposure to increasing intensities of noise. Green = Hsp90b1, red = CtBP2, white = DAPI. **(D)** Psmc5 levels increase after exposures to increasing noise intensity within inner hair cells. Green = Psmc5 and red = CtBP2. **(E)** Vcp levels are elevated in the outer hair cells after exposure to increasing damaging levels of noise. Green = Vcp, red = CtBP2, white = DAPI. **(F)** Spiral ganglion neurons from the second ganglion bundle from the top of the cochlea (12-16 kHz) in midmodiolar sections. *Left:* Arpc2 levels are elevated in SGNs after exposure to increasing damaging levels of noise. Similarly, Uba2 (*Middle*) levels were also seen to progressively increase within the spiral ganglion neuron cell bodies at increasing noise exposures. LtBP4 (*right*) levels are reduced in the spiral ganglion neurons after exposure to increasingly damaging levels of noise. Green = Arpc2, Uba2, and LtBP4 (left, middle, right) and red = NF200. Scale bar = 10 μm (A-F). Whole mount preparation for B-E and midmodiolar sections F.

Noise exposures causing hearing loss drive cochlear gene expression

To investigate if elevated protein levels can be explained by increased gene expression, we again exposed a new cohort of mice to ambient, moderate, or severe intensity noise for 30 minutes and collected cochlear extracts for analysis with paired-end RNA sequencing (RNA-Seq) analysis (Li and Dewey, 2011). We obtained greater than 75 million mapped reads at a total mapping rate > 95.3% from each biological replicate within each group, four per group. We then obtained differential gene expression profiles for 13,519 and 16,258 transcripts representing the moderate versus ambient and severe versus ambient datasets respectively. Violin plots were used to visualize the global gene expression, which demonstrated very similar overall distributions between each respective dataset **(Figure 25A)**. To investigate the reproducibility of our transcriptomic analysis, we assessed correlation of gene expression patterns between our datasets. Biological replicates clustered by noise exposure intensity and gene expression patters from cochlea exposed to severe noise were more alike ambient controls than to cochlea exposed to moderate intensity noise **(Figure 25B)**. We also performed principal component analysis and again found that the biological replicates clustered and datasets from mice exposure to severe noise were more similar to mice exposed to ambient rather than moderate intensity noise **(Figure 25C)**.

We visualized the noise induced changes to cochlear gene expression following exposure to moderate or severe intensity noise, relative to the ambient controls with volcano plots **(Figure 25D-E)**. Notably, we found nearly twice as many genes with significantly altered expression levels in the moderate condition compared to severe conditions. In both paradigms there were slightly more genes with elevated rather than reduced fold changes. Ddit4, Atf3, Fos, Jun, and

Cebpb were among the genes with the most dramatic elevations to gene expression after exposures to either moderate or severe intensity noise. Ddit4 gene expression is rapidly induced in response to changes in energy requirements, endoplasmic reticulum stress, and hypoxia (Kimball and Jefferson, 2012). Importantly, the elevated of Ddit4, Atf3, Fos, Jun, and Cebpb gene expression is consistent with previous findings demonstrating the involvement of these genes among hearing loss models (Low et al., 2010; Schiavon et al., 2018). Moreover, genes encoding individual proteasome subunits had significantly elevated fold change in moderate and severe datasets (15 vs 12 genes, respectively). Suggesting that the elevated levels of proteasome proteins observed with proteomics are partially due to elevated expression in response to noise.

We next compared the correlation of mRNA to protein fold changes observed after exposures to moderate or severe intensity noise, relative to ambient controls. Overall, there were 194 significantly regulated proteins with matching changes to expression levels, i.e. increased protein abundance and increased mRNA levels, in the moderate group, conversely only 47 protein-mRNA pairs were quantified within the severe dataset **(Figure 25F-G)**. Notably, we found that 45.6% or 74.6% of proteins with elevated fold changes also had elevated mRNA abundance in the moderate and severe datasets respectively. Suggesting that increased gene expression likely contributes but is not solely responsible for the elevation or reduction in protein abundance observed after exposure to damaging levels of noise.

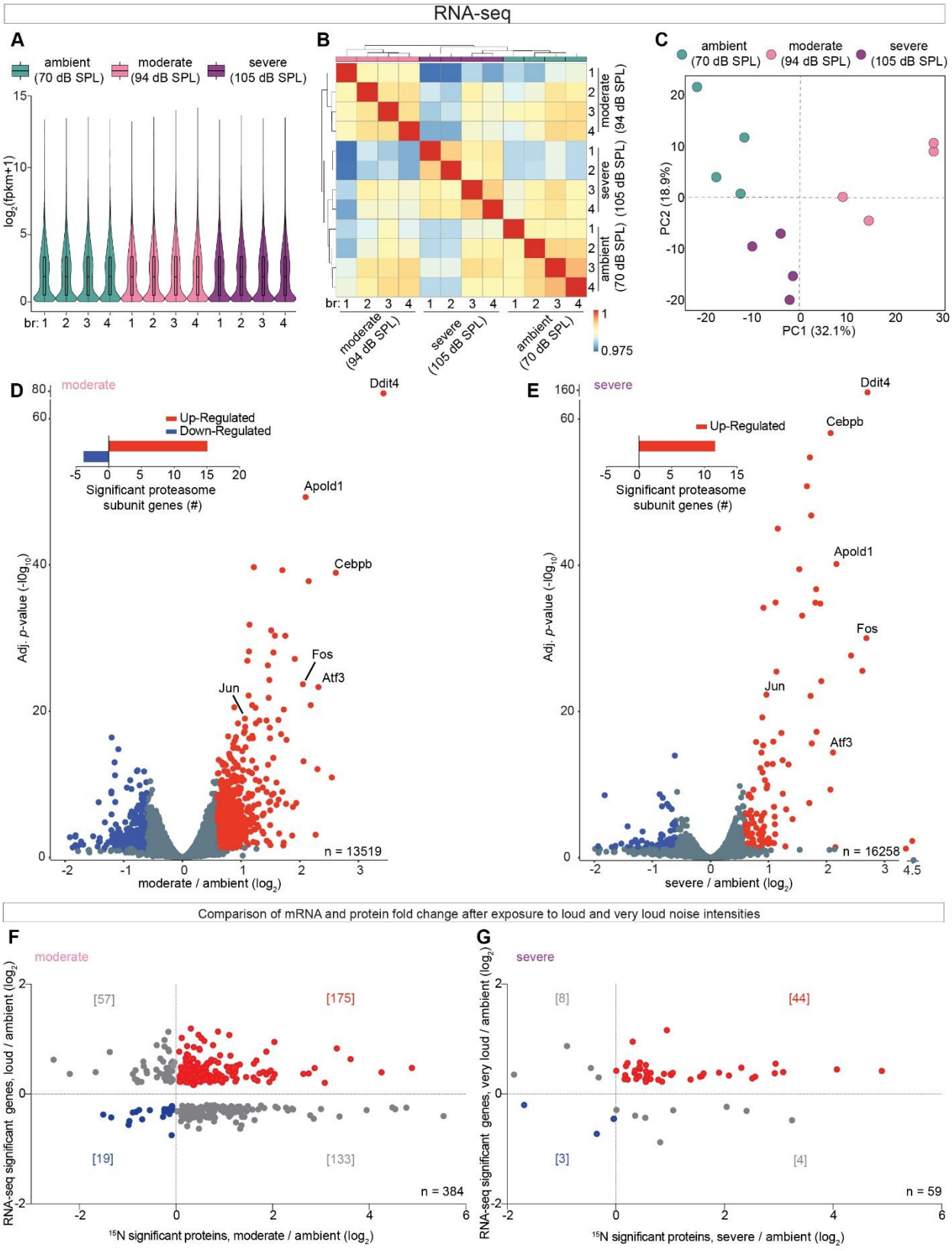
RNA-seq
A
ambient (70 dB SPL)
moderate (94 dB SPL)
severe (105 dB SPL)
log2(fpkm+1)
br: 1 2 3 4 1 2 3 4 1 2 3 4
B
moderate (94 dB SPL)
severe (105 dB SPL)
ambient (70 dB SPL)
1
0.975
C
PC2 (18.9%)
PC1 (32.1%)
D
moderate
Up-Regulated
Down-Regulated
Significant proteasome subunit genes (#)
Ddit4
Apold1
Cebpb
Fos
Atf3
Jun
Adj. p-value (-l0g10)
n = 13519
moderate / ambient (log2)
E
severe
Up-Regulated
Significant proteasome subunit genes (#)
Ddit4
Cebpb
Apold1
Fos
Jun
Atf3
n = 16258
severe / ambient (log2)
Comparison of mRNA and protein fold change after exposure to loud and very loud noise intensities
F
moderate
[57]
[175]
[19]
[133]
n = 384
RNA-seq significant genes, loud / ambient (log2)
15N significant proteins, moderate / ambient (log2)
G
severe
[8]
[44]
[3]
[4]
n = 59
RNA-seq significant genes, very loud / ambient (log2)
15N significant proteins, severe / ambient (log2)

Figure 25. RNA-Seq analysis demonstrated an overall increase in cochlear gene expression following exposure to moderate or severe intensity noise compared to ambient levels. (A) Visualization of global gene expression patterns with violin plots showed very similar overall distributions between the datasets. **(B)** Correlation of gene expression matrix demonstrated that biological replicates clustered based on noise exposure intensity. Notably, cochlea exposed to severe noise were more similar to ambient controls rather than to cochlea exposed to moderate intensity noise. **(C)** Principal component analysis shows that the biological replicates cluster, and demonstrated that the severe noise condition is more similar to the ambient condition rather than moderate noise condition based on transcriptomics. **(D-E)** Noise induced changes in cochlear gene expression were graphed as fold change after exposure to moderate or severe intensity noise, relative to ambient controls on volcano plots. Nearly twice as many genes with significantly altered fold change were found in the moderate compared to severe datasets. In both analysis paradigms there were slightly more genes with elevated rather than reduced fold change. *Insert*: 15 and 12 genes encoding individual proteasome subunits had significantly elevated fold change in moderate and severe datasets, respectively. **(F)** Comparison of corresponding mRNA and protein fold change after exposure to moderate or severe intensity noise relative to ambient controls. Roughly 45.6% or 74.6% of proteins with elevated fold changes also had elevated mRNA abundance in the moderate and severe datasets, respectively. N = 4 mice per noise exposure group (A-E)

Ubiquitin-proteasome system is activated after exposure to moderate and severe intensity noise

To independently validate the involvement of the proteostasis network within noise exposure, we investigated protein ubiquitylation utilizing three complementary assays. In the first assay, ubiquitylated proteins were biochemically enriched with Tandem Ubiquitin Binding Entities (TUBEs) from cochlear extracts harvested from mice exposed to ambient, moderate, or severe levels of noise (Hjerpe et al., 2009) **(Figure 26A)**. Western blot analysis of the TUBEs purified material indicating that exposure to moderate or intense noise causes an increase in protein ubiquitylation compared to the ambient condition **(Figure 26B)**. We then repeated the experiment with three independent groups of mice and analyzed the material enriched with TUBEs by LC-MS/MS based proteomics to identify which proteins were ubiquitinated. We identified 328 proteins which were either enriched or exclusive identified in at least two cochlear purifications within the moderate or severe intensity noise conditions compared to ambient controls. Interestingly, 108 of these proteins were also found with elevated protein fold change in the ^{15}N experiments **(Figure 26C)**.

To better assess direct evidence of protein ubiquitylation, we repeated our noise exposures in a new cohort of mice and purified the ubiquitylated peptides with antibodies for the "diGly remnant" C-terminal Lys-ε-Gly-Gly sequence, which results from the cleaving of ubiquitin (Peng et al., 2003b; Xu et al., 2010) **(Figure 26D)**. In total, we identified 324 diGly peptides from 202 identified proteins. In support of elevated cochlear protein ubiquitylation due to excess noise, we identified significantly more diGly peptides across the severe condition compared to ambient controls (165.0 ± 51.7 versus 83.7 ± 14.2, p value < 0.05) **(Figure 26E)**. To note, 46 diGly containing peptides from 36 proteins identified in at least two biological

replicates from the moderate or severe conditions were below the limit of detection in cochlear extracts harvested from ambient noise exposures. These proteins are predominantly associate with metabolism, the cytoskeleton, UPS, and the nucleus. Fifteen of these proteins observed elevated fold changes in our ^{15}N based analysis including Actg1, Tubb5, Vcp, and Vamp3 while only 5 had reduced fold changes in the ^{15}N experiments **(Figure 26F)**. Taken all together, these results show that cochlear protein ubiquitylation is elevated after exposure to damaging levels of noise.

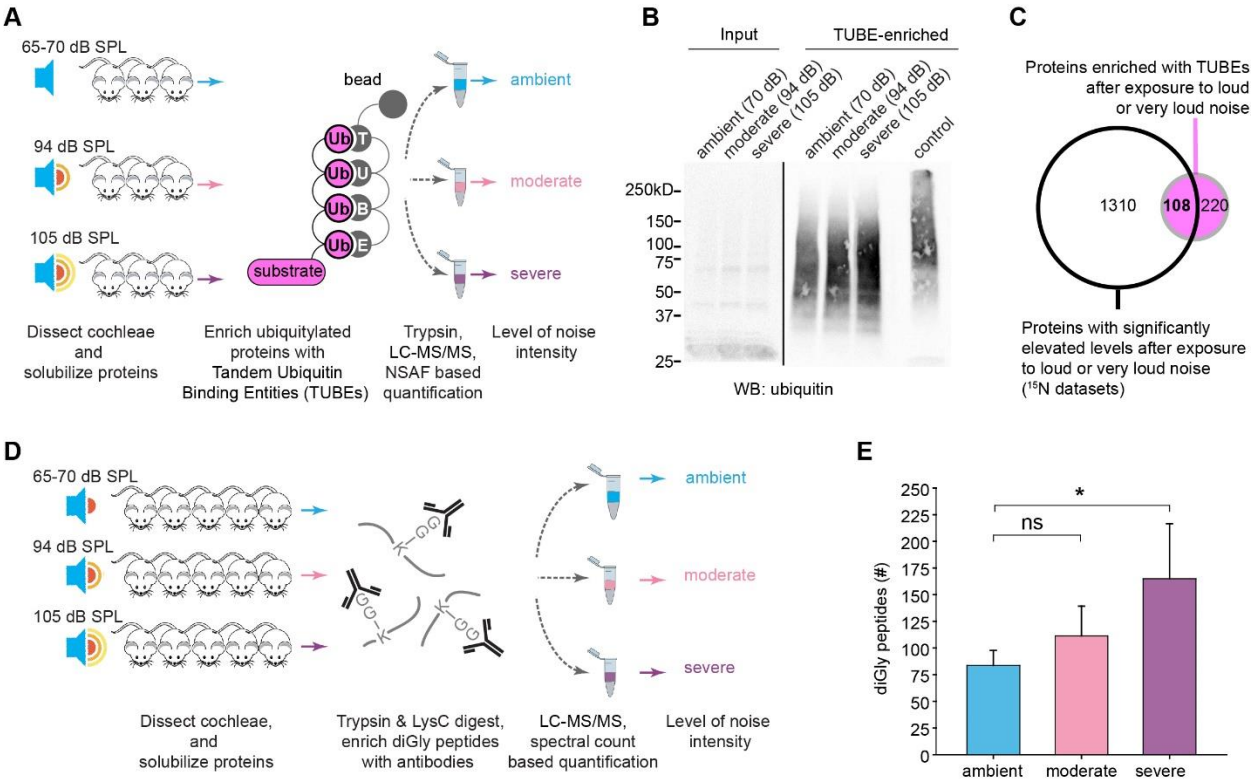
A
65-70 dB SPL
94 dB SPL
105 dB SPL
bead
substrate
ambient
moderate
severe
Dissect cochleae and solubilize proteins
Enrich ubiquitylated proteins with Tandem Ubiquitin Binding Entities (TUBEs)
Trypsin, LC-MS/MS, NSAF based quantification
Level of noise intensity
B
Input
TUBE-enriched
ambient (70 dB)
moderate (94 dB)
severe (105 dB)
control
250kD
150
100
75
50
37
25
WB: ubiquitin
C
Proteins enriched with TUBEs after exposure to loud or very loud noise
1310
108
220
Proteins with significantly elevated levels after exposure to loud or very loud noise (15N datasets)
D
65-70 dB SPL
94 dB SPL
105 dB SPL
ambient
moderate
severe
Dissect cochleae, and solubilize proteins
Trypsin & LysC digest, enrich diGly peptides with antibodies
LC-MS/MS, spectral count based quantification
Level of noise intensity
E
diGly peptides (#)
250
225
200
175
150
125
100
75
50
25
0
*
ns
ambient
moderate
severe
F
Cytoskeleton and molecular motors
K191 K326 Actg1
K344 Actn3
K141 Arl8b
K112 Cfl1
K118 Dlgap5
K110 K133 K152 K167 Kxd1
K1591 Myh4
K501 Pdcd6ip
K58 Tubb5
UPS and protein quality control
K250 Aup1
K539 Hspa8
K393 Itch
K115 Psmd13
K142 Skp1
K18 K109 Vcp
K50 Ywhae
Cell membranes
K503 Abcc1
K117 Chic2
K87 Cnp
K14 Imt2c
K299 P2rx3
K39 Vamp3
Nucleus
K325 Asxl2
K120 Hist2h2ab
K21 Hist2h2be
K80 H3c1
K448 K456 Nol10
Metabolism
K184 Alad
K261 Gapdh
K95 Glul
Translation
K58 Rps2
K51 Rps21
K188 Pabpc4
Hemoglobin
K8 Hba
K60 Hbb-b1
K67 Hbb-bs

Figure 26. The degree of ubiquitylation within the cochlea increases at progressively increasing levels of noise exposure compared to ambient controls. (A) Cartoon illustrating how cochleae were harvested from mice exposed to ambient, moderate, or severe intensity noise and prepared for enrichment of ubiquitylated proteins by Tandem Ubiquitin Binding Entities (TUBEs). **(B)** Western blot analysis of the TUBEs purified material suggesting that exposure to moderate or intense compared to ambient noise causes an increase in global protein ubiquitylation. MG132 treated HEK293 lysate were used as positive control. **(C)** TUBEs purifed material from each noise exposure group (n=4 mice, repeated 3 times) was analyzed by LC-MS/MS. In total, 328 proteins were enriched (based on NSAF) or exclusively identified in at least two purifications from either the moderate or severe groups compared to ambient controls (purple). Comparison of proteins found with elevated protein fold change in the ^{15}N experiments showed 108 proteins that were also enriched in the TUBE assay at increasing noise exposure intensities (moderate or severe). **(D)** Experimental schematic for diGly LC-MS/MS assay used to directly identify peptides with C-terminal Lys-ε-Gly-Gly ubiquitin residues. **(E)** In total, 324 diGly containing peptides from 202 proteins were identified from anti diGly purified cochlear extracts. Significantly more diGly peptides were identified in cochlear extracts from mice exposed to severe compared to ambient intensity noise (165.0 $\pm$ 51.7 versus 83.7 $\pm$ 14.2, *p* value < 0.05). **(F)** 46 diGly peptides from 36 proteins were identified in cochlear extracts from at least two biological replicates exposed to moderate or severe but were absent in extracts from ambient noise exposed mice. Fifteen of these proteins were found with elevated fold change including Actg1, Tubb5, Kxd1, Arl8b, Vcp, and Vamp3 (purple) while only 5 had reduced fold (blue) in the ^{15}N experiments. * = *p* value < 0.05 by Kruskal-Wallis and Tukey pairewise multiple comparison (E).

Protein translation machinery has selectively elevated fold change during the recovery period

Given the stark differences with respect to the potential for recovery from our moderate versus severe conditions, based on comparison of ABR responses 1DAN compared to 14DAN. We set out to determine if the cochlear proteome was significantly different after this two-week recovery period in the moderate vs severe noise exposure condition. If successful, the results of these experiments would provide critical insights into the potential cellular mechanisms underlying recovery potential. To this extent we analyzed how the cochlear proteome was altered two-weeks after exposure versus acutely after exposure to moderate or severe noise **(Figure 27A)**. Overall, we quantified 4,626 proteins and found more proteins with elevated rather than reduced fold change (recovery / acute) after both moderate and severe noise exposure **(Figure 27B-C)**. To gain further insights into the pathways involved in recovery we again performed GO:MF, GO:CC, and GO biological process (GO:BP) enrichment analysis of the significantly (p value < 0.05) altered proteins **(Figure 27D)**. Unexpectantly, we found no ontologies that were enriched among the proteins significantly altered in the severe datasets, while the significantly regulated proteins within the moderate noise datasets demonstrated significant enrichment of several pathways **(Figure 27D)**. In particular, GO:MF analysis revealed proteins associated with protein synthesis to be selectively elevated during recovery from moderate intensity noise. Specifically, the ontologies significantly enriched by GO:CC as well as by GO:BP were associated with ribosomes or ribonucleoproteins and translation or metabolism, respectively. To further visualize the protein fold change of the significantly altered proteins during recovery, we generated heat maps which revealed many ribosomal proteins co-clustered together, consistent with GO analysis **(Figure 27E)**.

The lack of ontologies identified under the severe condition suggests one of two possibilities. The first being a disorganized response to noise in response to severe intensities, potentially stemming from the increased cellular stress and damage to multiple pathways. Alternatively, the lack of enriched ontologies may stem from many of the same pathways elevated in the severe condition, which are elevated in response to noise, are also elevated in the moderate conditions thus failing to reach significance. To address this discrepancy, we expanded our investigation to compared changes in protein abundance two weeks after exposures within the severe or moderate conditions relative to ambient conditions **(Figure 28A-B)**. Similarly, we found that the translational machinery observed elevated levels during recovery, however, in this paradigm the phenomenon was present in both the moderate and severe conditions relative to ambient controls **(Figure 28D-F)**. Taken all together, the fact that the protein translation machinery has elevated levels two weeks after noise exposure suggests that protein synthesis may play a key role in the recovery phase of noise exposure.

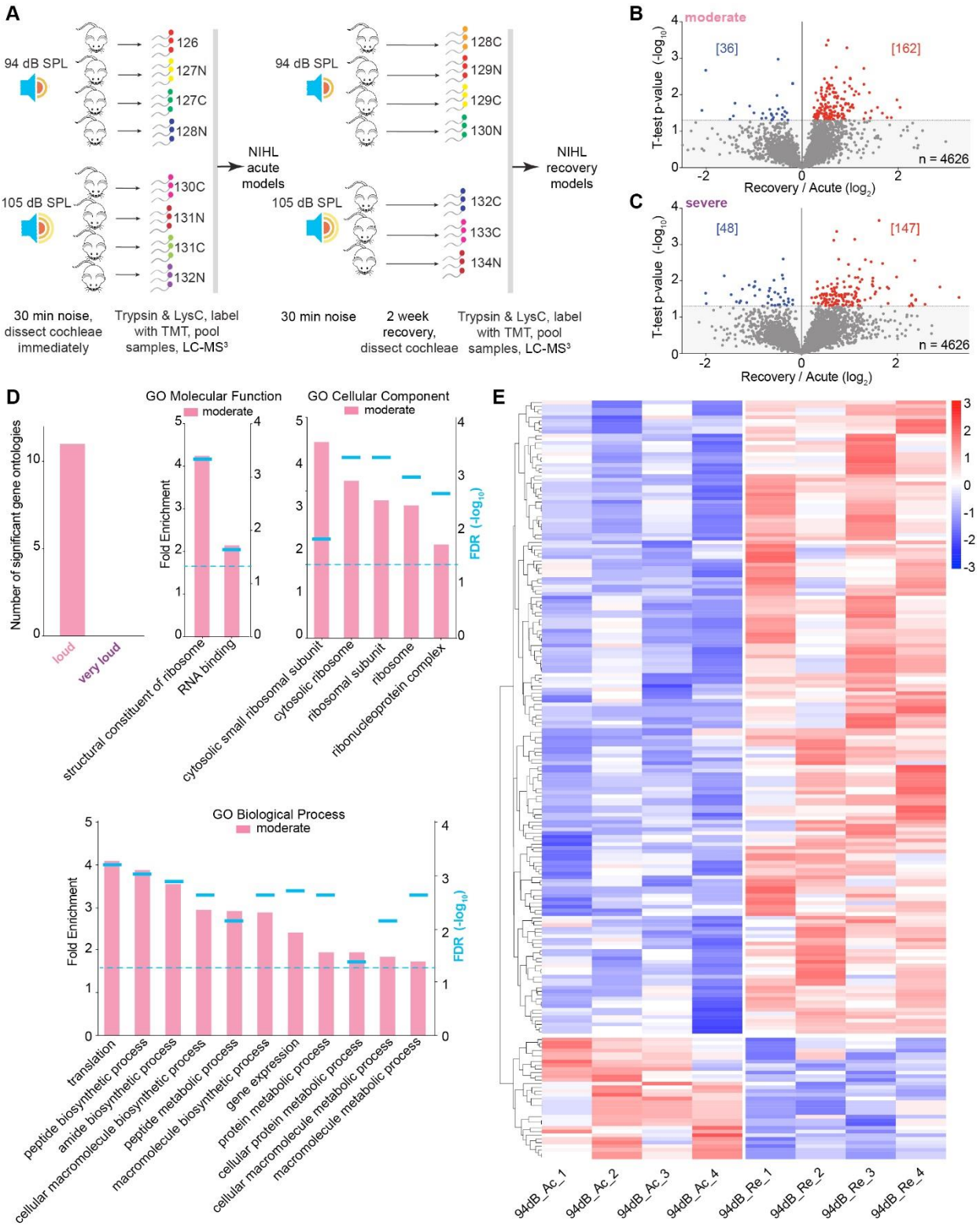
A
94 dB SPL
126
127N
127C
128N
105 dB SPL
130C
131N
131C
132N
NIHL acute models
94 dB SPL
128C
129N
129C
130N
105 dB SPL
132C
133C
134N
NIHL recovery models
30 min noise, dissect cochleae immediately
Trypsin & LysC, label with TMT, pool samples, LC-MS³
30 min noise
2 week recovery, dissect cochleae
Trypsin & LysC, label with TMT, pool samples, LC-MS³
B
moderate
[36]
[162]
T-test p-value (-log10)
n = 4626
Recovery / Acute (log2)
C
severe
[48]
[147]
T-test p-value (-log10)
n = 4626
Recovery / Acute (log2)
D
Number of significant gene ontologies
loud
very loud
GO Molecular Function
moderate
Fold Enrichment
FDR (-log10)
structural constituent of ribosome
RNA binding
GO Cellular Component
moderate
cytosolic small ribosomal subunit
cytosolic ribosome
ribosomal subunit
ribosome
ribonucleoprotein complex
GO Biological Process
moderate
Fold Enrichment
FDR (-log10)
translation
peptide biosynthetic process
amide biosynthetic process
cellular macromolecule biosynthetic process
peptide metabolic process
macromolecule biosynthetic process
gene expression
protein metabolic process
cellular protein metabolic process
cellular macromolecule metabolic process
macromolecule metabolic process
E
94dB_Ac_1
94dB_Ac_2
94dB_Ac_3
94dB_Ac_4
94dB_Re_1
94dB_Re_2
94dB_Re_3
94dB_Re_4

Figure 27. Proteomic assessment of the molecular mechanisms underlying the recovery of hearing sensitivity. (A) Quantitative proteomic analysis workflow by 15plex TMT was used to determine molecular processes associated with the recovery phases of moderate and severe noise exposure (n = 3-4 mice per condition). **(B and C)** Volcano plot of cochlear proteome comparing acute and recovery phase within moderate (B) or severe (C) levels of noise intensity for 30 minutes. Proteins meeting the statistical cutoff (T-test *p* value < 0.05) are shown either in red (elevated fold change) or blue (reduced fold change). **(D)** The number of significantly enriched gene ontologies from the biological processes category in the moderate or severe datasets (top left). Summary of GO enrichment analysis of significantly regulated proteins in moderate noise exposure condition based on GO: Molecular function, GO: Cellular Component and GO: Biological Process. **(E)** Heat maps depicting protein fold change for the significantly altered proteins in the acute versus recovery within moderate or severe intensity. Ac = acute and Re = recovery, n = 391 proteins, dotted blue line indicates FDR < 0.05 by Fisher's exact test (E).

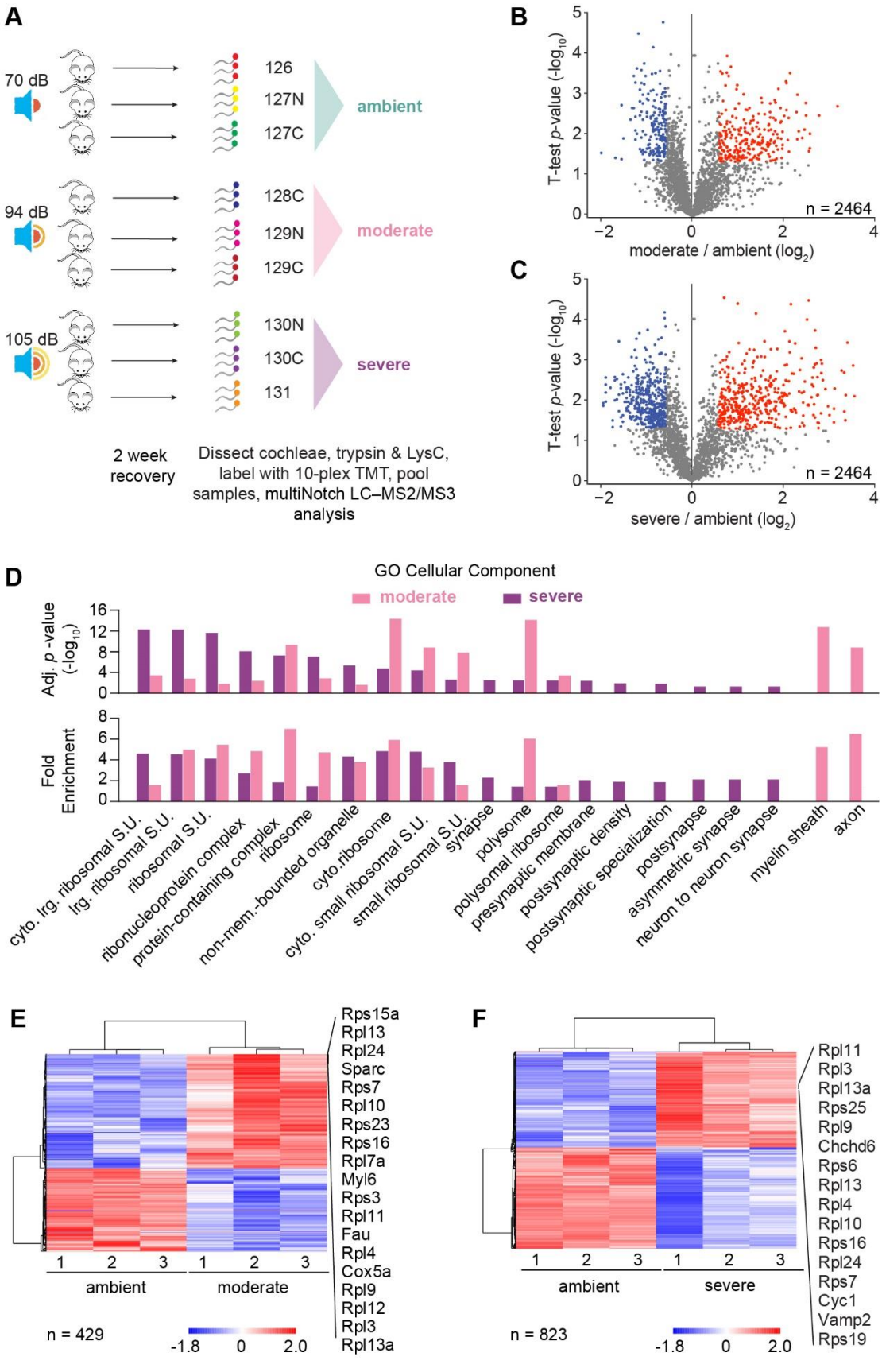
A
70 dB
94 dB
105 dB
126
127N
127C
128C
129N
129C
130N
130C
131
ambient
moderate
severe
2 week recovery
Dissect cochleae, trypsin & LysC, label with 10-plex TMT, pool samples, multiNotch LC–MS2/MS3 analysis
B
T-test p-value (-log10)
moderate / ambient (log2)
n = 2464
C
T-test p-value (-log10)
severe / ambient (log2)
n = 2464
D
GO Cellular Component
moderate
severe
Adj. p -value (-log10)
Fold Enrichment
cyto. lrg. ribosomal S.U.
lrg. ribosomal S.U.
ribosomal S.U.
ribonucleoprotein complex
protein-containing complex
ribosome
non-mem.-bounded organelle
cyto. ribosome
cyto. small ribosomal S.U.
small ribosomal S.U.
synapse
polysome
polysomal ribosome
presynaptic membrane
postsynaptic density
postsynaptic specialization
postsynapse
asymmetric synapse
neuron to neuron synapse
myelin sheath
axon
E
Rps15a
Rpl13
Rpl24
Sparc
Rps7
Rpl10
Rps23
Rps16
Rpl7a
Myl6
Rps3
Rpl11
Fau
Rpl4
Cox5a
Rpl9
Rpl12
Rpl3
Rpl13a
1 2 3 1 2 3
ambient
moderate
n = 429
-1.8 0 2.0
F
Rpl11
Rpl3
Rpl13a
Rps25
Rpl9
Chchd6
Rps6
Rpl13
Rpl4
Rpl10
Rps16
Rpl24
Rps7
Cyc1
Vamp2
Rps19
1 2 3 1 2 3
ambient
severe
n = 823
-1.8 0 2.0

Figure 28. Ribosomal proteins have elevated fold change during the hearing recovery period cochlear extracts after exposure to moderate or severe relative to ambient intensity noise. (A) Quantitative 9plex TMT proteomic analysis workflow to identify biological processes associated with the recovery phases of noise inducing temporary and permanent hearing loss relative to ambient controls. **(B)** Volcano plot depicting cochlear proteome remodeling two weeks after exposure to ambient versus moderate noise for 30 minutes. Proteins meeting the statistical cutoff (T-test p value < 0.05) and having at least a 1.5 fold change are red (elevated) or blue (reduced). **(C)** Same as (B) except volcano plot depicts measures from severe versus ambient intensity noise exposures. **(D)** GO: Cellular component enrichment analysis from the proteins with significantly altered fold change relative all the proteins identified. **(E and F)** Heatmaps depicting proteins with severely altered fold change for moderate versus ambient (E) and severe versus ambient (F) clustered based on one-minus correlation and average linkage. Ribosomal proteins robustly co-cluster in both datasets. N = 3 mice per group.

Chapter 6 Data in Progress: Mitigation of Cellular Stress Induced by Noise.

Introduction and Preliminary Data

Hearing is a metabolically demanding process which requires an inexhaustible pool of glutamate to be released presynaptically to accurately encode the various frequencies embedded in sound(Becker et al., 2018; Buran et al., 2010; Castellano-Munoz et al., 2016; Cheng *et al.*, 2005). This continuous signaling requires extensive calcium buffering postsynaptically to safeguard neurons from potential excitotoxicity. However, in instances of prolonged and elevated activity, calcium buffering alone is not enough to offset the cellular stress which results from deficits in available energy and oxygen reserves within the cochlea (Castellano-Munoz *et al.*, 2016; Fettiplace, 2017). In our lab we have shown that one of the hallmarks of moderate and severe intensity noise exposure is the recruitment of proteins associated with the proteosome and heat shock response (Jongkamonwiwat *et al.*, 2020). Together suggesting that overstimulation of the auditory system creates a demanding and stressful environment in which the potential for denaturation and protein damage is high. These findings have motivated our lab to ask if priming the cochlea's heat shock response prior to noise exposure would mitigate the resulting hearing impairments.

Indeed, preliminary data from our lab has demonstrated that injections of TRC051384, an HSP70 inducer, 2 hours prior to exposure to severe intensity noise increases the potential for recovery of hearing sensitivity. To follow up with this finding we acquired a proteosome activity reporter line, Tg(CAG-Ub*G76V/GFP)1Dant, which contains a green fluorescent protein (GFP) fused to a constitutively active degradation signal (UbG76V). Under normal circumstances the GFP fused UB is readily degraded but under situations in which the proteasome is impaired or

overwhelmed, GFP signal is expected to increase. Therefore, by monitoring the intensity of GFP we can gain insights into which cells are undergoing cellular stress in response to noise.

We then asked which cells would have the highest cellular stress following noise exposure. To address this, we exposed a cohort of mice to noise for two hours and compared the level of GFP signal by immunocytochemistry within cochlea. The intensity of GFP signal gradually increased with respect to noise exposure. Moreover, GFP signal appeared to localize primarily within the spiral bundles regardless of the intensity of noise **(Figure 29A-C)**. Suggesting that the spiral bundle is the primary target of cellular stress following noise exposure, consistent with previous reports (Chen et al., 2019; Furman *et al.*, 2013; Kujawa and Liberman, 2009). However, a potential caveat to this interpretation relies on the equal expression of *GFP* among all cell types within the cochlea. To properly gauge this, we used RNAScope in situ hybridization to visualize which cells within the cochlea express *GFP*. This analysis verified *GFP* expression among cells within the ganglion bundle, the organ of corti, spiral limbus and inferior spiral ligament **(Figure 30A)**. Given that we have previously shown a robust upregulation of cellular stress markers in response to noise (Jongkamonwiwat *et al.*, 2020). It is possible that during noise exposure, transcription is actively downregulated to conserve energy and ensure the survival of the cell. Nonetheless, these experiments demonstrate that *GFP* is expressed among all cell types of the cochlea. To independently validate our immunocytochemistry results, which observed a noise dependent increase of GFP intensity, we probed overall abundance of GFP via western blot. In this experiment we again exposed a cohort of mice to either ambient (65-70 dB SPL) or severe (105 dB SPL) levels of noise for 2 hours, then allowed mice to recover for 2 hours prior to harvesting the cochlea. This analysis

recapitulated the intensity dependent increase of GFP abundance following noise exposure observed by immunohistochemistry **(Figure 31)**.

We next asked whether administration of TRC051384 would result in an increase in GFP signal and if injection prior to noise reduces cellular stress. Consistent with the recruitment of the heat shock response, administration of TRC051384 elevated GFP signal above levels observed in ambient controls **(Figure 32A-B)**. Strikingly, the comparison of GFP signal in mice exposed to noise with and without TRC051384 demonstrated a significant reduction in overall intensity of GFP in the treated group **(Figure 32C-D)**. Western blot analysis independently validated the TRC051384 dependent reduction of GFP signal following noise exposure **(Figure 32E-F)**. Thus, these preliminary results strongly support the use of TRC051384 as a mitigator of cellular stress induced by noise exposures.

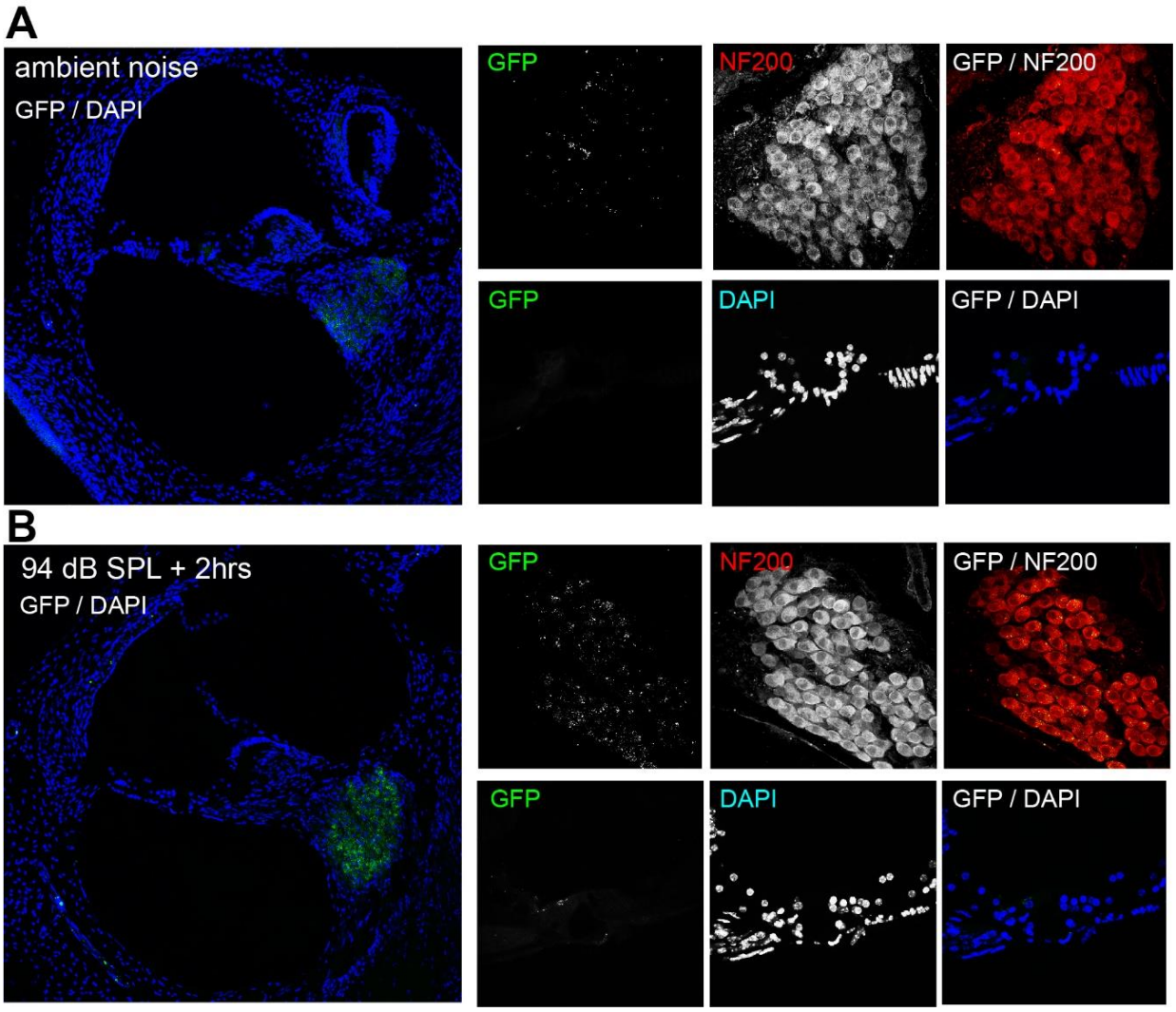
A
ambient noise
GFP / DAPI
GFP
NF200
GFP / NF200
GFP
DAPI
GFP / DAPI
B
94 dB SPL + 2hrs
GFP / DAPI
GFP
NF200
GFP / NF200
GFP
DAPI
GFP / DAPI

Figure 29. GFP signal intensity increases with noise exposure and is concentrated among the cells of the spiral bundle. (A) Representative images collected from 12 µm thick sections of the cochlea through the midmodiolar plane. GFP (green) was seen to colocalize within cells positive for NF200 (red) indicative of presence at the neurons within the spiral bundle. No appreciable signal was detected among the cells of the Organ of Corti. **(B)** GFP intensity was seen to increase 2 hours post exposure to 94 dB SPL among all cell types.

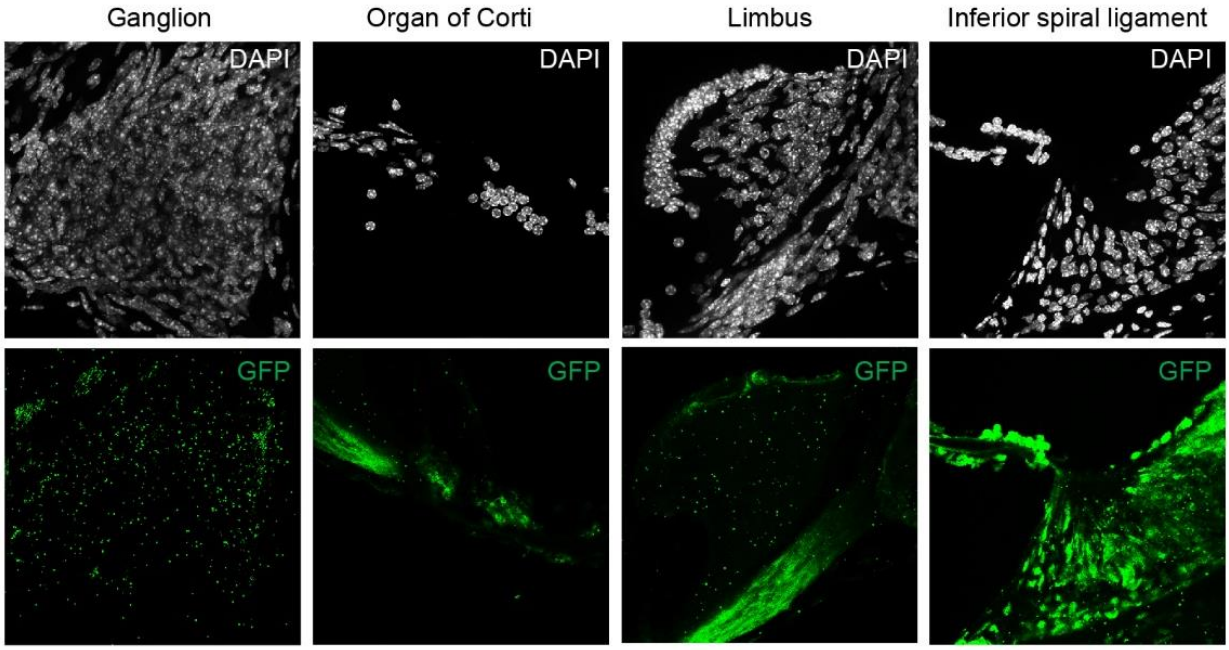
Ganglion
Organ of Corti
Limbus
Inferior spiral ligament
DAPI
DAPI
DAPI
DAPI
GFP
GFP
GFP
GFP

Figure 30. *GFP* is expressed among all cell types within the cochlea and expression is reduced following noise exposure. (A) Representative images of 12 µm thick midmodiolar sections of the cochlea probed against GFP directed *in situ* probed. Regions of the spiral ganglion, organ of Corti, spiral limbus and inferior spiral ligament all observed positive signal for *GFP* expression. Indicative of uniform expression amongst cochlear cell types Scale bar = 25µm.

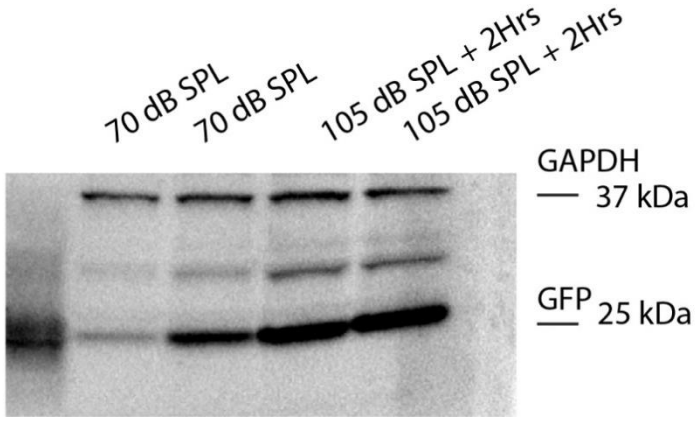
70 dB SPL
70 dB SPL
105 dB SPL + 2Hrs
105 dB SPL + 2Hrs
GAPDH
37 kDa
GFP
25 kDa

Figure 31. GFP levels increase 2 hours after exposure to 105 dB SPL noise. (A) Tg(CAG-Ub*G76V/GFP)1Dant mice were exposed to either ambient (65- 70dB SPL) or severe (105 dB SPL) intensity noise for 2 hours then allowed to rest for 2 hours prior to harvesting of cochlea. Western blot analysis demonstrated an increase in the overall abundance of GPF following noise exposure. N= 2 per condition.

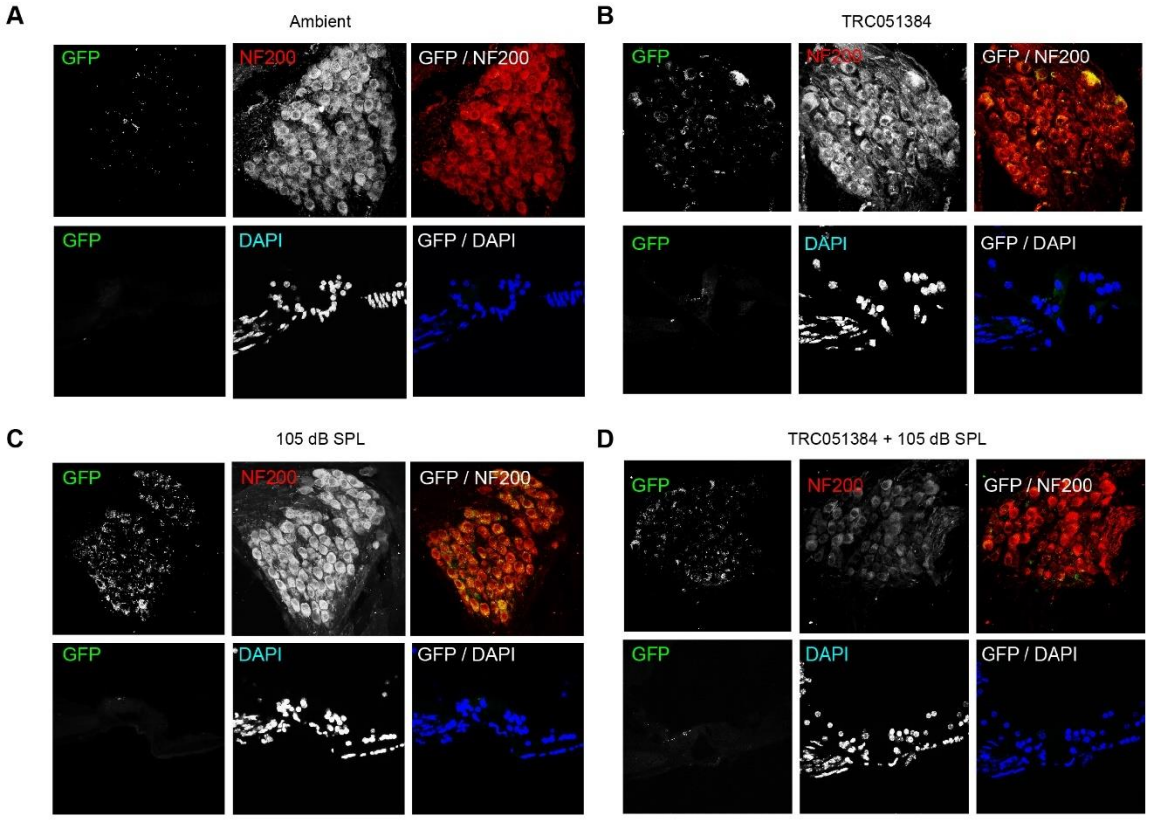
A
Ambient
GFP
NF200
GFP / NF200
GFP
DAPI
GFP / DAPI
B
TRC051384
GFP
NF200
GFP / NF200
GFP
DAPI
GFP / DAPI
C
105 dB SPL
GFP
NF200
GFP / NF200
GFP
DAPI
GFP / DAPI
D
TRC051384 + 105 dB SPL
GFP
NF200
GFP / NF200
GFP
DAPI
GFP / DAPI

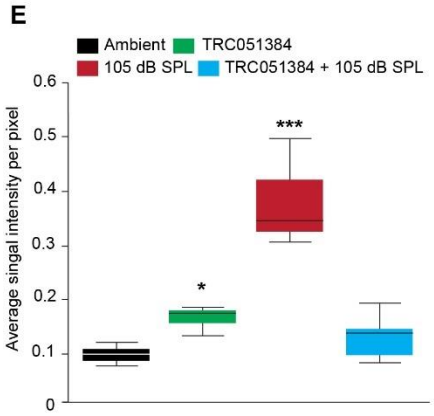
E
Ambient
TRC051384
105 dB SPL
TRC051384 + 105 dB SPL
Average singal intensity per pixel
0.6
0.5
0.4
0.3
0.2
0.1
0
***
*

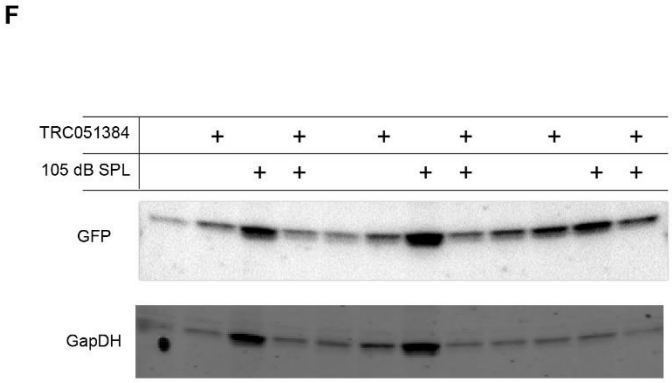
F
TRC051384
105 dB SPL
GFP
GapDH

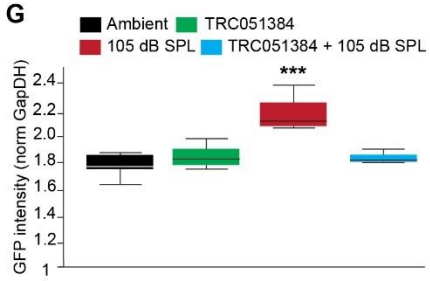
G
Ambient
TRC051384
105 dB SPL
TRC051384 + 105 dB SPL
GFP intensity (norm GapDH)
2.4
2.2
2.0
1.8
1.6
1.4
1.2
1
***

Figure 32. TRC051384 injections elevate GFP abundance prior to noise exposure which reduces cellular stress after noise exposure. (A-B) Representative images of the organ of Corti and the spiral bundle stained against GFP (green) and NF200 (red) from 12 µm thick midmodiolar cochlear sections. Administration of TRC051384 was seen to increase GFP signal intensity above levels observed under ambient conditions **(C-D)** Injection of TRC051384 two hours prior to noise exposure appears to reduce the overall intensity of GFP signal among spiral ganglion cells compared to cochlea that were only exposed to noise. **(E)** Quantification of (A-D) confirm that TRC051384 elevates GFP intensity above basal levels but injection prior to noise significantly reduces GFP signal, indicative of a reduction in overall proteasome stress following noise. **(F-G)** Independent western blot analysis confirms immunohistochemistry findings which demonstrate TRC051384 elevate GFP levels in the absence of noise but reduce overall GFP levels following noise exposure compared to control groups. N= 4 mice per condition (A-D), 3 mice per condition. * = p value < 0.05, *** = p value < 0.001 by one-way ANOVA with Tukey post hoc correction.

Chapter 7 Data in Progress: The Investigation of Long-Lived Proteins within the Cochlea, and the Quantification of Low-Abundance Proteins in Complex Cochlear Samples.

Introduction and Preliminary Data

Hair cells are post-mitotic and are not replaced throughout the life of an animal (Atkinson et al., 2015). Structures within the hair cells, like the stereocilia, have also been shown to be present throughout the life of the cell with minimal protein turnover (Zhang et al., 2012). These permanent structures pose key points of vulnerability as damage accumulated over the life of the cell or after acute cellular damage are likely to result in hearing impairments. We have previously shown that hair cells are enriched in proteins associated with deafness, leading us to ask if extremely long-lived proteins within the cochlea are enriched at the ribbon synapses.

Long-lived proteins, as the name implies, are maintained within cells for incredible lengths of time with low protein turnover (Savas *et al.*, 2012; Toyama et al., 2013). Thus, by comparing the localization of long-lived proteins we may begin to understand the impact of damages to static structures within the cochlea and hearing. To address this, we first fed mice exclusively Nitrogen-15 (^{15}N) enriched chow for four months (from P30 to P190), which will label newly synthesized proteins with "heavy" nitrogen. Proteins with the slowest turnover rates will not readily incorporate the heavy nitrogen and remain mostly "light". Thus, in these mice, unlabeled ^{14}N proteins must have been present before the labeling period at P30 and persisted within the cochlea until harvest. The differences in ^{15}N and ^{14}N can then be detected via mass spectrometry to determine if a protein is long-lived based on its enrichment of ^{14}N (Savas *et al.*, 2012; Toyama *et al.*, 2013).

Using this method, I first worked towards understanding which proteins within the cochlea are long-lived. To this extent we identified 285 proteins which were at least 0.5-fold more enriched in ^{14}N compared to ^{15}N containing peptides. To further investigate the diversity

among the panel of significant proteins, we performed gene ontology cellular component (GO:CC) enrichment analysis with PANTHER (Thomas *et al.*, 2006). The "collogen trimer (GO:0005581)", "basement membrane (GO:0005604)", "keratin filament (GO:0045095)" and "extracellular matrix (GO:0031012)" were among the top cellular pathways enriched in our long-lived panel of proteins **(Figure 33)**. Previously we highlighted collogen associated protein among the most significantly down-regulated proteins following noise exposure, suggesting that collogen structures within the cochlea are highly static, with potentially limited recovery following extensive cellular stress. Specifically, collogen IV has been shown to be enriched within the Reissner's membrane, a structure that separates the perilymph from the endolymph, and surrounding the blood vessels of the cochlea within the stria (Liu et al., 2015). While collogen II localizes to the tectorial membrane, a structure that sits atop the hair cells and is critical for the opening of hair cell mechanoreceptors (Liu *et al.*, 2015). Notably, both alpha- and beta-tectorin were shown to be extremely long-lived within the cochlea, further the large membranes within the cochlea as static structures.

Among the top 10 GO:CO enriched among the long-lived pool of proteins were the terms perisynaptic extracellular matrix" and "extracellular matrix", supporting the rational that proteins which bridge the synaptic cleft of the cochlear ribbon synapse may be long-lived static structures. Our characterization of neuroligins within the cochlear ribbon synapses have highlighted *Nlgn3* as a key contributor towards resistance to noise induced hearing loss. I was unable to detect any neuroligins among our quantified proteins but were able to identify Nrxn3 as long-lived. Although cursory, this finding potentially implies that neuroligins may also be long-lived within the cochlea. Given that higher intensities of noise exposure results in

considerable swelling of ANF terminal and uncoupling of ribbon synapse membranes (Furman *et al.*, 2013; Kujawa and Liberman, 2009). It is possible that during this swelling and decoupling that neurexins and neuroligins are sheered due to the forces generated by the expanding membranes or cleaved to release the pre- and post-synaptic membranes.

However, due to the low abundance of these proteins within the cochlea, traditional western blot and proteomic analysis are faced with significant challenges. Previous experiments aimed at exploring proteins in the hair cells have been met with challenges due to the relatively small proportions of hair cell specific proteins in the inner ear making mass spectrometry (MS) difficult (Hickox *et al.*, 2017). To overcome this challenge, I developed a method for parallel reaction monitoring (PRM) MS/MS to increase our understanding of neuroligins with respect to hearing. UniProt mouse protein database was imported into Skyline and used to create a spectral library for the selection of precursor ions specific to Nlgn3. Candidate precursor ions were required to have charges between 2-5 and rank among the top 5 predicted most intense precursor ions for Nlgn3 **(Figure 34A, C)**. I improved our inclusion list by generating "heavy" Nlgn3 standards with stable isotope labeling of cells in culture (SILAC) to validate the theoretically most intense precursor ions with LC-MS/MS. In brief, Hek203T cells were grown in SILAC heavy medium which replaces all available lysine and arginine amino acids with their heavy isotopes. Hek293T cells were then transfected with plasmids encoding Nlgn3-HA and grown for one week prior to immunoprecipitation (IP). This IP product was then digested and used as an internal standard for the validation of the theoretically most intense Nlgn3 precursor ions.

The major benefits of a PRM guided LC-MS/MS experiment lies in the predefined precursor ion selection list. The specific mass-to-charge ratios (m/z) of these precursors are

monitored and selected within the quadrupole, and are transferred, via the C-trap, to the HCD cell for fragmentation. Upon precursor detection, ions fill the C-trap for an extended period time, effectively increasing the signal-to-noise ratio of the ions eventually measured in the Orbitrap (Domon and Gallien, 2015; Gallien et al., 2012). Given that the similarities of heavy and light peptides with respect to MS retention times, the use of isotopically labeled internal standards can be used selectively drive PRM acquisitions of the endogenous peptides. Allowing for the detection and quantification of low abundance proteins within highly complex backgrounds, such as neuroligins within the cochlea. Within our trial experiments, I spiked heavy labeled Nlgn3 peptides into cochlear digests in a 1:1 ratio. Notably, both GNYGLLDQIQALR and ELVEQDIQPAR, rank 1 and 2 theoretically most abundant precursors for Nlgn3, were detected in the heavy Nlgn3 spiked cochlear samples **(Figure 34B, D)**. Moreover, the Nlgn3 precursor peptide ELVEQDIQPAR was able to detect endogenous levels of Nlgn3 across all 5 trial experiments **(Figure 34D)**.

To further improve upon this method, I utilized a linear regression analysis to predict the elution profile for the top precursor m/z to increase the specificity of the PRM by defining a scheduler **(Figure 35AB)**. To test the scheduler, I again spiked heavy Nlgn3 peptide standards into two micrograms of cochlear lysates and compared the specificity of our scheduled PRM with traditional data dependent acquisition (DDA) and S-PRM with heavy Nlgn3 standard alone. Trials for DDA and S-PRM were analyzed offline with Skyline to determine the specificity of precursor ion selection **(Figure 36A)**. Cochlea spiked with heavy standards observed similar selectivity of precursors at each specified retention time compared to heavy standard alone, however, the intensity of the measured ions was halved within the spiked cochlea **(Figure 36B)**.

Although S-PRM was seen to be more stringent compared to DDA alone, as it selectively identified Nlgn3 via 61 spectral counts. This method failed to robustly measure endogenous Nlgn3, as this protein could not be measured among the top 4 ranking precursor ions selected by S-PRM. Further refinement of our S-PRM method is necessary however, once complete it will be an invaluable tool in the analysis of low-abundance proteins.

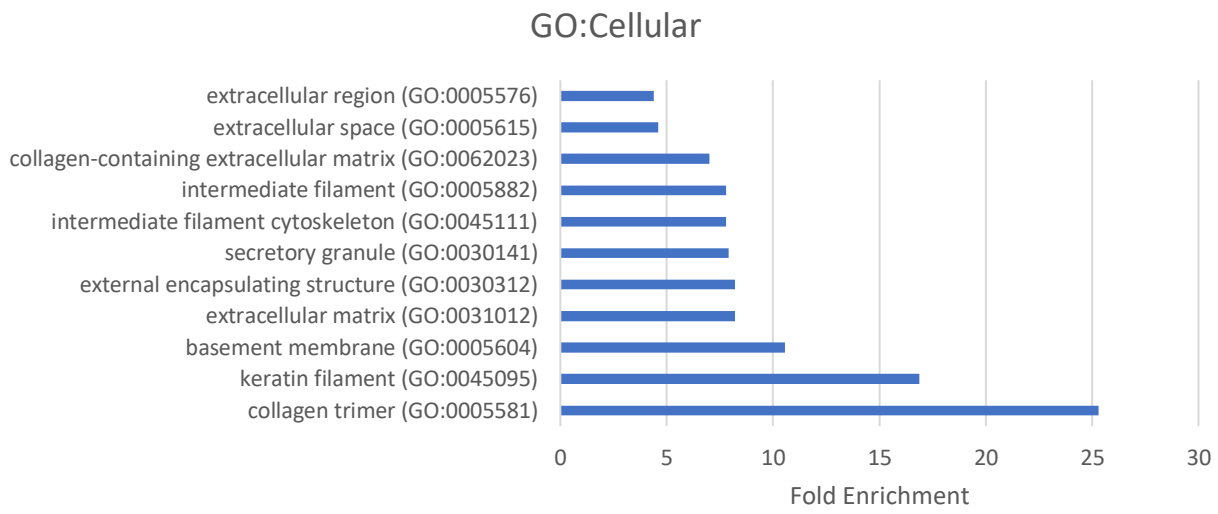
GO:Cellular
extracellular region (GO:0005576)
extracellular space (GO:0005615)
collagen-containing extracellular matrix (GO:0062023)
intermediate filament (GO:0005882)
intermediate filament cytoskeleton (GO:0045111)
secretory granule (GO:0030141)
external encapsulating structure (GO:0030312)
extracellular matrix (GO:0031012)
basement membrane (GO:0005604)
keratin filament (GO:0045095)
collagen trimer (GO:0005581)
0
5
10
15
20
25
30
Fold Enrichment

Figure 33. GO analysis of long-lived proteins within the cochlear determined an enrichment in collogen and extracellular matrix proteins. (A) GO:Cellular analysis of 285 proteins seen to have at least a 0.5 fold enrichment of ^{14}N following four months of ^{15}N labeling ($^{14}N/ (^{14}N+^{15}N)$). Proteins associated with the cellular ontologies “Collegen trimer”, “basement membrane”, and “extracellular matrix” were among the top 5 enriched ontologies.

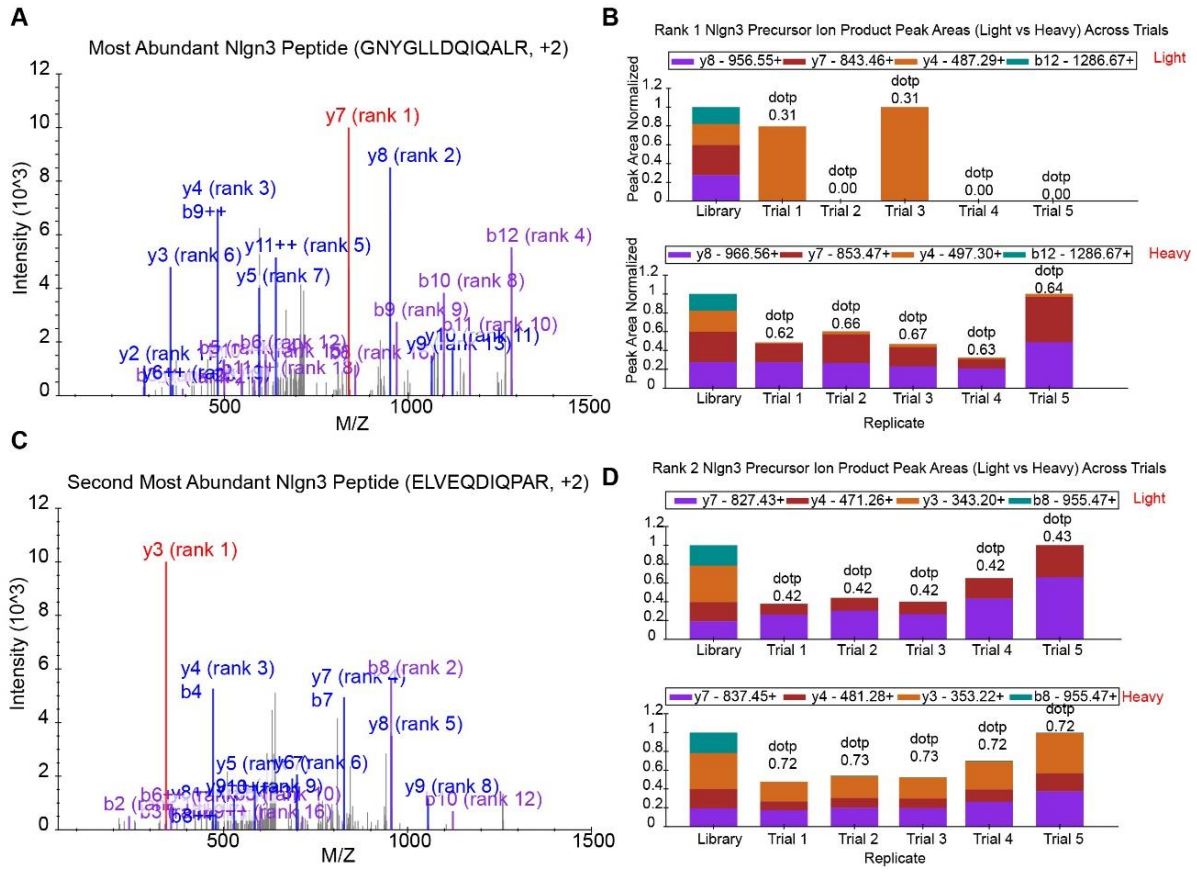
A
Most Abundant Nlgn3 Peptide (GNYGLLDQIQALR, +2)
Intensity (10^3)
M/Z
y7 (rank 1)
y8 (rank 2)
y4 (rank 3)
b9++
y3 (rank 6)
y11++ (rank 5)
y5 (rank 7)
b12 (rank 4)
b10 (rank 8)
b9 (rank 9)
B
Rank 1 Nlgn3 Precursor Ion Product Peak Areas (Light vs Heavy) Across Trials
y8 - 956.55+ y7 - 843.46+ y4 - 487.29+ b12 - 1286.67+ Light
y8 - 966.56+ y7 - 853.47+ y4 - 497.30+ b12 - 1286.67+ Heavy
Peak Area Normalized
Library
Trial 1
Trial 2
Trial 3
Trial 4
Trial 5
Replicate
C
Second Most Abundant Nlgn3 Peptide (ELVEQDIQPAR, +2)
y3 (rank 1)
y4 (rank 3)
b4
b8 (rank 2)
b7
y8 (rank 5)
y9 (rank 8)
b10 (rank 12)
D
Rank 2 Nlgn3 Precursor Ion Product Peak Areas (Light vs Heavy) Across Trials
y7 - 827.43+ y4 - 471.26+ y3 - 343.20+ b8 - 955.47+ Light
y7 - 837.45+ y4 - 481.28+ y3 - 353.22+ b8 - 955.47+ Heavy

Figure 34. Comparison of the theoretical top two most intense precursor and product ions with measured ions associated with Nlgn3. (A) Skyline was used to compile the theoretically most intense precursor ion for Nlgn3, “GNYGLLDQIQALR”, product ions expected to result from the fragmentation are ranked based on expected intensity. **(B)** Summary of expected product ion intensities compared to observed ions across 5 trials. Heavy Nlgn3 peptide standards were measured in each trial with endogenous Nlgn3 product ions observed in 2 of the 5 trials. **(C)** Theoretical product intensities for the second most abundant precursor ion associated with Nlgn3, “ELVEQDIQPAR”. **(D)** Summary of expected product ion intensities compared to observed ions across 5 trials. Heavy Nlgn3 peptide standards as well as endogenous Nlgn3 product ions were observed in all 5 trials.

A

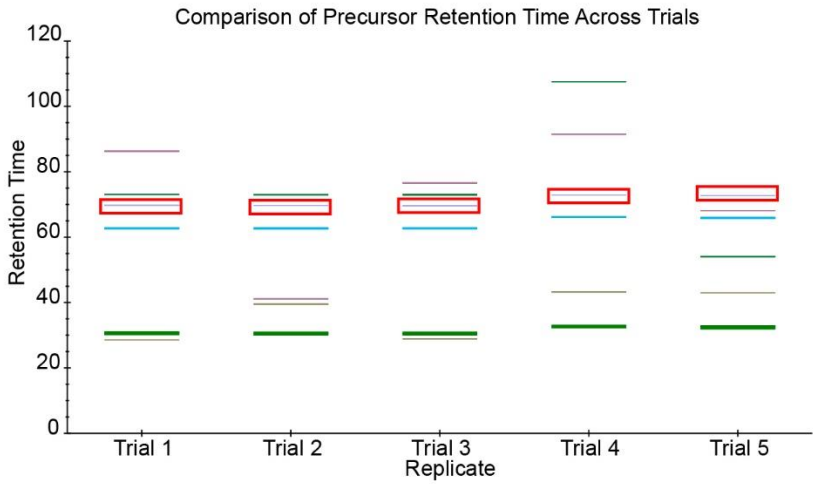
Comparison of Precursor Retention Time Across Trials
Retention Time
120
100
80
60
40
20
0
Trial 1
Trial 2
Trial 3
Trial 4
Trial 5
Replicate

B

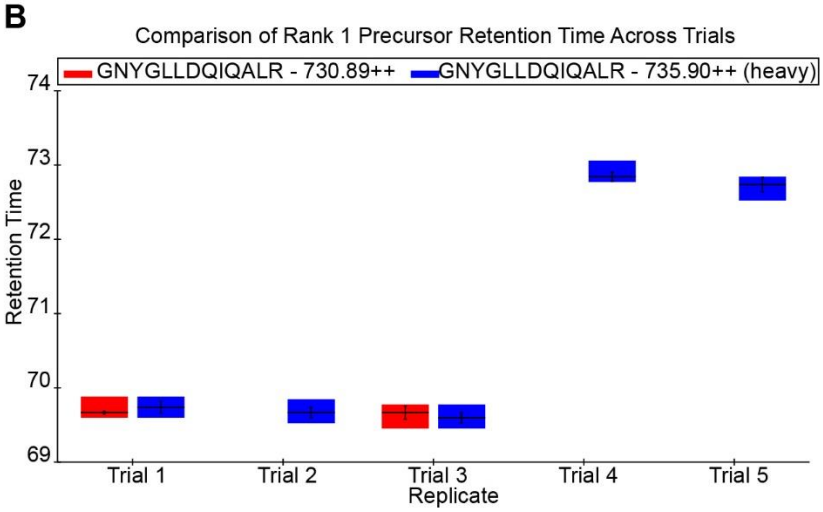
Comparison of Rank 1 Precursor Retention Time Across Trials
GNYGLLDQIQALR - 730.89++
GNYGLLDQIQALR - 735.90++ (heavy)
Retention Time
74
73
72
71
70
69
Trial 1
Trial 2
Trial 3
Trial 4
Trial 5
Replicate

Figure 35. Analysis of retention times associated with the 6 precursors used for PRM observed similar elution times across all trials. (A) Comparison of retention times across each two-hour MS/MS analysis observed similar elution patterns. Red boxes highlight product ion GNYGLLDQIQALR which is the theoretically most intense was measured in each trial at a similar time within analysis. **(B)** Higher resolution representation of product ions highlighting deviations in retention times, which on average were less than 1 min.

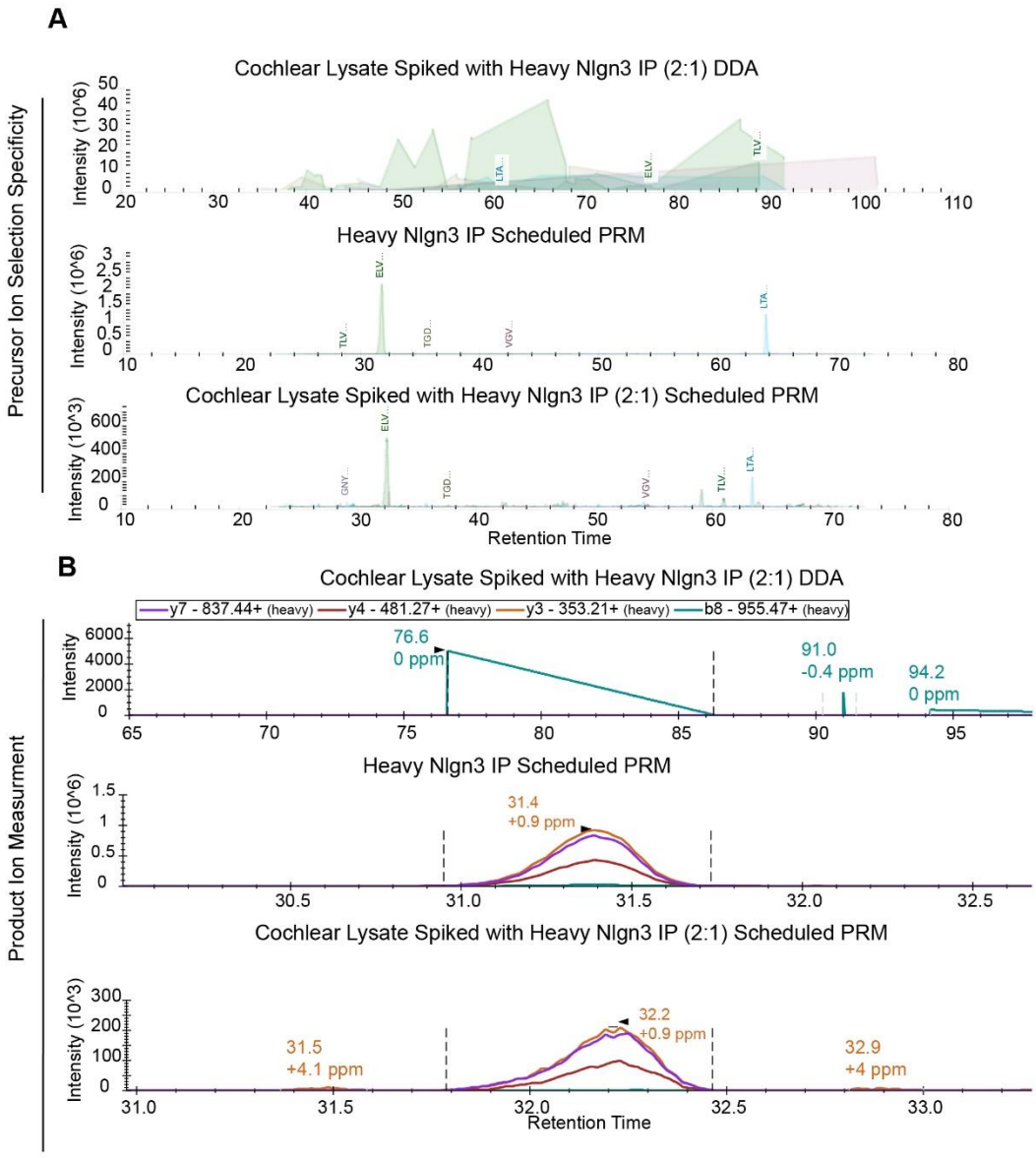
A
Precursor Ion Selection Specificity
Cochlear Lysate Spiked with Heavy Nlgn3 IP (2:1) DDA
Intensity (10^6)
Heavy Nlgn3 IP Scheduled PRM
Intensity (10^6)
Cochlear Lysate Spiked with Heavy Nlgn3 IP (2:1) Scheduled PRM
Intensity (10^3)
Retention Time
B
Product Ion Measurment
Cochlear Lysate Spiked with Heavy Nlgn3 IP (2:1) DDA
y7 - 837.44+ (heavy)
y4 - 481.27+ (heavy)
y3 - 353.21+ (heavy)
b8 - 955.47+ (heavy)
Intensity
76.6
0 ppm
91.0
-0.4 ppm
94.2
0 ppm
Heavy Nlgn3 IP Scheduled PRM
Intensity (10^6)
31.4
+0.9 ppm
Cochlear Lysate Spiked with Heavy Nlgn3 IP (2:1) Scheduled PRM
Intensity (10^3)
31.5
+4.1 ppm
32.2
+0.9 ppm
32.9
+4 ppm
Retention Time

Figure 36. Comparison of DDA and S-PRM methods demonstrate increasing levels of selectivity for Nlgn3 product ions. (A) Cochlear lysates were spiked with heavy Nlgn3 peptide standards in a 2:1 ratio prior to LC-MS/MS analysis. Similarly, heavy Nlgn3 standards were run as internal control with S-PRM. Each run was then analyzed within Skyline for comparison of precursor selection specificity. As anticipated, DDA resulted in the lowest specificity for Nlgn3 while the S-PRM method observed the most intense and specific ion selection. Cochlear lysates spiked with heavy Nlgn3 observed similar ion selection times, but the overall intensity of each precursor was halved compared to intensities measured for heavy Nlgn3 standards alone. **(B)** Area under the curve was used to gauge the ratio of ion intensity among Nlgn3 product ions across trials. DDA failed to trigger a precursor selection which identified a specific Nlgn3 product ion. Product ion intensities observed a 1-minute delay in retention time within cochlea spiked with heavy Nlgn3 standard compared to standard alone.

Chapter 8: General Discussion

Discussion I: Neuroligins and Hearing

Nlgn1 and Nlgn3 play key roles in the maturation of excitatory synapses in the CNS since neurons with reduced levels of either Nlgn1 or Nlgn3 fail to reach functional maturity (Chanda *et al.*, 2017; Chih et al., 2005; Jiang et al., 2017; Varoqueaux *et al.*, 2006; Zhang et al., 2015). Within this thesis I provide the first characterization of Nlgn1 and Nlgn3 with respect to their impact on hearing and ribbon synapse morphology. In chapter 3 we determined that both *Nlgn1* and *Nlgn3* are expressed by SGNs and are present at nearly 90% of cochlear ribbon synapses. In chapter 4 I then determined the functional deficits that manifest among the cochlear ribbon synapses of *Nlgn1* and *Nlgn3* KO. Interestingly, many of these cochlear phenotypes including reduced ribbon synapse number per inner hair cell, smaller ribbon synapse size, increases in the distance between pre- and postsynaptic membranes and mildly impaired cochlear function were shared among single KOs. However, ablation of both Nlgn1 and Nlgn3 generally resulted in a synergistic phenotype (i.e., worse than expected from the additive effects of the single KOs), suggesting essential overlapping functions for Nlgn1 and Nlgn3 in synapse formation and maintenance. For example, the dKO mice had a ~30% reduction in synapse number and a nearly five-fold reduction in synapse size. Cochlear function was also robustly impaired in the dKOs since their ABR thresholds, Wave I amplitudes, and latencies were significantly impaired for all probe frequencies.

Notably, throughout the establishment period of cochlear ribbon synapses (Michanski et al., 2019), only *Nlgn3* expression consistently increased, suggesting a prominent role for this protein in the maturation of ribbon synapses. Assessment of synaptic density at P12 and P30 again highlighted the importance of Nlgn3 for synapse maturation (Michanski *et al.*, 2019), as

only *Nlgn1* KO inner hair cell ribbon synapse number increased from P12 to P30. Synaptic density was significantly reduced at P30 in the single KOs suggesting that these proteins are closely related to the maintenance of cochlear ribbon synapse rather than the initial formation of these synapses. Indeed, the presence of ribbon synapses among double KO cochlea at P12 suggests that there exists a mechanism outside of neuroligins to aid in synapse formation. However, given that synaptic density is reduced at P30, it also suggests that these unknown proteins are not sufficient for the maintenance of all cochlear ribbon synapses.

The promiscuous interactions of neurexins and the presence of additional SAMs opens the door for future investigations of these synaptic organizing proteins within hearing. Leucine-rich repeat (LRR)-containing synaptic adhesion molecules (LRRTMS) in example have been readily studied and are known to interact with neurexins to support AMPAR activity through poorly characterized interactions within Schaffer collateral-CA1 synapses (de Wit *et al.*, 2009; Soler-Llavina et al., 2011). Similarly, knockdown of *Flrt3,* which can interact with neurexins and latrophilins, leads to reductions in mEPSC frequency and amplitude in dissociated hippocampal neurons (O'Sullivan et al., 2012). Investigating the impact of SAMs that do not interact with neurexins will also undoubtably highlight the significance of postsynaptic remodeling in hearing. For example, SALM2 (synaptic adhesion-like molecule) is of particular interest as it is not synaptogenic but rather promotes the maturation of excitatory synapses via clustering of both NMDA and AMPA receptors in dissociated hippocampal neurons (Nam et al., 2011). Current evidence suggests that SALM2 is predominately expressed, all be it lowly, by type Ia SGNs making it a preferential target for the characterization of low threshold fiber activity impairments (Shrestha *et al.*, 2018).

Indeed, the cochlear inner hair cell ribbon synapses provide a unique opportunity to discriminate the roles of Nlgn3 and Nlgn1 at distinct one-to-one synapses, where each auditory nerve fiber (i.e., SGN) is driven by an individual synapse. I found that the inner hair cells of *Nlgn1* KO but not of *Nlgn3* KO harbor orphan ribbons, suggesting that *Nlgn1* is particularly important for the physical coupling of pre- and post-synaptic membranes, likely via its interactions with intracellular structures. However, the number of orphan ribbons was increased five-fold in the dKO relative to *Nlgn1* KOs, suggesting that *Nlgn3* also contributes to transsynaptic coupling in the absence of *Nlgn1*. In support of this, analysis of the distance between pre and postsynaptic elements determined that *Nlgn1* and *Nlgn3* KOs both exhibited an increase in the distance between CtBP2 and GluA2 puncta.

ABR analysis of *Nlgn1* KOs show only a mild reduction in Wave I amplitudes at 8 kHz. In *Nlgn3* KO mice, ABR Wave I amplitudes were reduced across the 8-28 kHz frequency range, which more closely resembled the *Nlgn1/3* dKO phenotypes. These functional phenotypes in the absence of dramatic reductions in cochlear ribbon synapses suggest that integrity of the remaining synapse is perturbed. Indeed, evidence linking *Nlgn1* and *Nlgn3* to AMPAR recruitment and the orientation of nanodomains throughout the postsynaptic membrane has been previously reported (Luo et al., 2021; Shipman *et al.*, 2011). In addition to the displacement of AMPARs in the absence of either *Nlgn1* and *Nlgn3*, both neuroligins have been shown to influence the strength of AMPARs, potentially explaining why ABR phenotypes manifested among single KOs in the absence of a dramatic loss of synapses (Chanda *et al.*, 2017; Shipman *et al.*, 2011). The milder phenotypes observed in *Nlgn1* KOs are interesting albeit not easily explained. I determined by qPCR that Nlgn3 expression is increased in Nlgn1 KOs but the latter

is not true for Nlgn3 KOs, suggestive of a type of compensate only observed in Nlgn1 KOs. Potentially explaining why more dramatic functional phenotypes were able to manifest in the Nlgn3 KOs. Nonetheless, these reductions in the amplitude and increases in both the latency and duration of Wave I is suggestive of a desynchronization of SGN action potential generation at sound onset, as seen in mice lacking synaptic ribbons (Buran *et al.*, 2010). An increase in the jitter of first-spike latency in the auditory nerve is expected to result from a reduction of amplitude among the excitatory post-synaptic current (Rutherford et al., 2012), which is then expected to impair aspects of sound encoding that rely on spike timing and phase locking, such as sound source localization in the horizontal plane (Rutherford et al., 2021).

Similarly, the reduced responses to high-intensity tones in *Nlgn3* and *Nlgn*1/3 dKO mice are expected to impair suprathreshold hearing, similar to cochlear synaptopathy resulting from moderate-intensity noise exposure. With moderate noise exposure, a reduction in Wave I amplitude is present only at higher levels of stimulation because low-threshold SGNs are largely unaffected (Kujawa and Liberman, 2009). In contrast, the *Nlgn1/3* dKO phenotype included reduction of Wave I amplitudes at all sound levels, suggesting dysfunction of synapses driving both hi- and low-threshold SGNs. However, since Nlgn1 and Nlgn3 may function in synapses of the ascending auditory pathway, future experiments with conditional KO mice are needed to determine if those effects emanate directly from CNS deficiencies or indirectly from reduced cochlear output, or both.

Mutations to *Nlgn1* and *Nlgn3* have been previously linked to some forms of autism spectrum disorder (ASD)(Guang et al., 2018; Nguyen et al., 2020; Poulopoulos *et al.*, 2012; Taylor et al., 2020; Uzunova et al., 2014; Zhang *et al.*, 2017). Given our new understanding of the role

for Nlgn3 and Nlgn1 in hair cell ribbon synapse function, it is possible that altered noise sensitivity, in individuals with ASD stemming from neuroligin mutations, could be attributed to abnormalities in cochlear function or central auditory processing (Leekam et al., 2007; Miron et al., 2021). Alterations to sensory processing and hypersensitivity to stimuli are hallmarks of individuals with ASD. Moreover, the reduction to Wave I amplitudes observed in *Nlgn3* KOs in the absence of elevated hearing thresholds is of interest as this phenotype is similar to hearing deficits commonly referred to as hidden hearing loss (Shi *et al.*, 2016). In this condition, individuals show no impairments to overall hearing sensitivity but lose the ability to distinguish relevant auditory information in noisier environments. The specific loss of these "cocktail party neurons" thus result in what one would believe to be a very uncomfortable and frustrating experiences in music venues, movie theaters and large open classrooms.

Perhaps what manifests in individuals with ASD, resulting from neuroligin mutations, is not a hypersensitivity to stimuli but rather an inability to decipher relevant information from background stimuli like hidden hearing loss. However, what makes ASD curious is the lack of a singular lynchpin protein. Unlike diseases such as Huntington's, where a single mutation drives a progressive increase in cognitive deficits overtime or pathologies like Alzheimer's in which a protein drives the deterioration of the brain and body via protein-protein interactions. No such singular protein or gene mutation exists when we speak about ASD. Rather, ASD manifests as a collection of mutations and deficits lumped together on a spectrum (Abrahams and Geschwind, 2008; Etherton *et al.*, 2011a; Zhang *et al.*, 2017). This diversity among etiology leads to caveats, not only with respect to the conclusions we can draw from our investigations, but also limits how generalizable these conclusions are in the grand scheme of the disorder. With the prominence of

ASD rising rapidly, in 2012 the CDC reported that 1 in 88 children would be diagnosed with ASD which skyrocketed to 1 in 44 children in 2018. It is likely that the investigation of mutations associated with ASD will continue to expand our understanding of critical functions at the neuronal and circuit level.

Nonetheless, our novel findings reveal roles for *Nlgn1* and *Nlgn3* in cochlear ribbon synapse structure and function that have direct impacts on hearing through impairment of sound encoding in the cochlea and preservation after noise exposure.

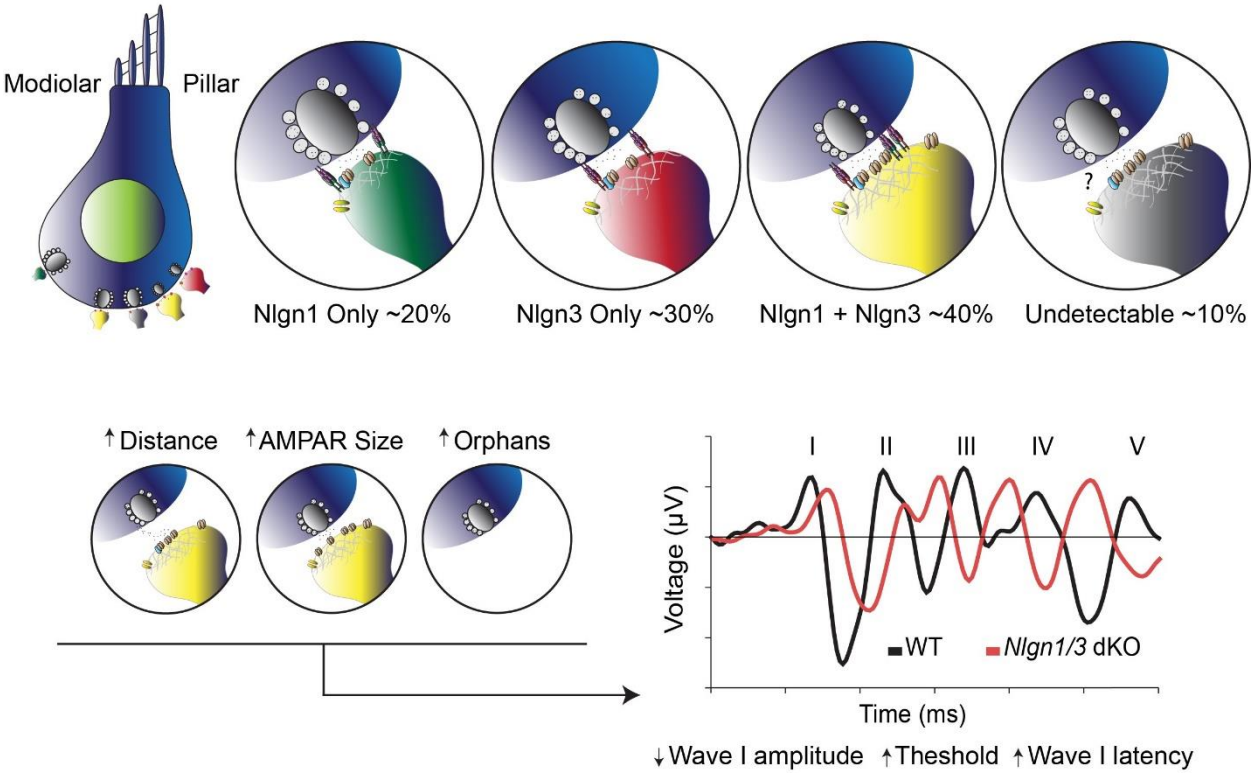
Modiolar
Pillar
Nlgn1 Only ~20%
Nlgn3 Only ~30%
Nlgn1 + Nlgn3 ~40%
Undetectable ~10%
?
↑Distance
↑AMPAR Size
↑Orphans
I
II
III
IV
V
Voltage (μV)
WT
Nlgn1/3 dKO
Time (ms)
↓Wave I amplitude
↑Theshold
↑Wave I latency

Figure 37. Summary of the Impact of Neuroligin 1/3 on Ribbon Synapse Structure and Function. Neuroligins 1 and 3 are present either alone or together among 90% of all cochlear ribbon synapses. Ablation of neuroligin expression leads to an increase in the physical distance between pre- and postsynaptic membranes, increases in the size of AMPAR puncta volumes and an increase in the number of orphans. This drives a reduction in the amplitude of Wave I in addition to an increase in ABR threshold levels. Double Nlgn1/3 KOs notably manifested a significant increase in ABR Wave I latency.

Discussion II: The Cellular Impact of Noise Exposure

The proteomic results outlined in chapter 5 add to the already compelling literature highlighting the complexity of the cochlear response to noise exposure. We found that cochlear overstimulation drives alterations to cochlear structures, gene expression, elevations in protein abundances, and general increases in global protein ubiquitylation. By focusing on noise exposures which induce auditory neuropathy, we were able to capture a snapshot of the molecular pathways elevated immediately following noise exposures. Recruitment of these pathways likely induce the deterioration of hair cells, loss of ribbon synapses, or are reflective of damages to the ANF terminals. Unexpectedly, our proteomic analysis determined that even moderate intensity noise exposures can broadly affect cochlear structures and cells.

The intensity dependent increase in protein abundance, we anticipate, is the result of either direct damage or associated cellular stress following noise exposure. This alterations to protein structure would then impair protein - protein interactions, driving the demand for protein synthesis to replace damaged proteins, contributing to overall abundance. This rational is supported by the recruitment of multiple nodes of the cochlear proteostasis network after both moderate and severe noise exposure. Specifically, HSP chaperones were seen to have elevated levels after noise exposure, notably members of the Hsp40 family (i.e. DnaJs), which prevent irreversible protein aggregation under cellular stress (Angles et al., 2017; Langer et al., 1992). HSPs, in addition, have been previously reported to be selectively elevated after noise exposure, likely playing protective roles (Gong et al., 2012; Lim et al., 1993). Consist with this finding, HSPs that localize to the cytosol (Hsp90aa1 and Hsp90ab1), in addition to the endoplasmic reticulum, nucleus, and plasma membrane (Hsp90b1) observed elevated levels after noise

exposure. Highlighting a systematic heat shock response among the various compartments of the cell, moreover, we also found that the heat shock response was non-uniform in its severity from inner hair cell to inner hair cell, highlighting the complexity of noise induced stress at the cellular level.

In addition to the heat shock response, we also found that numerous Ubiquitin-Proteasome system factors (Skp1, Usp19, Bag6, and Vcp) in addition to global ubiquitylation levels were elevated following noise. Suggestive of a significant level of damage to the cochlear proteome after noise exposure. Protein post-translational modifications within the cochlea have largely been studied under the lens of cellular development, leaving the importance of glycosylation, ubiquitylation and SUMOylation within the context of noise induced hearing loss poorly characterized (Mateo Sanchez et al., 2016). Although preliminary, our findings provide the first proteome wide analysis of cochlear protein ubiquitylation following noise exposure. The importance of ubiquitylation in NIHL is supported by findings from ubiquitin-specific protease 53 (Usp53), a member of the deubiquitinating enzyme family, mutant mice (Kazmierczak et al., 2015). Notably, loss of Usp53 drives increased susceptibility to noise induced trauma at high frequencies, which is believed to result from a weakening of the tight adherent junctions (Kazmierczak et al., 2015).

In our own datasets we discovered several collagen proteins, which provide structural support within the cochlea, with reduced protein abundance following exposures to moderate or severe intensity noise. Suggesting that these structures are damaged by excess noise, become ubiquitylated, and are subsequently degraded. This is further supported by our diGly MS analysis which determined that Col16a1 is ubiquitylated following severe levels of noise exposure.

Together potentially highlighting the importance of ubiquitylation with respect to noise induced hearing loss and the need for a more robust investigation into the role of ubiquitylated proteins following noise exposure.

Consistent with this finding, we found that two weeks after noise exposure that ribosomal proteins had robustly elevated levels suggesting one of two possibilities. The first is that ribosomes are actively turned over after noise exposure, potentially as a result of damage or that the ribosomes are upregulated due to the increased demands for protein synthesis during recovery to replace proteins that were damaged and degraded acutely following exposure (Anisimova et al., 2018; Shcherbik and Pestov, 2019; Zhou et al., 2015). The inability for proteins to function would suggest the potential for noise induced proteotoxicity, which likely creates a disequilibrium in protein homeostasis, ultimately suspending basic cellular functions thus leading to cell death (Balch et al., 2008; Morimoto, 2008).

The striking difference with respect to enriched cellular ontologies associated with moderate versus severe noise induced proteome remodeling may underline the differences in recovery potential. Namely, the lack of enriched ontologies observed in the severe condition suggests that this level of exposure may shift the proteome from protection mechanisms towards pathways emphasizing survival. Together suggesting that mitigating the denaturation of proteins or lessening the metabolic demands associated with the noise induced cellular stress are likely viable strategies for lessening the permeant loss of hearing sensitivity. Future research into the administration of drugs, such as TRC051384, to prime the cochlea for noise exposures are likely to greatly improve the overall quality of life for individuals that are exposed to dangerous levels of noise daily. Preliminary experiments have shown that TRC051384 is sufficient for reducing

the elevations in threshold levels two weeks following noise exposures. Investigation of the cellular impact of TRC051384 demonstrated an increase with respect to basal levels of cellar stress, observable by an increase in GFP signal intensity. However, cellular stress was significantly reduced following noise exposure compared to mice that were not pretreated with TRC051384, indicating that this “priming” of the cellular stress response prior to noise may mitigate damages which may be acquired because of prolonged exposures. Additional experiments are necessary to determine administration of TRC051384 following noise can still rescue threshold levels or if elevating the stress response following noise would drive more severe threshold shifts to manifest two-weeks after initial exposures.

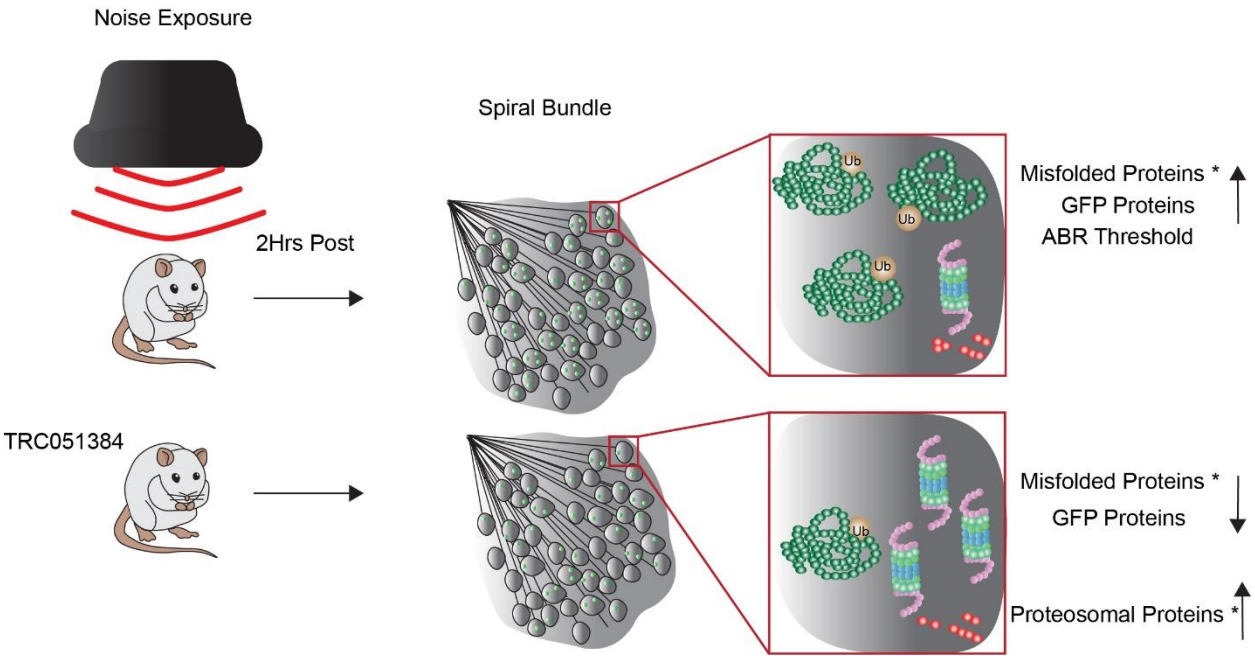
Noise Exposure
2Hrs Post
TRC051384
Spiral Bundle
Ub
Ub
Ub
Misfolded Proteins *
GFP Proteins
ABR Threshold
Ub
Misfolded Proteins *
GFP Proteins
Proteosomal Proteins *

Figure 38. Speculation on TRC051384's Effect on the Preservation of Hearing Following Noise. Pretreatment of TRC051384 prior to 2-hour exposures to noise dramatically reduces the frequency and intensity of GFP signal within the cells of the spiral bundle compared to mice that did not receive treatment. This suggests that misfolded proteins are cleared from cells faster than they can accumulate in TRC051384 treated tissues compared to controls. We have shown that the heat shock response and multiple proteasomal proteins are elevated following noise exposure. It is likely that TRC051384 elevated basal levels of these proteins prior to noise "priming" the cells for the accumulation of numerous misfolded proteins because of noise exposure. Clearance of these misfolded proteins likely accelerates recovery mechanisms leading to a reduction in threshold elevations observed two weeks after noise exposure in TRC051384 treated mice compared to untreated mice.

Chapter 9: References

1. Abrahams, B.S., and Geschwind, D.H. (2008). Advances in autism genetics: on the threshold of a new neurobiology. Nat Rev Genet *9*, 341-355. 10.1038/nrg2346.
2. Angles, F., Castanie-Cornet, M.P., Slama, N., Dinclaux, M., Cirinesi, A.M., Portais, J.C., Letisse, F., and Genevaux, P. (2017). Multilevel interaction of the DnaK/DnaJ(HSP70/HSP40) stress-responsive chaperone machine with the central metabolism. Sci Rep *7*, 41341. 10.1038/srep41341.
3. Anisimova, A.S., Alexandrov, A.I., Makarova, N.E., Gladyshev, V.N., and Dmitriev, S.E. (2018). Protein synthesis and quality control in aging. Aging (Albany NY) *10*, 4269-4288. 10.18632/aging.101721.
4. Atkinson, P.J., Huarcaya Najarro, E., Sayyid, Z.N., and Cheng, A.G. (2015). Sensory hair cell development and regeneration: similarities and differences. Development *142*, 1561-1571. 10.1242/dev.114926.
5. Balch, W.E., Morimoto, R.I., Dillin, A., and Kelly, J.W. (2008). Adapting proteostasis for disease intervention. Science *319*, 916-919. 10.1126/science.1141448.
6. Becker, L., Schnee, M.E., Niwa, M., Sun, W., Maxeiner, S., Talaei, S., Kachar, B., Rutherford, M.A., and Ricci, A.J. (2018). The presynaptic ribbon maintains vesicle populations at the hair cell afferent fiber synapse. Elife *7*. 10.7554/eLife.30241.
7. Berg, S., Kutra, D., Kroeger, T., Straehle, C.N., Kausler, B.X., Haubold, C., Schiegg, M., Ales, J., Beier, T., Rudy, M., et al. (2019). ilastik: interactive machine learning for (bio)image analysis. Nat Methods *16*, 1226-1232. 10.1038/s41592-019-0582-9.
8. Blundell, J., Blaiss, C.A., Etherton, M.R., Espinosa, F., Tabuchi, K., Walz, C., Bolliger, M.F., Sudhof, T.C., and Powell, C.M. (2010). Neuroligin-1 deletion results in impaired spatial memory and increased repetitive behavior. J Neurosci *30*, 2115-2129. 10.1523/JNEUROSCI.4517-09.2010.
9. Bolliger, M.F., Pei, J., Maxeiner, S., Boucard, A.A., Grishin, N.V., and Sudhof, T.C. (2008). Unusually rapid evolution of Neuroligin-4 in mice. Proc Natl Acad Sci U S A *105*, 6421-6426. 10.1073/pnas.0801383105.
10. Budreck, E.C., and Scheiffele, P. (2007). Neuroligin-3 is a neuronal adhesion protein at GABAergic and glutamatergic synapses. Eur J Neurosci *26*, 1738-1748. 10.1111/j.1460-9568.2007.05842.x.
11. Buran, B.N., Strenzke, N., Neef, A., Gundelfinger, E.D., Moser, T., and Liberman, M.C. (2010). Onset coding is degraded in auditory nerve fibers from mutant mice lacking synaptic ribbons. J Neurosci *30*, 7587-7597. 10.1523/JNEUROSCI.0389-10.2010.
12. Butko, M.T., Savas, J.N., Friedman, B., Delahunty, C., Ebner, F., Yates, J.R., 3rd, and Tsien, R.Y. (2013). In vivo quantitative proteomics of somatosensory cortical synapses shows which protein levels are modulated by sensory deprivation. Proc Natl Acad Sci U S A *110*, E726-735. 10.1073/pnas.1300424110.
13. Cai, T., Jen, H.I., Kang, H., Klisch, T.J., Zoghbi, H.Y., and Groves, A.K. (2015). Characterization of the transcriptome of nascent hair cells and identification of direct targets of the Atoh1 transcription factor. J Neurosci *35*, 5870-5883. 10.1523/JNEUROSCI.5083-14.2015.
14. Carter, L., Williams, W., Black, D., and Bundy, A. (2014). The leisure-noise dilemma: hearing loss or hearsay? What does the literature tell us? Ear Hear *35*, 491-505. 10.1097/01.aud.0000451498.92871.20.
15. Castellano-Munoz, M., Schnee, M.E., and Ricci, A.J. (2016). Calcium-induced calcium release supports recruitment of synaptic vesicles in auditory hair cells. J Neurophysiol *115*, 226-239. 10.1152/jn.00559.2015.

16. Chanda, S., Hale, W.D., Zhang, B., Wernig, M., and Sudhof, T.C. (2017). Unique versus Redundant Functions of Neuroligin Genes in Shaping Excitatory and Inhibitory Synapse Properties. J Neurosci *37*, 6816-6836. 10.1523/JNEUROSCI.0125-17.2017.
17. Chen, H., Shi, L., Liu, L., Yin, S., Aiken, S., and Wang, J. (2019). Noise-induced Cochlear Synaptopathy and Signal Processing Disorders. Neuroscience *407*, 41-52. 10.1016/j.neuroscience.2018.09.026.
18. Cheng, A.G., Cunningham, L.L., and Rubel, E.W. (2005). Mechanisms of hair cell death and protection. Curr Opin Otolaryngol Head Neck Surg *13*, 343-348. 10.1097/01.moo.0000186799.45377.63.
19. Chih, B., Engelman, H., and Scheiffele, P. (2005). Control of excitatory and inhibitory synapse formation by neuroligins. Science *307*, 1324-1328. 10.1126/science.1107470.
20. Chih, B., Gollan, L., and Scheiffele, P. (2006). Alternative splicing controls selective trans-synaptic interactions of the neuroligin-neurexin complex. Neuron *51*, 171-178. 10.1016/j.neuron.2006.06.005.
21. Choi, Y.B., Li, H.L., Kassabov, S.R., Jin, I., Puthanveettil, S.V., Karl, K.A., Lu, Y., Kim, J.H., Bailey, C.H., and Kandel, E.R. (2011). Neurexin-neuroligin transsynaptic interaction mediates learning-related synaptic remodeling and long-term facilitation in aplysia. Neuron *70*, 468-481. 10.1016/j.neuron.2011.03.020.
22. Cociorva, D., D, L.T., and Yates, J.R. (2007). Validation of tandem mass spectrometry database search results using DTASelect. Curr Protoc Bioinformatics *Chapter 13*, Unit 13 14. 10.1002/0471250953.bi1304s16.
23. Comoletti, D., Flynn, R.E., Boucard, A.A., Demeler, B., Schirf, V., Shi, J., Jennings, L.L., Newlin, H.R., Sudhof, T.C., and Taylor, P. (2006). Gene selection, alternative splicing, and post-translational processing regulate neuroligin selectivity for beta-neurexins. Biochemistry *45*, 12816-12827. 10.1021/bi0614131.
24. Craig, A.M., and Kang, Y. (2007). Neurexin-neuroligin signaling in synapse development. Curr Opin Neurobiol *17*, 43-52. 10.1016/j.conb.2007.01.011.
25. de Wit, J., O'Sullivan, M.L., Savas, J.N., Condomitti, G., Caccese, M.C., Vennekens, K.M., Yates, J.R., 3rd, and Ghosh, A. (2013). Unbiased discovery of glypican as a receptor for LRRTM4 in regulating excitatory synapse development. Neuron *79*, 696-711. 10.1016/j.neuron.2013.06.049.
26. de Wit, J., Sylwestrak, E., O'Sullivan, M.L., Otto, S., Tiglio, K., Savas, J.N., Yates, J.R., 3rd, Comoletti, D., Taylor, P., and Ghosh, A. (2009). LRRTM2 interacts with Neurexin1 and regulates excitatory synapse formation. Neuron *64*, 799-806. 10.1016/j.neuron.2009.12.019.
27. Domon, B., and Gallien, S. (2015). Recent advances in targeted proteomics for clinical applications. Proteomics Clin Appl *9*, 423-431. 10.1002/prca.201400136.
28. Elias, J.E., and Gygi, S.P. (2007). Target-decoy search strategy for increased confidence in large-scale protein identifications by mass spectrometry. Nat Methods *4*, 207-214. 10.1038/nmeth1019.
29. Eng, J.K., McCormack, A.L., and Yates, J.R. (1994). An approach to correlate tandem mass spectral data of peptides with amino acid sequences in a protein database. J Am Soc Mass Spectrom *5*, 976-989. 10.1016/1044-0305(94)80016-2.
30. Etherton, M., Foldy, C., Sharma, M., Tabuchi, K., Liu, X., Shamloo, M., Malenka, R.C., and Sudhof, T.C. (2011a). Autism-linked neuroligin-3 R451C mutation differentially alters hippocampal and cortical synaptic function. Proc Natl Acad Sci U S A *108*, 13764-13769. 10.1073/pnas.1111093108.

31. Etherton, M.R., Tabuchi, K., Sharma, M., Ko, J., and Sudhof, T.C. (2011b). An autism-associated point mutation in the neuroligin cytoplasmic tail selectively impairs AMPA receptor-mediated synaptic transmission in hippocampus. EMBO J *30*, 2908-2919. 10.1038/emboj.2011.182.
32. Fettiplace, R. (2017). Hair Cell Transduction, Tuning, and Synaptic Transmission in the Mammalian Cochlea. Compr Physiol *7*, 1197-1227. 10.1002/cphy.c160049.
33. Furman, A.C., Kujawa, S.G., and Liberman, M.C. (2013). Noise-induced cochlear neuropathy is selective for fibers with low spontaneous rates. J Neurophysiol *110*, 577-586. 10.1152/jn.00164.2013.
34. Gallien, S., Duriez, E., Crone, C., Kellmann, M., Moehring, T., and Domon, B. (2012). Targeted proteomic quantification on quadrupole-orbitrap mass spectrometer. Mol Cell Proteomics *11*, 1709-1723. 10.1074/mcp.O112.019802.
35. Gibson, J.R., Huber, K.M., and Sudhof, T.C. (2009). Neuroligin-2 deletion selectively decreases inhibitory synaptic transmission originating from fast-spiking but not from somatostatin-positive interneurons. J Neurosci *29*, 13883-13897. 10.1523/JNEUROSCI.2457-09.2009.
36. Gilels, F., Paquette, S.T., Zhang, J., Rahman, I., and White, P.M. (2013). Mutation of Foxo3 causes adult onset auditory neuropathy and alters cochlear synapse architecture in mice. J Neurosci *33*, 18409-18424. 10.1523/JNEUROSCI.2529-13.2013.
37. Glowatzki, E., and Fuchs, P.A. (2002). Transmitter release at the hair cell ribbon synapse. Nat Neurosci *5*, 147-154. 10.1038/nn796.
38. Gong, T.W., Fairfield, D.A., Fullarton, L., Dolan, D.F., Altschuler, R.A., Kohrman, D.C., and Lomax, M.I. (2012). Induction of heat shock proteins by hyperthermia and noise overstimulation in hsf1 -/- mice. J Assoc Res Otolaryngol *13*, 29-37. 10.1007/s10162-011-0289-9.
39. Gorga, M.P., Neely, S.T., Ohlrich, B., Hoover, B., Redner, J., and Peters, J. (1997). From laboratory to clinic: a large scale study of distortion product otoacoustic emissions in ears with normal hearing and ears with hearing loss. Ear Hear *18*, 440-455. 10.1097/00003446-199712000-00003.
40. Gouw, J.W., Krijgsveld, J., and Heck, A.J. (2010). Quantitative proteomics by metabolic labeling of model organisms. Mol Cell Proteomics *9*, 11-24. 10.1074/mcp.R900001-MCP200.
41. Guang, S., Pang, N., Deng, X., Yang, L., He, F., Wu, L., Chen, C., Yin, F., and Peng, J. (2018). Synaptopathology Involved in Autism Spectrum Disorder. Front Cell Neurosci *12*, 470. 10.3389/fncel.2018.00470.
42. Haas, K.T., Compans, B., Letellier, M., Bartol, T.M., Grillo-Bosch, D., Sejnowski, T.J., Sainlos, M., Choquet, D., Thoumine, O., and Hosy, E. (2018). Pre-post synaptic alignment through neuroligin-1 tunes synaptic transmission efficiency. Elife *7*. 10.7554/eLife.31755.
43. He, L., Diedrich, J., Chu, Y.Y., and Yates, J.R., 3rd (2015). Extracting Accurate Precursor Information for Tandem Mass Spectra by RawConverter. Anal Chem *87*, 11361-11367. 10.1021/acs.analchem.5b02721.
44. Heine, M., Thoumine, O., Mondin, M., Tessier, B., Giannone, G., and Choquet, D. (2008). Activity-independent and subunit-specific recruitment of functional AMPA receptors at neurexin/neuroligin contacts. Proc Natl Acad Sci U S A *105*, 20947-20952. 10.1073/pnas.0804007106.
45. Hettling, H., and van Beek, J.H. (2011). Analyzing the functional properties of the creatine kinase system with multiscale 'sloppy' modeling. PLoS Comput Biol *7*, e1002130. 10.1371/journal.pcbi.1002130.

46. Hickox, A.E., Wong, A.C., Pak, K., Strojny, C., Ramirez, M., Yates, J.R., 3rd, Ryan, A.F., and Savas, J.N. (2017). Global Analysis of Protein Expression of Inner Ear Hair Cells. J Neurosci *37*, 1320-1339. 10.1523/JNEUROSCI.2267-16.2016.
47. Hjerpe, R., Aillet, F., Lopitz-Otsoa, F., Lang, V., England, P., and Rodriguez, M.S. (2009). Efficient protection and isolation of ubiquitylated proteins using tandem ubiquitin-binding entities. EMBO Rep *10*, 1250-1258. 10.1038/embor.2009.192.
48. Jiang, M., Polepalli, J., Chen, L.Y., Zhang, B., Sudhof, T.C., and Malenka, R.C. (2017). Conditional ablation of neuroligin-1 in CA1 pyramidal neurons blocks LTP by a cell-autonomous NMDA receptor-independent mechanism. Mol Psychiatry *22*, 375-383. 10.1038/mp.2016.80.
49. Jongkamonwiwat, N., Ramirez, M.A., Edassery, S., Wong, A.C.Y., Yu, J., Abbott, T., Pak, K., Ryan, A.F., and Savas, J.N. (2020). Noise Exposures Causing Hearing Loss Generate Proteotoxic Stress and Activate the Proteostasis Network. Cell Rep *33*, 108431. 10.1016/j.celrep.2020.108431.
50. Kazmierczak, M., Harris, S.L., Kazmierczak, P., Shah, P., Starovoytov, V., Ohlemiller, K.K., and Schwander, M. (2015). Progressive Hearing Loss in Mice Carrying a Mutation in Usp53. J Neurosci *35*, 15582-15598. 10.1523/JNEUROSCI.1965-15.2015.
51. Kim, D.K., Park, Y., Back, S.A., Kim, H.L., Park, H.E., Park, K.H., Yeo, S.W., and Park, S.N. (2014). Protective effect of unilateral and bilateral ear plugs on noise-induced hearing loss: functional and morphological evaluation in animal model. Noise Health *16*, 149-156. 10.4103/1463-1741.134915.
52. Kim, J.A., Kim, D., Won, S.Y., Han, K.A., Park, D., Cho, E., Yun, N., An, H.J., Um, J.W., Kim, E., et al. (2017). Structural Insights into Modulation of Neurexin-Neuroligin Trans-synaptic Adhesion by MDGA1/Neuroligin-2 Complex. Neuron *94*, 1121-1131 e1126. 10.1016/j.neuron.2017.05.034.
53. Kimball, S.R., and Jefferson, L.S. (2012). Induction of REDD1 gene expression in the liver in response to endoplasmic reticulum stress is mediated through a PERK, eIF2alpha phosphorylation, ATF4-dependent cascade. Biochem Biophys Res Commun *427*, 485-489. 10.1016/j.bbrc.2012.09.074.
54. Ko, J., Zhang, C., Arac, D., Boucard, A.A., Brunger, A.T., and Sudhof, T.C. (2009). Neuroligin-1 performs neurexin-dependent and neurexin-independent functions in synapse validation. EMBO J *28*, 3244-3255. 10.1038/emboj.2009.249.
55. Kujawa, S.G., and Liberman, M.C. (2006). Acceleration of age-related hearing loss by early noise exposure: evidence of a misspent youth. J Neurosci *26*, 2115-2123. 10.1523/JNEUROSCI.4985-05.2006.
56. Kujawa, S.G., and Liberman, M.C. (2009). Adding insult to injury: cochlear nerve degeneration after "temporary" noise-induced hearing loss. J Neurosci *29*, 14077-14085. 10.1523/JNEUROSCI.2845-09.2009.
57. Langer, T., Lu, C., Echols, H., Flanagan, J., Hayer, M.K., and Hartl, F.U. (1992). Successive action of DnaK, DnaJ and GroEL along the pathway of chaperone-mediated protein folding. Nature *356*, 683-689. 10.1038/356683a0.
58. Le Prell, C.G., Yamashita, D., Minami, S.B., Yamasoba, T., and Miller, J.M. (2007). Mechanisms of noise-induced hearing loss indicate multiple methods of prevention. Hear Res *226*, 22-43. 10.1016/j.heares.2006.10.006.
59. Leekam, S.R., Nieto, C., Libby, S.J., Wing, L., and Gould, J. (2007). Describing the sensory abnormalities of children and adults with autism. J Autism Dev Disord *37*, 894-910. 10.1007/s10803-006-0218-7.

60. Letellier, M., Sziber, Z., Chamma, I., Saphy, C., Papasideri, I., Tessier, B., Sainlos, M., Czondor, K., and Thoumine, O. (2018). A unique intracellular tyrosine in neuroligin-1 regulates AMPA receptor recruitment during synapse differentiation and potentiation. Nat Commun *9*, 3979. 10.1038/s41467-018-06220-2.
61. Li, B., and Dewey, C.N. (2011). RSEM: accurate transcript quantification from RNA-Seq data with or without a reference genome. BMC Bioinformatics *12*, 323. 10.1186/1471-2105-12-323.
62. Li, J., Li, Q., Tang, J., Xia, F., Wu, J., and Zeng, R. (2015). Quantitative Phosphoproteomics Revealed Glucose-Stimulated Responses of Islet Associated with Insulin Secretion. J Proteome Res *14*, 4635-4646. 10.1021/acs.jproteome.5b00507.
63. Liberman, L.D., Wang, H., and Liberman, M.C. (2011). Opposing gradients of ribbon size and AMPA receptor expression underlie sensitivity differences among cochlear-nerve/hair-cell synapses. J Neurosci *31*, 801-808. 10.1523/JNEUROSCI.3389-10.2011.
64. Liberman, M.C. (1978). Auditory-nerve response from cats raised in a low-noise chamber. J Acoust Soc Am *63*, 442-455.
65. Liberman, M.C. (1982). Single-neuron labeling in the cat auditory nerve. Science *216*, 1239-1241.
66. Liberman, M.C. (2016). Noise-Induced Hearing Loss: Permanent Versus Temporary Threshold Shifts and the Effects of Hair Cell Versus Neuronal Degeneration. Adv Exp Med Biol *875*, 1-7. 10.1007/978-1-4939-2981-8_1.
67. Liberman, M.C. (2017). Noise-induced and age-related hearing loss: new perspectives and potential therapies. F1000Res *6*, 927. 10.12688/f1000research.11310.1.
68. Lim, H.H., Jenkins, O.H., Myers, M.W., Miller, J.M., and Altschuler, R.A. (1993). Detection of HSP 72 synthesis after acoustic overstimulation in rat cochlea. Hear Res *69*, 146-150. 10.1016/0378-5955(93)90102-7.
69. Lin, H.W., Furman, A.C., Kujawa, S.G., and Liberman, M.C. (2011). Primary neural degeneration in the Guinea pig cochlea after reversible noise-induced threshold shift. J Assoc Res Otolaryngol *12*, 605-616. 10.1007/s10162-011-0277-0.
70. Liu, P., Edassery, S.L., Ali, L., Thomson, B.R., Savas, J.N., and Jin, J. (2019). Long-lived metabolic enzymes in the crystalline lens identified by pulse-labeling of mice and mass spectrometry. Elife *8*. 10.7554/eLife.50170.
71. Liu, W., Atturo, F., Aldaya, R., Santi, P., Cureoglu, S., Obwegeser, S., Glueckert, R., Pfaller, K., Schrott-Fischer, A., and Rask-Andersen, H. (2015). Macromolecular organization and fine structure of the human basilar membrane - RELEVANCE for cochlear implantation. Cell Tissue Res *360*, 245-262. 10.1007/s00441-014-2098-z.
72. Low, W.K., Kong, S.W., and Tan, M.G. (2010). Ototoxicity from combined Cisplatin and radiation treatment: an in vitro study. Int J Otolaryngol *2010*, 523976. 10.1155/2010/523976.
73. Lu, J., Li, W., Du, X., Ewert, D.L., West, M.B., Stewart, C., Floyd, R.A., and Kopke, R.D. (2014). Antioxidants reduce cellular and functional changes induced by intense noise in the inner ear and cochlear nucleus. J Assoc Res Otolaryngol *15*, 353-372. 10.1007/s10162-014-0441-4.
74. Luo, J.K., Melland, H., Nithianantharajah, J., and Gordon, S.L. (2021). Postsynaptic Neuroligin-1 Mediates Presynaptic Endocytosis During Neuronal Activity. Front Mol Neurosci *14*, 744845. 10.3389/fnmol.2021.744845.
75. MacCoss, M.J., Wu, C.C., Liu, H., Sadygov, R., and Yates, J.R., 3rd (2003). A correlation algorithm for the automated quantitative analysis of shotgun proteomics data. Anal Chem *75*, 6912-6921. 10.1021/ac034790h.

76. Mateo Sanchez, S., Freeman, S.D., Delacroix, L., and Malgrange, B. (2016). The role of post-translational modifications in hearing and deafness. Cell Mol Life Sci *73*, 3521-3533. 10.1007/s00018-016-2257-3.
77. Maulucci, G., Troiani, D., Eramo, S.L., Paciello, F., Podda, M.V., Paludetti, G., Papi, M., Maiorana, A., Palmieri, V., De Spirito, M., and Fetoni, A.R. (2014). Time evolution of noise induced oxidation in outer hair cells: role of NAD(P)H and plasma membrane fluidity. Biochim Biophys Acta *1840*, 2192-2202. 10.1016/j.bbagen.2014.04.005.
78. McAlister, G.C., Nusinow, D.P., Jedrychowski, M.P., Wuhr, M., Huttlin, E.L., Erickson, B.K., Rad, R., Haas, W., and Gygi, S.P. (2014). MultiNotch MS3 enables accurate, sensitive, and multiplexed detection of differential expression across cancer cell line proteomes. Anal Chem *86*, 7150-7158. 10.1021/ac502040v.
79. McDonald, W.H., Tabb, D.L., Sadygov, R.G., MacCoss, M.J., Venable, J., Graumann, J., Johnson, J.R., Cociorva, D., and Yates, J.R., 3rd (2004). MS1, MS2, and SQT-three unified, compact, and easily parsed file formats for the storage of shotgun proteomic spectra and identifications. Rapid Commun Mass Spectrom *18*, 2162-2168. 10.1002/rcm.1603.
80. Meyer, A.C., Frank, T., Khimich, D., Hoch, G., Riedel, D., Chapochnikov, N.M., Yarin, Y.M., Harke, B., Hell, S.W., Egner, A., and Moser, T. (2009). Tuning of synapse number, structure and function in the cochlea. Nat Neurosci *12*, 444-453. 10.1038/nn.2293.
81. Mi, H., Poudel, S., Muruganujan, A., Casagrande, J.T., and Thomas, P.D. (2016). PANTHER version 10: expanded protein families and functions, and analysis tools. Nucleic Acids Res *44*, D336-342. 10.1093/nar/gkv1194.
82. Mi, H.Y., Muruganujan, A., and Thomas, P.D. (2013). PANTHER in 2013: modeling the evolution of gene function, and other gene attributes, in the context of phylogenetic trees. Nucleic Acids Res *41*, D377-D386. 10.1093/nar/gks1118.
83. Michanski, S., Smaluch, K., Steyer, A.M., Chakrabarti, R., Setz, C., Oestreicher, D., Fischer, C., Mobius, W., Moser, T., Vogl, C., and Wichmann, C. (2019). Mapping developmental maturation of inner hair cell ribbon synapses in the apical mouse cochlea. Proc Natl Acad Sci U S A *116*, 6415-6424. 10.1073/pnas.1812029116.
84. Miron, O., Delgado, R.E., Delgado, C.F., Simpson, E.A., Yu, K.H., Gutierrez, A., Zeng, G., Gerstenberger, J.N., and Kohane, I.S. (2021). Prolonged Auditory Brainstem Response in Universal Hearing Screening of Newborns with Autism Spectrum Disorder. Autism Res *14*, 46-52. 10.1002/aur.2422.
85. Mondin, M., Labrousse, V., Hosy, E., Heine, M., Tessier, B., Levet, F., Poujol, C., Blanchet, C., Choquet, D., and Thoumine, O. (2011). Neurexin-neuroligin adhesions capture surface-diffusing AMPA receptors through PSD-95 scaffolds. J Neurosci *31*, 13500-13515. 10.1523/JNEUROSCI.6439-10.2011.
86. Morimoto, R.I. (2008). Proteotoxic stress and inducible chaperone networks in neurodegenerative disease and aging. Genes Dev *22*, 1427-1438. 10.1101/gad.1657108.
87. Muller, U., and Barr-Gillespie, P.G. (2015). New treatment options for hearing loss. Nat Rev Drug Discov *14*, 346-365. 10.1038/nrd4533.
88. Nam, C.I., and Chen, L. (2005). Postsynaptic assembly induced by neurexin-neuroligin interaction and neurotransmitter. Proc Natl Acad Sci U S A *102*, 6137-6142. 10.1073/pnas.0502038102.
89. Nam, J., Mah, W., and Kim, E. (2011). The SALM/Lrfn family of leucine-rich repeat-containing cell adhesion molecules. Semin Cell Dev Biol *22*, 492-498. 10.1016/j.semcdb.2011.06.005.

90. Nguyen, T.A., Lehr, A.W., and Roche, K.W. (2020). Neuroligins and Neurodevelopmental Disorders: X-Linked Genetics. Front Synaptic Neurosci *12*, 33. 10.3389/fnsyn.2020.00033.
91. O'Sullivan, M.L., de Wit, J., Savas, J.N., Comoletti, D., Otto-Hitt, S., Yates, J.R., 3rd, and Ghosh, A. (2012). FLRT proteins are endogenous latrophilin ligands and regulate excitatory synapse development. Neuron *73*, 903-910. 10.1016/j.neuron.2012.01.018.
92. Oku, S., Feng, H., Connor, S., Toledo, A., Zhang, P., Zhang, Y., Thoumine, O., Zhang, C., and Craig, A.M. (2020). Alternative splicing at neuroligin site A regulates glycan interaction and synaptogenic activity. Elife *9*. 10.7554/eLife.58668.
93. Park, S.K., Aslanian, A., McClatchy, D.B., Han, X., Shah, H., Singh, M., Rauniyar, N., Moresco, J.J., Pinto, A.F., Diedrich, J.K., et al. (2014). Census 2: isobaric labeling data analysis. Bioinformatics *30*, 2208-2209. 10.1093/bioinformatics/btu151.
94. Park, S.K., Venable, J.D., Xu, T., and Yates, J.R., 3rd (2008). A quantitative analysis software tool for mass spectrometry-based proteomics. Nat Methods *5*, 319-322. 10.1038/nmeth.1195.
95. Peng, J., Elias, J.E., Thoreen, C.C., Licklider, L.J., and Gygi, S.P. (2003a). Evaluation of multidimensional chromatography coupled with tandem mass spectrometry (LC/LC-MS/MS) for large-scale protein analysis: the yeast proteome. J Proteome Res *2*, 43-50.
96. Peng, J., Schwartz, D., Elias, J.E., Thoreen, C.C., Cheng, D., Marsischky, G., Roelofs, J., Finley, D., and Gygi, S.P. (2003b). A proteomics approach to understanding protein ubiquitination. Nat Biotechnol *21*, 921-926. 10.1038/nbt849.
97. Petitpre, C., Wu, H., Sharma, A., Tokarska, A., Fontanet, P., Wang, Y., Helmbacher, F., Yackle, K., Silberberg, G., Hadjab, S., and Lallemend, F. (2018). Neuronal heterogeneity and stereotyped connectivity in the auditory afferent system. Nat Commun *9*, 3691. 10.1038/s41467-018-06033-3.
98. Poulopoulos, A., Soykan, T., Tuffy, L.P., Hammer, M., Varoqueaux, F., and Brose, N. (2012). Homodimerization and isoform-specific heterodimerization of neuroligins. Biochem J *446*, 321-330. 10.1042/BJ20120808.
99. Raso, C., Cosentino, C., Gaspari, M., Malara, N., Han, X., McClatchy, D., Park, S.K., Renne, M., Vadala, N., Prati, U., et al. (2012). Characterization of breast cancer interstitial fluids by TmT labeling, LTQ-Orbitrap Velos mass spectrometry, and pathway analysis. J Proteome Res *11*, 3199-3210. 10.1021/pr2012347.
100. Rauniyar, N., and Yates, J.R., 3rd (2014). Isobaric labeling-based relative quantification in shotgun proteomics. J Proteome Res *13*, 5293-5309. 10.1021/pr500880b.
101. Reijntjes, D.O.J., and Pyott, S.J. (2016). The afferent signaling complex: Regulation of type I spiral ganglion neuron responses in the auditory periphery. Hear Res *336*, 1-16. 10.1016/j.heares.2016.03.011.
102. Robertson, D. (1983). Functional-Significance of Dendritic Swelling after Loud Sounds in the Guinea-Pig Cochlea. Hearing Res *9*, 263-278. Doi 10.1016/0378-5955(83)90031-X.
103. Ruel, J., Wang, J., Rebillard, G., Eybalin, M., Lloyd, R., Pujol, R., and Puel, J.L. (2007). Physiology, pharmacology and plasticity at the inner hair cell synaptic complex. Hear Res *227*, 19-27. 10.1016/j.heares.2006.08.017.
104. Rutherford, M.A., Chapochnikov, N.M., and Moser, T. (2012). Spike encoding of neurotransmitter release timing by spiral ganglion neurons of the cochlea. J Neurosci *32*, 4773-4789. 10.1523/JNEUROSCI.4511-11.2012.
105. Rutherford, M.A., von Gersdorff, H., and Goutman, J.D. (2021). Encoding sound in the cochlea: from receptor potential to afferent discharge. J Physiol *599*, 2527-2557. 10.1113/JP279189.

106. Ryan, A.F., Kujawa, S.G., Hammill, T., Le Prell, C., and Kil, J. (2016). Temporary and Permanent Noise-induced Threshold Shifts: A Review of Basic and Clinical Observations. Otol Neurotol *37*, e271-275. 10.1097/MAO.0000000000001071.
107. Saunders, G.H., and Griest, S.E. (2009). Hearing loss in veterans and the need for hearing loss prevention programs. Noise Health *11*, 14-21.
108. Savas, J.N., Park, S.K., and Yates, J.R., 3rd (2016). Proteomic Analysis of Protein Turnover by Metabolic Whole Rodent Pulse-Chase Isotopic Labeling and Shotgun Mass Spectrometry Analysis. Methods Mol Biol *1410*, 293-304. 10.1007/978-1-4939-3524-6_18.
109. Savas, J.N., Toyama, B.H., Xu, T., Yates, J.R., 3rd, and Hetzer, M.W. (2012). Extremely long-lived nuclear pore proteins in the rat brain. Science *335*, 942. 10.1126/science.1217421.
110. Scheffer, D.I., Shen, J., Corey, D.P., and Chen, Z.Y. (2015). Gene Expression by Mouse Inner Ear Hair Cells during Development. J Neurosci *35*, 6366-6380. 10.1523/JNEUROSCI.5126-14.2015.
111. Scheiffele, P., Fan, J., Choih, J., Fetter, R., and Serafini, T. (2000). Neuroligin expressed in nonneuronal cells triggers presynaptic development in contacting axons. Cell *101*, 657-669. 10.1016/s0092-8674(00)80877-6.
112. Schiavon, E., Smalley, J.L., Newton, S., Greig, N.H., and Forsythe, I.D. (2018). Neuroinflammation and ER-stress are key mechanisms of acute bilirubin toxicity and hearing loss in a mouse model. PLoS One *13*, e0201022. 10.1371/journal.pone.0201022.
113. Shcherbik, N., and Pestov, D.G. (2019). The Impact of Oxidative Stress on Ribosomes: From Injury to Regulation. Cells *8*. 10.3390/cells8111379.
114. Shi, L., Chang, Y., Li, X., Aiken, S., Liu, L., and Wang, J. (2016). Cochlear Synaptopathy and Noise-Induced Hidden Hearing Loss. Neural Plast *2016*, 6143164. 10.1155/2016/6143164.
115. Shipman, S.L., and Nicoll, R.A. (2012). Dimerization of postsynaptic neuroligin drives synaptic assembly via transsynaptic clustering of neurexin. Proc Natl Acad Sci U S A *109*, 19432-19437. 10.1073/pnas.1217633109.
116. Shipman, S.L., Schnell, E., Hirai, T., Chen, B.S., Roche, K.W., and Nicoll, R.A. (2011). Functional dependence of neuroligin on a new non-PDZ intracellular domain. Nat Neurosci *14*, 718-726. 10.1038/nn.2825.
117. Shrestha, B.R., Chia, C., Wu, L., Kujawa, S.G., Liberman, M.C., and Goodrich, L.V. (2018). Sensory Neuron Diversity in the Inner Ear Is Shaped by Activity. Cell *174*, 1229-1246 e1217. 10.1016/j.cell.2018.07.007.
118. Soler-Llavina, G.J., Fuccillo, M.V., Ko, J., Sudhof, T.C., and Malenka, R.C. (2011). The neurexin ligands, neuroligins and leucine-rich repeat transmembrane proteins, perform convergent and divergent synaptic functions in vivo. Proc Natl Acad Sci U S A *108*, 16502-16509. 10.1073/pnas.1114028108.
119. Song, J.Y., Ichtchenko, K., Sudhof, T.C., and Brose, N. (1999). Neuroligin 1 is a postsynaptic cell-adhesion molecule of excitatory synapses. Proc Natl Acad Sci U S A *96*, 1100-1105. 10.1073/pnas.96.3.1100.
120. Strimbu, C.E., Prasad, S., Hakizimana, P., and Fridberger, A. (2019). Control of hearing sensitivity by tectorial membrane calcium. Proc Natl Acad Sci U S A *116*, 5756-5764. 10.1073/pnas.1805223116.
121. Sudhof, T.C. (2008). Neuroligins and neurexins link synaptic function to cognitive disease. Nature *455*, 903-911. 10.1038/nature07456.
122. Sudhof, T.C. (2017). Synaptic Neurexin Complexes: A Molecular Code for the Logic of Neural Circuits. Cell *171*, 745-769. 10.1016/j.cell.2017.10.024.

123. Sun, S., Babola, T., Pregernig, G., So, K.S., Nguyen, M., Su, S.M., Palermo, A.T., Bergles, D.E., Burns, J.C., and Muller, U. (2018). Hair Cell Mechanotransduction Regulates Spontaneous Activity and Spiral Ganglion Subtype Specification in the Auditory System. Cell *174*, 1247-1263 e1215. 10.1016/j.cell.2018.07.008.
124. Szklarczyk, D., Morris, J.H., Cook, H., Kuhn, M., Wyder, S., Simonovic, M., Santos, A., Doncheva, N.T., Roth, A., Bork, P., et al. (2017). The STRING database in 2017: quality-controlled protein-protein association networks, made broadly accessible. Nucleic Acids Res *45*, D362-D368. 10.1093/nar/gkw937.
125. Tabb, D.L., McDonald, W.H., and Yates, J.R., 3rd (2002). DTASelect and Contrast: tools for assembling and comparing protein identifications from shotgun proteomics. J Proteome Res *1*, 21-26.
126. Takahashi, S., Sun, W., Zhou, Y., Homma, K., Kachar, B., Cheatham, M.A., and Zheng, J. (2018). Prestin Contributes to Membrane Compartmentalization and Is Required for Normal Innervation of Outer Hair Cells. Front Cell Neurosci *12*, 211. 10.3389/fncel.2018.00211.
127. Taylor, S.C., Ferri, S.L., Grewal, M., Smernoff, Z., Bucan, M., Weiner, J.A., Abel, T., and Brodkin, E.S. (2020). The Role of Synaptic Cell Adhesion Molecules and Associated Scaffolding Proteins in Social Affiliative Behaviors. Biol Psychiatry *88*, 442-451. 10.1016/j.biopsych.2020.02.012.
128. Thomas, P.D., Kejariwal, A., Guo, N., Mi, H., Campbell, M.J., Muruganujan, A., and Lazareva-Ulitsky, B. (2006). Applications for protein sequence-function evolution data: mRNA/protein expression analysis and coding SNP scoring tools. Nucleic Acids Res *34*, W645-650.
129. Toyama, B.H., Savas, J.N., Park, S.K., Harris, M.S., Ingolia, N.T., Yates, J.R., 3rd, and Hetzer, M.W. (2013). Identification of long-lived proteins reveals exceptional stability of essential cellular structures. Cell *154*, 971-982. 10.1016/j.cell.2013.07.037.
130. Ullrich, B., Ushkaryov, Y.A., and Sudhof, T.C. (1995). Cartography of neurexins: more than 1000 isoforms generated by alternative splicing and expressed in distinct subsets of neurons. Neuron *14*, 497-507. 10.1016/0896-6273(95)90306-2.
131. Uzunova, G., Hollander, E., and Shepherd, J. (2014). The role of ionotropic glutamate receptors in childhood neurodevelopmental disorders: autism spectrum disorders and fragile x syndrome. Curr Neuropharmacol *12*, 71-98. 10.2174/1570159X113116660046.
132. Varoqueaux, F., Aramuni, G., Rawson, R.L., Mohrmann, R., Missler, M., Gottmann, K., Zhang, W., Sudhof, T.C., and Brose, N. (2006). Neuroligins determine synapse maturation and function. Neuron *51*, 741-754. 10.1016/j.neuron.2006.09.003.
133. Wang, S., Wu, R., Lu, J., Jiang, Y., Huang, T., and Cai, Y.D. (2022). Protein-protein interaction networks as miners of biological discovery. Proteomics, e2100190. 10.1002/pmic.202100190.
134. Weisz, C.J., Glowatzki, E., and Fuchs, P.A. (2014). Excitability of type II cochlear afferents. J Neurosci *34*, 2365-2373. 10.1523/JNEUROSCI.3428-13.2014.
135. Weisz, C.J., Lehar, M., Hiel, H., Glowatzki, E., and Fuchs, P.A. (2012). Synaptic transfer from outer hair cells to type II afferent fibers in the rat cochlea. J Neurosci *32*, 9528-9536. 10.1523/JNEUROSCI.6194-11.2012.
136. Xu, G., Paige, J.S., and Jaffrey, S.R. (2010). Global analysis of lysine ubiquitination by ubiquitin remnant immunoaffinity profiling. Nat Biotechnol *28*, 868-873. 10.1038/nbt.1654.
137. Xu, T., Park, S.K., Venable, J.D., Wohlschlegel, J.A., Diedrich, J.K., Cociorva, D., Lu, B., Liao, L., Hewel, J., Han, X., et al. (2015). ProLuCID: An improved SEQUEST-like algorithm with enhanced sensitivity and specificity. J Proteomics *129*, 16-24. 10.1016/j.jprot.2015.07.001.
138. Yates, J.R., 3rd, Link, A.J., and Schieltz, D. (2000). Direct analysis of proteins in mixtures. Application to protein complexes. Methods Mol Biol *146*, 17-26. 10.1385/1-59259-045-4:17.

139. Yates, J.R., 3rd, McCormack, A.L., Schieltz, D., Carmack, E., and Link, A. (1997). Direct analysis of protein mixtures by tandem mass spectrometry. J Protein Chem *16*, 495-497. 10.1023/a:1026365528484.
140. Yoshida, T., Yamagata, A., Imai, A., Kim, J., Izumi, H., Nakashima, S., Shiroshima, T., Maeda, A., Iwasawa-Okamoto, S., Azechi, K., et al. (2021). Canonical versus non-canonical transsynaptic signaling of neuroligin 3 tunes development of sociality in mice. Nat Commun *12*, 1848. 10.1038/s41467-021-22059-6.
141. Zhang, B., Chen, L.Y., Liu, X., Maxeiner, S., Lee, S.J., Gokce, O., and Sudhof, T.C. (2015). Neuroligins Sculpt Cerebellar Purkinje-Cell Circuits by Differential Control of Distinct Classes of Synapses. Neuron *87*, 781-796. 10.1016/j.neuron.2015.07.020.
142. Zhang, B., Seigneur, E., Wei, P., Gokce, O., Morgan, J., and Sudhof, T.C. (2017). Developmental plasticity shapes synaptic phenotypes of autism-associated neuroligin-3 mutations in the calyx of Held. Mol Psychiatry *22*, 1483-1491. 10.1038/mp.2016.157.
143. Zhang, D.S., Piazza, V., Perrin, B.J., Rzadzinska, A.K., Poczatek, J.C., Wang, M., Prosser, H.M., Ervasti, J.M., Corey, D.P., and Lechene, C.P. (2012). Multi-isotope imaging mass spectrometry reveals slow protein turnover in hair-cell stereocilia. Nature *481*, 520-524. 10.1038/nature10745.
144. Zhou, X., Liao, W.J., Liao, J.M., Liao, P., and Lu, H. (2015). Ribosomal proteins: functions beyond the ribosome. J Mol Cell Biol *7*, 92-104. 10.1093/jmcb/mjv014.